COMPOSITE LOW TEMPERATURE HYDROGEN STORAGE MATERIAL ON THE BASIS OF IRON-TITANIUM ALLOY; SYNTHESIS AND STRUCTURE

NKELE ONYEGBULE

A thesis submitted in fulfilment of the requirements for the degree of Magister Scientiae
In the Department of Chemistry, University of the Western Cape.

UNIVERSITY of the
WESTERN CAPE

Supervisor: Prof. V.M. Linkov

Co-supervisor: Dr. A. Nechaev

November 2006

DECLARATION

I declare that *Composite low temperature hydrogen storage materials on the basis of iron-titanium; synthesis and structure* is my own work, that it has not been submitted for any degree or examination in any other University and that all the sources I have used or quoted have been indicated and acknowledged by the complete references.

Nkele Onyegbule November 2006

Signed:…….

ACKNOWLEDGEMENTS

I express profound gratitude to the Almighty God for the gift of life, and opportunities for the fulfillment of ambition.

My late parents Mr. and Mrs. Onyegbule, for my forthright upbringing and legacy of self-belief; May their souls rest in peace.

Prof. V.M Linkov and other staff of the South African Institute for Advanced Materials Chemistry, for their camaraderie and financial leverage in actualizing this research.

Dr. A. Nechaev for his guidance and tutelage; you were more than a supervisor to me, you were a father.

Dr. Patrick Ndungu for his immense scientific contributions; many thanks.

Dr. Remy Butcher for his input in XRD measurements.

The University of Western Cape, Department of Physics for their assistance with SEM and TEM characterization.

Finally, my brothers and friends; Goke, Nelson, Ojiugo and co. This would not have been possible without your moral support.

UNIVERSITY of the
WESTERN CAPE

ABSTRACT

It is widely believed that hydrogen will within a few tens of years become the means of storing and transporting energy. The reason is the depletion of hydrocarbons and the relatively facile production of hydrogen from various renewable sources of energy. Hydrogen can be combusted in an efficient way in a fuel cell with water as emission product. As concerns over air pollution and global warming increase, the incentive to switch to clean and efficient hydrogen economy becomes greater and the transition may occur well before hydrocarbon reserves are extinct.

The overall goal of the project is to develop the knowledge base for solid-state hydrogen storage technology suitable for stationary and mobile applications. In order to accomplish this goal, the project will have a dual focus which includes the synthesis of novel nano-structured hydrogen storage materials and systems that can accurately analyze the materials.

The aim of this research is to develop a novel composite hydrogen storage material with high wt% storage capacity, high intrinsic safety, appropriate thermodynamics, high mechanical strength, reversibility of the system and fast kinetics based on a well known “low temperature” intermetallic alloy (Ti/Fe) as the core. In the course of achieving this objective, the structural, thermal, chemisorptive and physisorptive attributes of this material on a nano-scale have been evaluated considering that nano-structuring is a potentially promising approach for controlling bond strength, kinetics, and sorption temperatures and pressures. By combining different materials with suitable catalytic and thermodynamic properties, a new class of hybrid hydrogen storage material has been developed. More importantly, the focus was to increase the capacity of hydrogen sorption in this material. This goal was achieved with the mechano-chemical pre-treatment of Ti/Fe alloy and surface modification with carbon nanotubes, binary palladium and magnesium metals via a layer-by-layer modification technique. The chemical and mechanical stability of hydrogen storage materials is of great importance because hydrogen storage materials must withstand repeated adsorption and desorption cycles. The layer by layer approach that was used in this project allowed the investigation of the chemical and mechanical stability of the materials as each layer was added. Through this layer by layer approach suitable nano-particles were introduced that are chemically and mechanically stable. The knowledge emanating from this investigation is expected to allow the directed design of new, higher-efficiency, recyclable hydride-based materials in pursuance of the 6.0 wt% goal set forth by the US Department of Energy.

UNIVERSITY of the
WESTERN CAPE

LIST OF TABLES

Table2.1	Qualitative overview of hydride types and attributes.
Table3.1	All materials used and suppliers
Table 3.2	Reference data for the constituent phases of the commercial alloy
Table 4.1	Influence of ball diameter on surface area of alloy
Table 4.2	Quantitative EDS data from points 1 (a) and 2 (b) on Fe/Ti sample
Table 4.3	Quantitative EDS data for the total surface of Fe/Ti sample
Table 4.4	Results of the Rietveld refinement of the as-delivered T/iFe sample (Figure 4.7)
Table 4.5	Influence of carbon nanotubes on surface area of different samples milled with 3cm balls
Table 4.6	Results of the Rietveld refinement of the hydrogenated Ti/Fe + 30% TiH_2 sample, ball-milled for 1hour (Figure 4.29).

UNIVERSITY of the
WESTERN CAPE

LIST OF FIGURES

Fig 2.1 Relation between weight and volume hydrogen capacities for binary and intermetallic hydrides on the basis of transition metals (I), and binary and complex hydrides of the light elements (II).

Fig 2.2 A schematic representation of the idealized PCT diagram of hydrogen — metal system: a -pressure - composition isotherms at the temperatures T1<T2<T3<Tc; b - temperature dependence of plateau pressure

Fig 2.3 Family tree of hydriding alloys and complexes

Fig 2.4 Temperatures of hydrogen desorption from the different Metal Hydrides

Fig 3.1 Schematic diagram of the CVD set-up for carbon nanotube synthesis using LPG

Fig 3.2 Schematic diagram of the Sieverts apparatus at SAIAMC

Fig 4.1 Influence of milling time on the samples milled with 3cm balls at 350 rpm

Fig 4.2 SEM images of the pristine Fe/Ti sample

Fig 4.3 Secondary X-ray image of the Ti/Fe sample (the same region and magnification as for Figure 4.3d). The points correspond to the regions from where the local EDS data were collected (1 – impurity phase, 2 – matrix phase)

Fig 4.4 Energy spectra of secondary X-rays collected from points 1 (a) and 2 (b) of the Ti/Fe sample.

Fig 4.5 Energy spectra of secondary X-rays collected from the total surface of the Ti/Fe sample.

Fig 4.6 SEM images of Fe/Ti ball milled after 60 minutes with 3cm balls at 350 rpm

Fig 4.7 XRD pattern of the as-delivered Ti/Fe sample

Fig 4.8 X-ray diffractographs showing broadening of the intensity peaks of Fe/Ti alloy with extended milling time for samples milled with 3cm balls at 350 rpm

Fig 4.9 SEM images of CNT grown on different substrates at 800^{o}C and 30 minutes LPG deposition time (a) nickel foils (b) cobalt foils (c) nickel porous membrane

UNIVERSITY of the
WESTERN CAPE

Fig 4.10 SEM image showing LPG deposit on the alloy after 10 minutes for sample ball milled 60 minutes-350 rpm-3cm balls

Fig 4.11 SEM image showing LPG deposit on the alloy after 30 minutes for same sample

Fig 4.12 SEM image showing LPG deposit on the alloy after 60 minutes for same sample

Fig 4.13 TEM images confirming the nanotubes with (a) hollow centre and diameter of ~20 nm and (b) filled centre and diameter of ~70 nm for LPG deposit on the alloy after 60 minutes for same sample

Fig 4.14 LPG deposition time Vs surface area showing increase in surface area of composite from 2.0289 m^2/g-12.8406 m^2/g with progressive LPG deposition time for samples ball milled for 60 minutes at 350 rpm using 3cm balls

Fig 4.15 Micrograph A is carbon nanotubes grown on the surface of the iron titanium alloy. Micrograph B is an image of the palladium functionalized nanotubes on the alloy

Fig 4.16 EDS peaks showing the presence of palladium deposited on the composite

Fig 4.17 SEM images showing magnesium functionalized composite

Fig 4.18 EDS peak showing the presence of magnesium deposited on the composite

Fig 4.19 Schematic representation of parameters monitored by the Set-up

Fig 4.20 TGA absorption/desorption patterns for the unmilled Fe/Ti sample

Fig 4.21 TGA absorption/desorption patterns for the sample milled for 60 mins – 3cm balls – 350 rpm

Fig 4.22 TGA absorption/desorption patterns for the sample milled for 60 mins – 3cm balls – 350 rpm + CNT

Fig 4.23 TGA absorption/desorption patterns for the sample milled for 60 mins – 3cm balls – 350 rpm + CNT + Pd

Fig 4.24 TGA absorption/desorption patterns for the sample milled for 60 mins – 3cm balls – 350 rpm + CNT + Pd + Mg

Fig 4.25 Progressive increase in mass % hydrogen capacity in composite layers

Fig 4.26 Dynamics of hydrogen absorption by the as-delivered Ti/Fe sample. Numbers of curves correspond to the number of cycle including vacuum heating at T=450 ^oC for 1 hour followed by hydrogen absorption at T=25^oC and starting H_2 pressure ~30 bar.

4.27 XRD pattern of the mixture Ti/Fe + 30% TiH_2 before ball-milling

UNIVERSITY of the WESTERN CAPE

4.28 XRD pattern of the Ti/Fe + 30% TiH_2 sample, ball-milled for 1 hour

4.29 XRD pattern of the hydrogenated Ti/Fe + 30% TiH_2 sample, ball-milled for 1 hour.

4.30 Dynamics of hydrogen absorption by the sample Ti/Fe + 30% TiH_2 sample, ball-milled for 1 hour. Numbers of curves correspond to the number of cycle including vacuum heating at T=450^{o}C for 1 hour followed by hydrogen absorption at T=25^{o}C and starting H2 pressure ~30 bar.

UNIVERSITY of the
WESTERN CAPE

ABBREVIATIONS

TGA	Thermogravimetric Analysis
BET	Brunauer-Emmett-Teller
SEM	Scanning Electron Microscopy
TEM	Transmission Electron Microscopy
XRD	X-ray Diffractometry
Fe/Ti	Iron-Titanium
IMH	Inter-metallic hydride
IMC	Inter-metallic compound
MH	Metal hydride
LPG	Liquefied Petroleum Gas
CNT	Carbon nanotube
SWNT	Single walled nanotube
MWNT	Multi walled nanotube
SSA	Specific surface area
P-C-T	Pressure-Composition-Temperature
CVD	Chemical Vapor Deposition
HP-DSC	High Pressure Differential Scanning Calorimeter
HPPS	High Performance Particle Sizing
EDS	Energy Dispersive Spectroscopy
H/D	Hydrogenation/Dehydrogenation
DOE	Department of Energy

UNIVERSITY of the WESTERN CAPE

TABLE OF CONTENTS PAGE

Acknowledgements ii

Abstract iii

List of Tables iv

List of Figures v

Abbreviations viii

CHAPTER 1 Introduction 1

Problem identification and motivation of research 1

CHAPTER 2 Literature review 7

2.1 Overview of physico-chemical methods of hydrogen storage 7

2.2 Physical methods for hydrogen storage 9

- *Storage as compressed gas (in high-pressure cylinders)* 10
- *Encapsulation of hydrogen in glass microsphere* 10
- *Hydrogen storage as liquid hydrogen (LH_2)* 11
- *Hydrogen storage in carbon nanomaterials* 12

2.3 Chemical methods for hydrogen storage 13

- *Storage in ammonia and methanol* 13
- *Hydrogen in organic hydrides and fullerenes* 14
- *Hydrogen in water reacting metals* 15
- *Hydrogen storage in metal hydrides* 15
- *Hydrogen storage in complex hydrides (alanates)* 16
- *Hydrogen in zeolites and metal-organic adsorbents* 17

2.4 Main principles of hydrogen storage in metal hydrides (Solid-state hydrogen storage) 18

2.4.1 Thermodynamic aspects of hydrogen absorption/desorption in metal hydrides. 22

2.4.2 Intermetallic alloys – *analysis of the problems associated with compounds* 25

UNIVERSITY of the WESTERN CAPE

- *AB_5 compounds* 27
- *AB_2 compounds* 28
- *AB compounds* 28
- *A_2B compounds* 29

2.4.3 Application of Intermetallic hydrides according to thermodynamic properties. 31

2.5 Carbon nanotubes as novel material for hydrogen storage 37

2.5.1 Methods of synthesis of carbon nanotubes 39

2.5.2 Carbon nanotubes adsorption properties 44

2.6 Composite hydrogen storage material based on Intermetallic Hydrides 46

2.6.1 Approaches for increasing weight capacity of hydrogen adsorption in intermetallic compounds 49

2.6.2 Approaches for eliminating impurity effects in intermetallic hydrides 52

2.6.3 Approaches for increasing the activation kinetics of intermetallic hydrides 55

2.6.4 Approaches for elimination of problems relating to pyrophoricity and decrepitation 58

2.7 Summary. 59

CHAPTER 3 Materials and Methods 61

3.1 Research Materials and Methodology 61

3.1.1 Materials 61

3.1.2 Methods of synthesis 62

3.2 Structural characterization of composite materials 65

3.2.1 X-ray Diffractometry 65

3.2.2 Scanning electron microscopy 67

3.2.3 Transmission electron microscopy 68

3.2.4 Surface area and porosity determination by N_2 physisorption 69

UNIVERSITY of the WESTERN CAPE

3.3 Thermal and Gravimetric characterization of the core alloy and composite materials 70

3.4 Volumetric characterization of the core alloy and composite 71

3.5 Synopsis of main points 74

CHAPTER 4 Experimental and Discussion 75

4.1. Application of ball milling technique for mechano-chemical pre-treatment of Ti/Fe alloy 75

4.1.1 Influence of rotation speed and ball size on the agglomeration of Ti/Fe particles 77

4.1.2 Crystallinity change in Ti/Fe alloy after ball milling 85

4.2 Development of carbon nanotube deposition technique for the surface modification of Ti/Fe alloy 89

4.2.1 Implementation of LPG pyrolysis for growing carbon nanotubes on the surface of Ni and Co catalysts (model experiment) 91

4.2.2 Modification of the surface of Ti/Fe alloy with carbon nanotubes by LPG pyrolysis for composite material preparation 93

- Optimization of pyrolysis parameters for carbon nanotube deposition on Ti/Fe alloy 93
- Structure and morphology of Ti/Fe-CNT composite 94
- Influence of CNT deposition on surface area of Ti/Fe 97

4.3 Development of methods for surface modification of composite Ti/Fe-CNT material using binary metal hydride 100

4.3.1 Deposition of palladium layer to improve activation kinetics of composite 101

UNIVERSITY of the WESTERN CAPE

4.3.2 Deposition of magnesium layer to increase hydrogen weight capacity of composite 104

4.4 The Investigation of hydrogen storage properties of composite material based on Ti/Fe alloy obtained by layer-by-layer technique 107

4.4.1 Thermo-gravimetric study of hydrogen sorption properties of Ti/Fe based composite materials. 112

4.4.2 Volumetric study of Ti/Fe as a core material. 115

4.5 Overview of main points 122

CHAPTER 5 Conclusions and Recommendations 124

REFERENCES 128

UNIVERSITY of the
WESTERN CAPE

Chapter 1

1. Problem identification and motivation for research:

Hydrogen is a clean and zero emission fuel when its source is water. With the rising concern of environmentally harmful pollutants from current hydrocarbon-based fuels, hydrogen is an ideal fuel which can potentially eliminate the problems found with modern hydrocarbon fuels [1, 2, 3]. Compared to hydrocarbons, hydrogen has an energy density that is 3 times greater than the average hydrocarbon fuel [1-4]. Relative to hydrocarbon based fuels, only 4 kg of hydrogen is needed for a 400 km journey in a modern car, while 24 kg of a hydrocarbon-based fuel is needed [1, 2, 4].The majority of hydrogen is present in water, thus in terms of procurement and distribution of hydrogen as a fuel source, a country's reliance on foreign energy resources can be drastically reduced. Therefore hydrogen presents immense positive socio-economic incentives. However, one of the largest stumbling blocks towards the widespread use of hydrogen as an energy source is its effective storage [1-4].

UNIVERSITY of the
WESTERN CAPE

Problem identification

Modern technology can and does compress hydrogen in high strength stainless steel cylinders. Conventional high pressure cylinders are usually filled to a maximum operating pressure of 20 MPa, and at this pressure the amount of hydrogen by mass is 4.0%, which is below the target (6%) generally accepted as benchmark for widespread use in mobile applications [1-5]. To increase the mass of hydrogen stored to 6.0%, many industries have set a goal of producing a cylinder that can withstand pressures of 70 MPa, and have a mass of 110kg. However, safety issues of using a compressed gas cylinder in ground transportation is still a primary concern and the actual work needed to compress the hydrogen is usually a complicated and a high energy process [1-5].

Hydrogen has a critical temperature of -241 ºC, above this temperature hydrogen cannot exist as a liquid no matter what pressure is used. When storing hydrogen as a liquid, efficient cryogenic containers are needed, and some kind of open system is required to prevent excessive over-pressures.

Liquefying hydrogen is an energy intensive and complicated process. First, hydrogen is pre-cooled with liquid nitrogen; this is done to get the temperature of hydrogen to below its inversion

temperature of -71 ºC. Once at this temperature, hydrogen can cool upon expansion and produce some liquid [4]. Overall, the energy needed to liquefy hydrogen is on average 15.2 kWh/kg, whereas if hydrogen were to be burned in a simple combustion process the energy gained would be 33.3kWh/kg. The gain over current hydrocarbon fuels, combustion of which yields approximately 12.4kWh/kg, would be negated [2, 4].

Boil-off of liquid hydrogen is exacerbated by heat leaks from the storage vessel, and from the exothermic process of hydrogen converting from the ortho- to para- form of hydrogen. The high cost of liquefying hydrogen, the problems of storing liquid hydrogen at cryogenic temperatures, and the problems due to boil-off have limited the use of liquid hydrogen to applications where cost is not an issue, such as rockets, and has prevented its widespread use [2-4].

Solid-state storage, in which the hydrogen is absorbed in a solid material, holds considerable promise for meeting the hydrogen economy targets, but no completely satisfactory material has yet been identified. The operating requirements for effective solid-state hydrogen storage for commercial application include the following [6-7]:

- Appropriate thermodynamics.
- Fast kinetics (quick uptake and release).
- High storage capacity (specific capacity to be determined by usage).
- Effective heat transfer.
- High gravimetric and volumetric densities (light in weight and conservative in space).
- Long cycle lifetime for hydrogen sorption.
- High mechanical strength and durability.
- Safety under normal use and acceptable risk under abnormal conditions.

UNIVERSITY of the WESTERN CAPE

The fundamental questions that need to be asked for any potential solid-state hydrogen storage material include the following:

- Does hydrogen undergo a physisorption mechanism or is it chemisorbed?
- Does it bind molecularly or dissociatively?
- Where does the hydrogen reside?
- What is the nature of hydrogen diffusion?
- What are the activation barriers for hydrogen desorption?
- What adverse effect does hydrogen have on the structural and mechanical stability of the host material?

- What is the nature of the bonding of hydrogen with host atoms — ionic, covalent, or metallic?
- What roles do surface morphology and defects play in hydrogen sorption?
- In what ways is it beneficial to store hydrogen in novel materials, such as nanostructures and porous materials?
- How do catalysts help in reducing the operating temperature and pressure for hydrogen uptake and release?

The overall goal of this project is to develop the knowledge base for solid-state hydrogen storage technology suitable for stationary and mobile applications. In order to accomplish this goal, the project will have a bi-focal direction which includes the synthesis of a novel nano-structured hydrogen storage material and analysis of the structure and hydrogen capacity of this material. In more detail, this goal will be reached by achieving the following targets:

- Solid-state hydrogen storage technology “know how”
- High capacity hydrogen storage materials of highly divided nature including nanomaterials that are applicable for storing hydrogen at low temperature and release of hydrogen at a reasonable rate;
- Produce a hydrogen storage prototype container/cylinder.

UNIVERSITY of the
WESTERN CAPE

The following steps will be used to reach the stated targets:

- to understand hydrogen uptake and release from hydrogen storage materials;
- to investigate hydrogen uptake and release from hydrogen storage materials in both physico-chemical and kinetic aspects;
- to improve the kinetics of hydrogen uptake and release from hydrogen storage materials;
- to improve hydrogen storage capacity;

Rationale and motivation

Hydrogen storage is a “critical path” technology that will facilitate the commercialization of hydrogen energy. Research on gaseous and liquid methods to inexpensively store hydrogen in a safe, compact and lightweight package has been ongoing for more than a decade. The U.S.A Department of Energy (DOE) Hydrogen, Fuel Cells & Infrastructure Technologies programme has been instrumental in developing state-of-the-art compressed hydrogen tanks. However, the future focus will be on solid-state materials that will enable the storage of hydrogen at low

pressure. Such storage may be achieved by absorption on high surface area materials like carbon nanotubes; adsorption into metal hydrides; and hydrogen binding in chemical compounds such as sodium boro-hydrides. Despite tremendous advances in recent years, no approach currently meets the storage density and/or charge-discharge requirements [8-11].

Most countries import more than 80% of their petroleum, and this value is projected to rise by 2025. The transportation sector is the major consumer of petroleum imports. Use of hydrogen as a fuel offers the opportunity to shift the energy requirements for transportation from imported oil to diverse, domestically available resources. Hydrogen-powered fuel cell vehicles are a tremendously attractive alternative to gasoline and diesel powered automobiles as they emit only water with essentially no critical pollutants. The hydrogen fuel itself may be generated by several different means, including thermo-chemical processing of primary energy sources such as coal, oil, biomass, or generated by electrolysis using electricity which may be derived from renewable sources such as wind power, and/or photo-voltaics. Producing hydrogen at central locations will enable pollutants and greenhouse gases to be contained and more easily dispensed. The high efficiency of fuel cells will make hydrogen a cost effective, energy efficient, and environmentally friendly alternative to current fuels when considering the full lifecycle. Thus, the concept of a hydrogen-based energy and transportation system offers energy resource flexibility and the potential for energy independence, as well as the elimination of net carbon dioxide, sulphur dioxide, and nitrogen oxides emissions.

UNIVERSITY of the
WESTERN CAPE

Solid-state storage refers to the storage of hydrogen in metal hydrides, chemical storage materials, and in nanostructured materials. This method of hydrogen storage offers perhaps the best opportunities for meeting the requirements for onboard storage. In these materials, hydrogen can be stored both physically and chemically according to the DOE classification [12].

The metal hydride method of hydrogen storage which is our primary focus is based on the process of the reversible hydrogen adsorption into hydride forming metals or intermetallic compounds with the formation of hydrides (MH). In this process, hydrogen is placed inside the interstitials of the crystal structure of the matrix of the metal, as individual H atoms, and not associated as molecules. The reaction is reversible, which means a small change of temperature or pressure will change the process from charging with hydrogen to the opposite (hydrogen discharge) and vice versa. The advantage of the system is that hydrogen is being stored as a metal at low pressure and being stored with less volume than compressed gaseous or liquid hydrogen. The hydrogen is absorbed at a lower temperature and when the hydrogen gas is needed the gas is recaptured by lowering the pressure below, or raising the temperature of the metal hydride above

the absorption process. The hydrating alloy is stored in stainless steel tubes and according to the Van't Hoff equation, hydrogen reacts with the metal alloy granules in the tank at a specific temperature and pressure. The steel tubes are surrounded by a water jacket that facilitates heat exchange during absorption and desorption of hydrogen gas [1, 13].

When a material is modified from its bulk phase to a nanostructured phase, the chemical and physical properties are altered significantly. The processes used to alter a material to a nanostructured phase is one of the most promising approaches for controlling bond strength, kinetics, and adsorption/desorption temperatures and pressures. A large number of the intermetallic hydride materials form a nanostructured phase in terms of the grain structures and/or the particle sizes on charging and discharging with hydrogen. While this capability can be desirable in maximizing the hydrogen diffusion path and enhancing the rate of charging and discharging, it may also have disadvantages in increasing the susceptibility to corrosion and reducing stability, which will be a key factor in determining the practical suitability of the materials synthesized [14].

One of the simplest mechano-chemical methods to achieve nanostructured materials is by ball milling. Through ball milling, various intermetallic alloys (LaMmNi4, Fe/Ti), light metal hydrides (NaAlH4), and binary metal hydrides (Mg, Pd) will have a reduced particle size, and an altered nanostructured grain. However, ball milling can introduce contaminants into the material being ball milled. The level of contamination may or may not affect the hydrogen storage properties of the chosen material.

UNIVERSITY of the
WESTERN CAPE

Combining different intermetallic hydrogen storage materials with suitable "dopants", will introduce new catalytic and thermodynamic properties into the hydrogen storage materials, and thus new classes of hybrid hydrogen storage materials can be developed. For example, a core material could be selected because of its thermodynamic properties, and the mantle could be chosen for its catalytic activity. The combination of functional materials in a layered fashion could open up completely new routes for optimizing the overall performance of such a sorption material. One potential material that can be used to create the novel encapsulated nanostructured materials is carbon nanotubes.

Carbon nanotubes are, to date, one of the most promising materials for current and future applications in nanotechnology. Carbon nanotubes possess high mechanical strength, good electrical and thermal conductivity, and the relatively stable chemical properties. The applications that have been demonstrated are numerous, and include additives in polymers to produce composite materials with higher mechanical strength and/or greater electrical conductivity, probes in atomic force microscopy, supports for various catalysts, drug delivery

agents, components in various logic circuits, as field emission devices, and as hydrogen storage materials. It is because of the innate potential of carbon nanotubes to be used in a surprisingly wide range of applications, and the potential to use the carbon nanotubes as scaffolds to build and stabilize metal nano-particles, that make carbon nanotubes make an attractive candidate for developing nanostructured composite materials [15, 16].

Researchers believe that metal hydrides may represent ideal storage systems. Although a database (http://hydpark.ca.sandia.gov) lists more than 2,000 elements, compounds, and alloys that form hydrides, none of these materials has yet been demonstrated to meet all the required targets to be used in a fuel cell system.

In addition to limits in hydrogen availability, other issues need to be considered as new hydrogen storage materials are developed and characterized, such as the ease of activation, sensitivity to gas impurities, rate of hydrogen absorption/desorption, heat transfer, cyclic stability, and physical properties (e.g., volume change and decrepitation). From an engineering perspective, the design and optimization of practical storage beds may well require at least a factor of 2-4 percent increase in the hydrogen mass and volume that would be necessary for use in thermal management.

Needed breakthroughs in hydrogen storage technology will require revolutionary new materials to meet the hydrogen storage requirements, and not simple, incremental improvements in current technologies. These breakthroughs require fundamental research to develop and examine new materials and obtain an atomic- and molecular-level understanding of the physical and chemical processes involved in hydrogen storage and release. The knowledge gained from this research will allow the tailored design and synthesis of new materials that will meet the requirements for efficient hydrogen storage.

UNIVERSITY of the WESTERN CAPE

Chapter 2

2.1. Overview of physico- chemical methods of hydrogen storage:

Hydrogen is the lightest known substance, and so presents a huge problem in terms of storage in containers. The main disadvantage of hydrogen is the extremely low volumetric density, because at usual conditions it exists in the gaseous form, having a very low boiling point (-252.8^{o}C). 1 kg of hydrogen gas at room temperature and atmospheric pressure has a volume of 11m^3, so to provide 100km run for mobile applications, it is necessary to have on board at least 33m^3 of gaseous hydrogen [1, 17]. This necessitates the need for an effective method of compact hydrogen storage. A viable hydrogen storage method (especially for mobile application), should store up to 6.6% wt H (according to United States Department Of Energy requirement), have a reversible hydrogen storage capacity of more than 75% of the total material, operate at temperatures not higher than 100^{o}C, have a self discharge time (dormancy) of less than a month, possess good mechanical strength and show good kinetics in terms of charge/discharge. It is also desirable that the system could operate at moderate pressures, would have low heat losses, and be serviceable if charged with hydrogen contaminated with impurities of oxygen, water vapor, traces of methane, carbon dioxide and carbon monoxide. On the strength of literature on hydrogen storage materials, it is concluded that the best competitive position in the future will have combined methods realizing a fusion of chemical and physical methods of hydrogen storage and processing. The combination would produce small, medium and large scale hydrogen storage units. Conditionally, all the materials which are able to store bounded hydrogen can be divided starting from the bond energy of the hydrogen atom or molecule either with the matrix (host material) or with the other atoms in a molecule. It is physically adsorbed (*absorption*) hydrogen having the weakest bond and chemically adsorbed (*chemisorption*) involving bounded hydrogen in ionic or atomic form. It is quite logical to assume that the materials binding hydrogen physically would contain minimal quantity of the gas and possess the ability to return it under normal conditions, whereas the chemically reacting materials would probably store more hydrogen but form stable compounds and consequently prove more difficult to return the gaseous H_2.

The storage of hydrogen can be narrowed down to two general types namely; physical methods and chemical methods. The United States D.O.E has proposed the following methods as having the best commercial viability;

Physical methods:

- *Storage as compressed gas (in high-pressure cylinders)*
- *Encapsulation of hydrogen in glass microsphere*
- *Hydrogen storage as liquid hydrogen (LH_2)*
- *Hydrogen storage in carbon nanomaterials*

Chemical methods:

- *Storage in ammonia and methanol*
- *Hydrogen in organic hydrides and fullerenes*
- *Hydrogen in water reacting metals*
- *Hydrogen storage in metal hydrides*
- *Hydrogen storage in complex hydrides (alanates)*
- *Hydrogen in zeolites and metal-organic adsorbents*

The processes are described in more detail below for better understanding of the mechanisms.

UNIVERSITY of the WESTERN CAPE

2.2. Physical methods of hydrogen storage:

These are physical methods which use physical processes to compact hydrogen gas. These methods are practically based on physisorption. Resonant fluctuations in charge distributions, which are called dispersive or Van der Waals interactions, are the origin of the physisorption of gas molecules onto the surface of a solid. In this process, a gas molecule interacts with several atoms at the surface of a solid. The interaction is composed of two terms: an attractive term, which diminishes with the distance between the molecule and the surface to the power of -6, and a repulsive term, which diminishes with distance to the power of -12 [3]. The potential energy of the molecule, therefore, shows a minimum at a distance of approximately one molecular radius of the adsorbate. Because of the weak interaction, significant physisorption is only observed at low temperatures <273 K [18]. The storage of hydrogen can rely on physisorption because the adsorbed gas can be released reversibly. There are different mechanisms of absorption depending on the geometry of the absorbent and the temperature of absorption. Multilayer mechanism functions if the absorption happens on an open surface and volume filling would happen in a pore narrower than 2 nm. Capillary condensation could happen in a pore larger than 2 but smaller than 50 nm. Absorption in a pore larger than 50 nm is the same as that on open surfaces. However, all the mechanisms here mentioned assume the possibility of condensation of the absorbed absorbates. Such possibility does not exist at above-critical temperatures; therefore, a different mechanism of absorption must assume. There is only one mechanism for the absorption of supercritical gases on any kind of absorbents, which is the monolayer surface coverage. When the surface is completely covered with a layer of absorbate, more gas molecules would be absorbed above the first layer due to the interaction between the same species of absorbate molecules forming the second layer, and so on for the subsequent layers. The interaction force received by the first layer molecules is, thus, different from that received by the second and subsequent layers. The binding energy of the second and subsequent layers of absorbate molecules is, therefore, similar to the latent heat of sublimation or vaporization of the absorbate. Obviously, the subsequent layers from the second cannot exist at above-critical temperatures, otherwise a classical law of physics, i.e. gas cannot be liquefied at above critical temperatures no matter how high pressure applied, would be false.

In summary, the physisorption of supercritical gases follows two basic rules: the monolayer absorption mechanism, and the exponential decrease of absorption with the increasing temperature. It follows that the absorption capacity of hydrogen on a material depends on the specific surface area of the material and that higher temperatures will lower the absorption

UNIVERSITY of the WESTERN CAPE

capacity. The total storage capacity in a porous solid is, however, not only the absorption capacity, but also the sum of contributions due to absorption on solid surface and that due to compression in the void space [2].

Presented here are the various known methods of physical hydrogen storage;

- *Storage as compressed gas (in high-pressure cylinders)*: Hydrogen storage in high-pressure cylinders is the most convenient and industrially approved method. Usually, steel gas cylinders of low (up to 12 liters) or medium (20 to 50liters) capacity are in use for the storage and transportation of the moderate quantities of compressed hydrogen at the environment temperature of from -50 to 60^{o}C. The industrial cylinders of larger capacity, up to several cubic meters are produced as well. Gas pressure in the commercial cylinders is 150 bar for the countries of the former USSR and 200 bar for West Europe and USA. Even for cylinders of large volume, the weight hydrogen storage capacity does not exceed 2-3% [19]. The cylinders provide hydrogen storage under the pressure up to 350 bar. The further improvement of the material and layout of the high-pressure cylinders (mainly due to the replacement of fibre glass by carbon fibres) allowed creating the advanced composite gas cylinders rated to pressure up to 690 bar. The weight and volume efficiency of the advanced cylinders is 80% higher than for the commercial ones, but are far more expensive.

  The advantage of hydrogen storage in cylinders is the simplicity in the realization and absence of power consumption to supply hydrogen. However, because of potential explosion risk for the high- pressure hydrogen, safety is the main problem of hydrogen storage in gas cylinders especially for vehicular application. Besides, hydrogen compression itself is a complicated enough engineering problem. These sky-rockets the final cost of the cylinder storage method by compression of the gas.

UNIVERSITY of the WESTERN CAPE

- *Encapsulation of hydrogen in glass microsphere*:

  This process involves the use of hollow glass spheres, 5-500 microns in diameter and ~1 micron in wall thickness, developed by spraying gels. The glass is permeable for hydrogen at moderate temperatures, which ensures that hydrogen can fill the micro-spheres.

Storage of high-pressure hydrogen in glass microspheres has long been proposed as a solution to the problems inherent in hydrogen storage and transport. The high tensile strength of glass microspheres allows containment of hydrogen at pressures up to 100 MPa. As envisioned in past system designs, the microspheres are filled by heating in high-pressure hydrogen to temperatures sufficient for rapid diffusion of hydrogen into the microspheres. Upon cooling, the low diffusivity of hydrogen at ambient temperatures causes the gas to be retained in the microspheres. Hydrogen is then released when needed by reheating the microspheres. Due to the inherently poor thermal conductivity of inorganic glasses, a problem further exacerbated by the morphology and size of hollow microspheres, poor hydrogen release rates have limited further development and implementation of this hydrogen storage method [20].

- *Hydrogen storage as liquid hydrogen (LH_2)*:

  This method involves use of cryogenic vessels having screen-vacuum heat isolation to store liquefied hydrogen. This method shows a higher storage capacity and better safety considerations than the gas storage in cylinders due to the much lower operational pressure required. It is especially useful in aerospace applications. However its viability for commercial use is limited due to very high power inputs required for sustaining the process. Hydrogen stored in a liquid form is substantially more compressed than in gaseous form and superficially it appears an appealing means of energy storage but there are various contributory negative factors. Primarily, that the liquefaction requires a large expenditure of energy and secondly, through the use of insulation, liquid hydrogen must be continually kept at a low temperature (<20K). There are risks associated with this constant low temperature, due to the high expansion ratio of liquid hydrogen to gaseous hydrogen. If there was a warming of liquid hydrogen extremely high pressures could accumulate and result in damage or an explosion. The boil off rate of hydrogen from a liquid storage vessel because of heat leaks is a function of its size, shape, and thermal insulation. Since boil-off losses as a result of heat leaks are proportional to the surface-to-volume ratio, the evaporation rate diminishes as the storage tank size increases. For double-walled, vacuum-insulated spherical dewars, boil-off losses are typically 0.4% per day for those with a storage volume of 50 m^3, 0.2% for 100 m^3 tanks, and 0.06% for 20 000 m^3 tanks [3].

UNIVERSITY of the WESTERN CAPE

The large amount of energy necessary for liquefaction and the continuous boil-off of hydrogen limit the possible use of liquid hydrogen storage systems to applications where the cost of hydrogen is not an issue and the gas is consumed in a short time, e.g. air and space applications.

- *Hydrogen storage in carbon nano-materials*:

Carbon inhabits a multitude of different nano-scale morphologies, including recently discovered fullerenes and nanotubes, as well as graphite nanofibres. All these materials are of significant interest concerning their applications for hydrogen storage. With the exception of fullerenes that exhibit a chemical interaction with hydrogen, similar to the formation/ decomposition of organic hydrides, the other carbon nanomaterials interact with hydrogen gas either via "Van der Waals" attractive forces (physisorption) or via a dissociative chemisorption of H_2 molecules [21-23].

The available literature data concerning hydrogen sorption capacity of carbon nanomaterials are conflicting up to this point. At ambient temperatures and pressures the H_2 sorption capacity of similarly prepared single walled nanotubes ranges from 8% to ≤ 1 wt% H. There are also available, the data concerning extremely high (up to 60 wt % H) hydrogen sorption capacity of some kind of carbon nanofibres [24, 25]. However these reports are yet to be ratified. The main conclusion from these studies is that H_2 storage does not take place in carbon nanotubes and nanofibres at considerable room temperatures.

Apart from differences in the structure of the materials used by different authors, sample weights, degree of purity, and pressure-temperature (P-T) conditions, an additional source of disagreements in the reported storage capacities of carbon nanomaterials could lie in inappropriate techniques of the volumetric measurements. The major source of errors is incorrect volume calibrations, probably caused by not properly determining the density of the sample. For high pressure experiments, a proper thermal management of the measurement system (avoiding temperature fluctuations and taking into consideration the exothermal effects from the introduction of pressurized gas into the reactor, and the temperature increase as a result of the absorption processes) should be achieved as well.

No doubt that the research of the hydrogen sorption properties of different carbon nanomaterials having well defined structures is very interesting from the fundamental point of view, and growing research activities in this field will result in better

UNIVERSITY of the WESTERN CAPE

understanding of gas - solid interaction mechanism. However, the initial optimism concerning creation of very efficient hydrogen storage material on the basis of nanoscale carbon seems to be taking quite a while to materialize.

2.3. Chemical methods for hydrogen storage:

This storage method is characterized by strong interaction between H atoms or molecular H_2 and the storage material. The process of this adsorption of molecules or atoms on surfaces is one of the key steps in molecule-surface reactions. The adsorption of a molecule or atom can take place through several mechanisms. The molecule might break apart into two fragments which both form chemical bonds to the surface. This is called dissociative chemisorption. The molecule may also break into two with one fragment remaining on the surface and one escaping to the gas phase. This is called abstraction [26]. First of all, it is very important to understand how crystal structural evolution takes place in the course of hydrogenation. In some cases, there is no change in the crystal structure of the hydride formed with that of the starting material since only the lattice expansion and the lattice distortion are introduced into them during hydrogenation. In other words, hydrogen atoms occupy a part of the interstitial sites in the crystal lattice and any substantial changes of crystal structure do not occur in the course of hydrogenation except for the onset of lattice expansion and distortion in it. Therefore, it is supposed that the ease of the lattice expansion and distortion during hydrogenation will be important in considering the hydride stability and this will be controlled by the nature of the chemical bonds between atoms in the starting materials. On the other hand, some hydrides witness a completely different crystal structure from the starting material in the course of hydrogenation, especially at elevated temperatures. In this case, the importance of the metal–hydrogen interaction increases as well as the metal– metal interaction if the reacting medium is a metal. It is noticed that the M–H chemical bond plays a more important role in the hydride stability of such media. A classic example of such a scenario is the formation of Mg_2NiH_4 [27]. Presented below are some of the well known chemical adsorption methods of hydrogen storage.

UNIVERSITY of the WESTERN CAPE

- ***Chemical interaction with hydrogen***

  Storage in ammonia and methanol: The advantage of hydrogen storage and transportation in the form of ammonia or methanol is in high hydrogen volume density (109 g/1 for liquid NH_3 at T=15 °C, P = 7.2 bar; and 99 g/1 for CH_3OH at room temperature). This is higher, in both cases, than for LH_2. Hydrogen is obtained by the following catalytical reactions:

$2NH_3 \rightarrow N_2 + 3H_2$ -92 kJ

$CH_3OH + H_2O \rightarrow CO_2 + 3\ H_2$ -49 kJ

The dissociation of ammonia is carried out at temperatures 800-900 °C using iron as a catalyst. The process of hydrogen generation from methanol requires temperature 300-400 °C in presence of the zinc - chromium catalyst. Both for ammonia and for methanol, the storage medium is used only once. This irreversibility, as well as too high power inputs for hydrogen generation, restricts a wider implementation of the above-mentioned hydrogen storage methods. Besides, the corrosion activity of ammonia is also a serious factor restricting its usage in hydrogen storage. At the same time, if the temperature of methanol decomposition reaction can be reduced, its usage as hydrogen storage medium can be competitive in a number of applications, including motor transport.

UNIVERSITY of the
WESTERN CAPE

- *Hydrogen in organic hydrides and fullerenes*: An example of organic chemical system allowing storing hydrogen reversibly is a system "benzene-cyclohexane"

$C_6H_6 + 3\ H_2 \leftrightarrow C_6H_{12} + 206.2$ kJ/ mole

The hydrogenation / dehydrogenation processes take place at 200-400 °C and 10-100 bar H2 in the presence of a catalyst (Pt, Pd, Mo_2O_3). Hydrogen storage in organic hydrides is very efficient concerning weight and volume storage capacities (5-7 wt. % or 70-100 g/1 H volume density). However, the energy consumption for the heating of the storage system providing the necessary reaction temperature is too large. It is higher than the one for cryogenic hydrogen storage. So this method can be used only in some specific cases (e.g. in chemical industry) when a waste heat source having sufficient temperature potential is available.

A similar option of hydrogen storage is a reversible catalytic hydrogenation of the double C=C bonds in fullerenes. In such a process, the C_{60} fullerene can be hydrogenated up to the composition $C_{60}H_{48}$ that corresponds to 6.3 wt. % H. The hydrides of intermetallic compounds are proved to be the efficient catalyzers of the reversible hydrogenation / dehydrogenation processes. However, the dehydrogenation temperature (more than 400°C) is still too high for the practical purposes.

- *Hydrogen in water reacting metals*: The process of hydrogen generation by a high-temperature reaction of water vapors with sponge iron is known for a long time. The following reaction, taking place at T=550-600 °C, is a basis of this hydrogen storage method:

  $3\ Fe + 4\ H_2O \rightarrow Fe_3O_4 + 4\ H_2$

  It is possible to make this process reversible, because the starting iron can be recovered by reducing Fe_3O_4, for example using carbon monoxide. By arranging the thermodynamic cycle of water decomposition using sponge iron, including an appropriate selection of the catalyst, the temperature of hydrogen generation and further recovery of iron can be reduced to some extent. However, an economic and environmental analysis of this technology has resulted in a conclusion that it is not efficient enough on a competitive scale.

UNIVERSITY of the WESTERN CAPE

- ***Bulk absorption in solids***

  Hydrogen storage in metal hydrides: Metal hydride method of hydrogen storage is based on the process of the reversible hydrogen adsorption in hydride forming metals or intermetallic compounds with the formation of hydrides (MH). The process is a gas-solid reaction represented by the equation:

  $M\ (s) + x/2\ H_2\ (g) \leftrightarrow MHx\ (s) + heat$

  As seen from the equation, it is an exothermic reaction with the release of heat accompanying the metal-hydride formation. The hydrogen is adsorbed at a lower temperature and when the hydrogen gas is needed the gas is recaptured by lowering the pressure below, or raising the temperature of the metal hydride above the adsorption process. The need for a compressor is eliminated in the hydride system as the hydriding and dehydriding reactions occur at specified temperature and pressure depending on the electrolyzer specifications. Binary hydrides with the general formula MH_x, and intermetallic hydrides with the general formula $A_xB_xH_x$ are formed by this reaction. Details of this reaction mechanism are presented in a subsequent section *(2.4)*. This

hydrogen storage method has shown great potential for commercial application in recent years and is the subject of wide spread research.

- *Hydrogen storage in complex hydrides (alanates)*: Recently, some of the complex hydrides (alanates) became a subject of intensive research concerning their applications as hydrogen storage materials. Indeed, these compounds have relatively high weight hydrogen fraction. For many years these compounds have been seen as "non-reversible" chemical hydrides and have not yet been considered fully as reversible MH storage systems. However in 1997 it was discovered that in the presence of $TiCl_3$ as a catalyst the following two-stage reaction is possible:

$NaAlH_4 \leftrightarrow 1/3\ Na_3AlH_6 + 2/3\ Al + H_2 \leftrightarrow NaH + Al + 3/2\ H_2$

The net reaction gives a theoretical reversible hydrogen storage capacity of 5.6 wt.% with the potential of hydrogen release about 100^{o}C. Now the alanate systems are the subject of intensive research worldwide. Nevertheless, in our opinion, this direction has no commercial potential, in particular because of clumsy kinetics of the reversible hydrogen absorption- desorption thereby prolonging cycling unnecessarily. Also the issue of degradation of the hydrogen sorption properties during prolonged cycling is a worry. These problems perhaps could be solved, but not the other principal flaw of the alanates. This problem is the extremely high chemical activity of the alanates with respect to the traces of oxygen and water vapors, which has the tendency to cause explosion. In this case if safety is a major consideration as we highlighted earlier then alanates may not be advisable for practical application especially vehicular, when compared to metal hydrides.

UNIVERSITY of the WESTERN CAPE

- ***Adsorption***

Hydrogen in zeolites and metal-organic adsorbents: Hydrogen adsorption by some zeolites can be applied to achieve reversible hydrogen storage in the temperature range 20-200 °C and pressures 25-100 bar. However, the maximum storage capacity (less than 10 cm^3g) is still too low to exhibit a competition with other storage systems. Nevertheless, it is possible to improve hydrogen storage performances of zeolites by

realization of the low-temperature adsorption, as well as by applying modern techniques of their synthesis and modification. The latter approach can also have some perspectives concerning the creation of new synthetic hydrogen adsorbents with similar microporous structure. Metal organic frameworks (MOF) are example of such compounds. One representative of MOF is the compound $Zn_4O[O_2C\text{-}C_6H_4\text{-}CO_2]_3$, whose structure is the high-porosity cubic frame having specific surface area of 2500-3000 m^2/g. This compound adsorbs up to 4.5 wt.% H at 70 K and 20 bar, or up to 1 wt.% H at the room temperature and the same pressure. The question about possibility to increase hydrogen sorption capacity of this class of compounds, as well as about their synthesis in large quantities and for acceptable prices remains unclear yet [19].

UNIVERSITY of the
WESTERN CAPE

2.4. Main principles of hydrogen storage in metal hydrides (solid-state hydrogen storage):

Metals can absorb hydrogen in atomic form and thereby act as hydrogen "sponges". Around 50 metallic elements of the periodic table can absorb hydrogen in great quantity and the possible choices of hydrogen storage materials are therefore enormous. The volume of this storage device is potentially less than a factor of two greater than the equivalent gasoline tank [28-29]. Metal hydride method of hydrogen storage is based on the process of the reversible hydrogen adsorption in hydride forming metals or intermetallic compounds with the formation of hydrides (MH). In this process, hydrogen is placed in interstitials of crystal structure of the matrix of the metal, as individual, not associated in molecules, H atoms. This process can be described as gas-solid reaction represented by the equation:

$$M\,(s) + x/2\ H_2\,(g) \leftrightarrow MHx\,(s) + heat$$

where M denotes hydride forming metal or intermetallic compound; s, g denote the solid and gas phase respectively .The reaction is reversible, which means a small change of temperature or pressure will change the process from charging with hydrogen to the opposite(hydrogen discharge) and vice versa. The advantage of the system is that hydrogen being stored as a metal at low pressure and that it stores more volume than compressed gaseous or liquid hydrogen [30, 19].
Hydrogen storage in metal hydrides is characterized by strong interaction between H atoms and the material. On some metallic surfaces, particularly if *d* electrons are present, it dissociates without activation barrier into chemisorbed atomic H. The solution of H in the bulk of the solid or the formation of a new compound with H might energetically be favorable. This gas-phase reaction of a solid with molecular H is absolutely analogous to the reaction with other gases like nitrogen or oxygen. If the starting solid is a metal we may end up with hydrides, nitrides or oxides as new compounds. Below the critical temperature one finds three domains: solid solution phase, new compound and domain of coexistence of both phases.
The processes of solution and compound formation are reversible in principle; however, quite extreme conditions (high *T*, low *p*) are required for the reversed reactions in some cases. The interest in hydrides grew so much because metallic alloys were found which reversibly form hydrides close to room temperature and atmospheric pressure and thus offer ways to absorb, store and desorb hydrogen gas as a synthetic fuel in a very safe and compact way. The following phenomena are involved in the bulk adsorption:

UNIVERSITY of the WESTERN CAPE

- The H atoms occupy interstitial sites and deform the host lattice. Most host-metal lattices expand upon H solution and hydride formation. The shape of ductile elemental metal samples deforms, but they remain compact. Brittle intermetallic compounds, however, fracture and disintegrate (irreversibly) into powder when they go through the coexistence region of the little-expanded solution phase and the expanded hydride phase.
- The proton of the H atom acts as an attractive potential for the host electrons. Hybridization effects including the H electron fundamentally modify the distribution of electron states in space and energy; a new electronic structure appears. Consequently physical properties are modified e.g. electric, magnetic and optical properties as well as mechanical properties. Phase transitions e.g. from normal conducting to superconducting behavior, from metals to semiconductors or insulators or from ferromagnetic to paramagnetic occur (reversible). Band-structure calculations and photoelectron spectroscopy are appropriate analytical tools, also recently, in situ X-ray absorption spectroscopy allowing for higher H pressure or in situ electrochemical charging. Principally the host metal lattice might contribute to bring H or the H-metal alloy into the superconducting state. Other evident transformations observed include;
- Order–disorder transitions of the H atoms on their sub-lattice are observed as a function of temperature and H content
- Disorder effects on the host lattice, potentially leading to amorphization or vacancy formation, even to superabundant formation of vacancies in stoichiometric ratios
- Formation of strong, possibly selective chemical bonds with components of the host, e.g. to saturate dangling bonds or to precipitate a hydride of an elemental metal out of an intermetallic compound leaving other non-hydrogenated phases. Many hydrides of intermetallic compounds are thermodynamically unstable as ternary compounds, but tend to disintegrate into a hydride of a constituting element and another intermetallic compound or component
- The reversible deformation of a ductile host metal is linked to the H concentration. Inhomogeneous and time dependent H distribution leads to inhomogeneous and time-dependent deformation, known as the Gorsky effect [31]. The reversible deformation of the H-containing metal by external forces causes H redistribution.
- The presence of hydrogen in the host lattice and its local motion enhance the local mobility of the host atoms. Some of the phenomena are particularly strong at the surface in the near surface-region or at interfaces.
- Adsorbed H atoms are known to cause geometrical rearrangements of the host surface atoms leading to reconstructed surfaces and often well-defined two-dimensional surface phases
- Adsorbed H atoms lead to new surface electronic and magnetic properties

UNIVERSITY of the WESTERN CAPE

- Adsorbed gases induce selective reactions with host compound constituents and subsequent near-surface phase separation and segregation [31].

Hydrogen reacts with many individual metals to form binary hydrides, MHx. The formation of the binary hydrides is accompanied by essential changes in the mutual location of the M atoms taking place. The latter either remains invariant, or in major cases rearranges itself [30, 3]. A strong M-H bond must be formed for the efficiency of this system.

Apart from the binary hydrides, there is also another class of hydrides called intermetallic hydrides denoted by a formula $A_xB_xH_x$ .This group are the compounds of two or more metals, wherein A has a strong affinity for hydrogen i.e. forms a stable binary hydride. Component B does not interact with hydrogen at usual conditions [19, 26]. They are generally characterized by excellent kinetics of reversible hydrogen sorption – desorption taking place at moderate temperatures. Metal hydrides have the potential for reversible on-board hydrogen storage and release at low temperatures and pressures.

One of the major issues with metal hydride materials, due to the reaction enthalpies involved, is thermal management during refueling. Depending on the amount of hydrogen stored and refueling times required, megawatts to half a gigawatt could be handled during recharging on-board vehicular systems with metal hydrides. Reversibility of these new materials is also an issue. The hydrogen volumetric density which sometimes goes up to 0.56g/cm^3 for intermetallic hydrides has been found to be up to 8 times higher than that of binary hydrides [19]. Another factor that validates the feasibility of MH hydrogen storage system is the multi functionality of the system (possibility of hydrogen purification due to high selectivity of hydrogen adsorption/ desorption processes, easy pressure control at the output of the MH storage unit, the increased chemical activity of supplied hydrogen, etc) these factors make the systems the most preferable for example in laboratory applications, and hopefully soon, a wide range of other applications. Important also to note that the amount of hydrogen that a material can release, rather than only the amount the material can hold, is the key parameter used to determine system (net) gravimetric and volumetric capacities.

Widely researched binary and intermetallic hydrides are presented in the figure below with regard to their reversibility, weight and volume capacities. A comparison is also drawn with compressed hydrogen and liquid hydrogen:

UNIVERSITY of the WESTERN CAPE

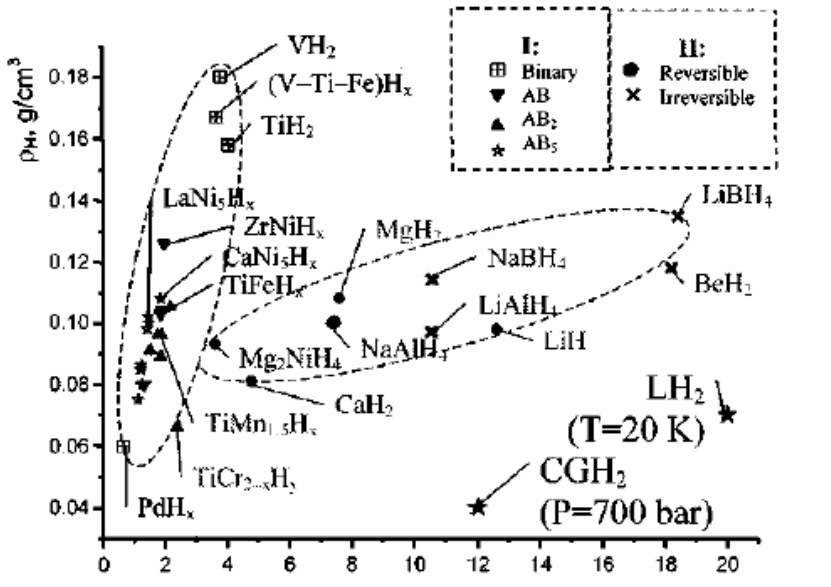

Fig 2.1: Relation between weight and volume hydrogen capacities for binary and intermetallic hydrides on the basis of transition metals (I), and binary and complex hydrides of the light elements (II). [19]

UNIVERSITY of the
WESTERN CAPE

2.4.1. Thermodynamic aspects of hydrogen adsorption/desorption process in metal hydrides:

This section presents a general description of the thermodynamic requirements for metal hydride systems. It is imperative to briefly address this area since different thermodynamic implications apply to different applications. This section is meant to offer us the answers to questions regarding selection of metal hydrides based on their pressure-composition-temperature (PCT) properties, for specific applications. The kinetics of hydrogen adsorption/desorption is of paramount interest to us since we desire metal hydride systems with near ambient operating conditions.

Most experimental measurements are routinely investigated by volumetric analysis, the Sievert's type apparatus and to a less extent by calorimetry or thermogravimetry. Nevertheless, there are difficulties of producing reliable thermodynamic data [32, 7]. Whatever the application, the most important properties are related to the 'plateau' pressure, which represents the coexistence of two condensed phases when hydrogen is loaded over the solubility limit. Assuming reversible and equilibrium conditions, the Gibbs phase rule gives a variance of one for two components, H and IMC and three phases, one gas phase and two solid phases. In the first one, hydrogen forms a solid solution in the matrix of the metal M (a-phase); in so doing its equilibrium concentration, C = H/M, is determined by the pressure, *P,* of hydrogen gas and the temperature, *T.* The relation can be approximately described by the Henry – Sievert's law [6]:

UNIVERSITY of the
WESTERN CAPE

$c = K(T)P^{1/2}$

After reaching a higher limit which corresponds to the hydrogen concentration in the saturated solid solution, $C = a$, the further hydrogen sorption (second stage) is accompanied by hydride (β-phase) formation with hydrogen concentration $C = b$ $(b > a)$, so as the material balance of the reaction (1) can be written as:

l/(b-a) **MHa** (s) + 1/2 H_2 (g) ↔ l/(b-a) **MHb** (s).

According to the Gibbs phase rule, the process above is reversible at the constant hydrogen pressure, *PD,* which corresponds to the appearance of the plateau on the pressure - composition isotherm, e.g. the dependence of the equilibrium hydrogen pressure (P) on hydrogen concentration (C) at constant temperature (T). After complete transition of the solid solution to

the hydride, further hydrogen sorption (third stage) is hydrogen dissolution in the hydride β-phase. In so doing, hydrogen equilibrium concentration increases with the pressure, asymptotically approaching to its upper limit, *Cmax* which is determined by hydrogen capacity of the metal, or the number of the available hydrogen insertion interstitials per the number of the metal atoms.

Starting from the equilibrium condition in the plateau region, that is the equality of hydrogen chemical potentials in the gas phase and two solid ones (solution **MHa** and hydride **MHb**), the known Van't Hoff relation determining the temperature dependence of plateau pressure can be derived:

$$In\ P_D = \frac{\Delta S^0}{R} + \frac{\Delta H^0}{RT},$$

where ΔH and ΔS are correspondingly standard enthalpy and entropy of the hydride formation reduced to 1 mole of hydrogen gas. The dependence of plateau pressure on the temperature in $In\ P_D$ - l/T coordinates is a straight line whose slope is proportional to $\Delta H°$ and ordinate of crossing with pressure axis at ($1/T$=0) - to the ΔS value.

The concentration limits *(a, b)* of the existence of the two-phase (α+β) plateau region (miscibility gap) are temperature-dependent. They become closer when the temperature increases, and coincide when it becomes equal to a critical value, *Tc,* - this corresponds to plateau degeneration into inflection point. Above the critical temperature, hydrogen in metal exists only as α-solution. The above-mentioned dependence between equilibrium pressure / concentration values and the temperature (PCT diagram) is the most practically important characteristic for hydride forming metals and intermetallides. As a rule, the reference literature presents its simplified parameters that are hydrogen capacity of the hydride and the enthalpy and the entropy of its formation determining temperature dependence of plateau pressure. The enthalpy, ΔH, is considered to be approximately equal to the heat effect, *Q,* of reaction *(1)* [19].

UNIVERSITY of the WESTERN CAPE

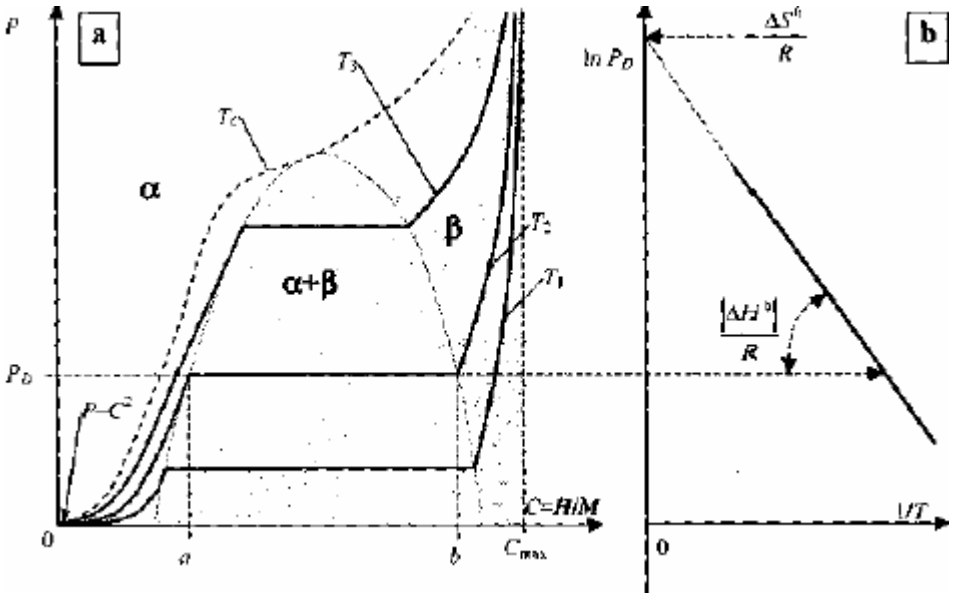

Fig 2.2: A schematic representation of the idealized PCT diagram of hydrogen — metal system: a -pressure - composition isotherms at the temperatures T1<T2<T3<Tc; b - temperature dependence of plateau pressure. [19]

UNIVERSITY of the
WESTERN CAPE

2.4.2. Intermetallic alloys- *analysis of the problems associated with modern compounds*

From the family of hydriding alloys and complexes presented below, intermetallic compounds appear to be of utmost interest in recent reports of international research. In order to capitalize on practical applications of reversible hydrides, we will be required to combine strong hydride forming elements A with weak hydriding elements B to form intermetallic compounds that have the desired intermediate thermodynamic affinities for hydrogen. This extraordinary ability to 'interpolate' between the extremes of elemental hydriding behavior has led to the modern world of reversible hydrides.

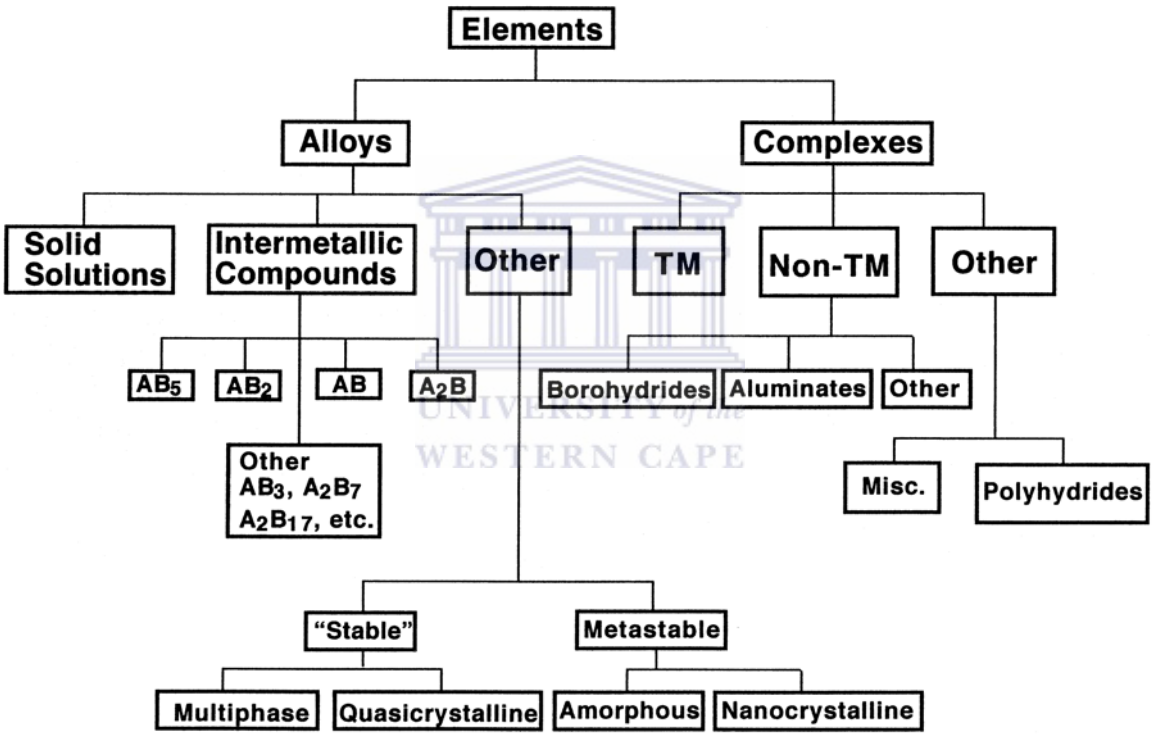

Fig 2.3: Family tree of hydriding alloys and complexes, TM = transition metal. [6]

The group of hydrides referred to as intermetallic compounds or hydrides (IMH) are denoted by the general formula $A_mB_nH_x$. In this hydride structure, two or more metals are involved. These metals must adhere to the following obligations (i) A should have a strong affinity for hydrogen. (ii) B should not interact with hydrogen in ambient conditions. Hydride forming intermetallides are generally grouped based on their ratio of hydride forming A to the non hydride forming B

components. The most widely acclaimed families of intermetallic hydrides are AB_5 e.g. $LaNi_5$, AB_2 e.g. $TiMn_2$, AB e.g. TiFe and A_2B e.g. Mg_2Cu. Rare earth metals and calcium are usually the A component in the AB_5. For the AB_2 and AB, A is commonly a member of the titanium sub group. For the A_2B, the A component is commonly magnesium. In all cases, The B component is usually of the transition metals group (Fe, Co, Ni, V, Mn, Cr, etc.). Formation of intermetallic hydrides usually involves expansion of the crystal lattices. The symmetry of the metal matrix is expected to be unchanged in the course of hydride formation. However in some cases (e.g. TiFe) due to the high rate of hydrogenation of component A, more significant changes may occur in the arrangement of metallic atoms that may either effect a change in symmetry or even cause degradation, with the formation of the mixture of stable A-based binary hydride and B-enriched intermetallic compounds (like in A_2B) [19, 7]. Intermetallic hydrides have a propensity for excellent kinetics of hydrogen absorption – desorption, according to the above described mechanisms. Added advantage to this is the fact that these reactions occur at ambient temperatures or close. Intermetallic hydrides show the strongest potential as hydrogen storage materials compared to the forms of hydrides, and this has encouraged extensive research for their use in recent years. The two basic properties, which make IMH attractive, are their high and reversible hydrogen storage capacity per mole of compound, and the high energy stored per unit volume. The mass of hydrogen that can be stored per unit volume of hydride is larger than can be stored in liquid form while the energy stored may be more than 10 MJ l^{-1} of hydride [7]. These figures and the fact that hydrogen plays an important role as a nonpolluting fuel in internal combustion engines, as well as a nonpolluting working fluid in chemical heat pumps lend strong arguments for supporting research in clean energy systems based on IMHs. The applications can be partitioned according to their operating mode, ‘closed’ or ‘opened’. In the former case, the same amount of hydrogen is recycled; while in the latter new hydrogen must be fed into the system, or continuously supplied. This implies that depending upon the operating mode, the presence of chemical impurities (O_2, H_2O, CO_2, CO…) affect differently the storage properties of the system over the long term. The main flaw of IMH’s, with the exception of magnesium hydrides is their low hydrogen weight percentage which, for the most common commercial IMH’s still remains below 2 wt.% [30, 12]. The weight limitation is less important for stationary hydrogen storage but is a handicap for transportation. Finally, the ability to maintain the absorption properties over the long-term is of paramount importance, although the constraints differ strongly according to the use. Obviously, the first step in hydride technology is to find the ‘best’ IMC amongst the hundreds proposed, to operate over the requested pressure and

UNIVERSITY of the WESTERN CAPE

temperature range. It follows that the prime criterion in helping selection is correlated to the thermodynamic characterization of the IMC–H_2 systems.

The synthesis of IMH is obtained by direct reaction of the hydrogen gas with intermetallic solid. This step allows determining the thermodynamic parameters of the M–H_2 system. The technological future of the compound depends upon the system behavior with regard to impurities and cycling. The dynamics of the transformation e.g. (heat and mass transport properties) as well as other technical aspects also need to be well established. For technological use, the M–H_2 system must be fully activated by repeated hydriding/dehydriding cycles.

We shall present in more detail, the structure and properties of the different intermetallic compounds that are generating international interest.

AB_5 compounds:

TheAB_5 hydriding intermetallics generally have a hexagonal crystal structure. The near ambient PCT properties of these hydrides were first discovered accidentally in 1969 at Philips Eindhoven while the magnet alloy $SmCo_5$ was being studied [6]. This family of hydrides exhibit extraordinary versatility because many different elemental species can be substituted in the A and B lattice sites. A- elements tend to be one or more of the lanthanides with atomic number ranging from 57- 71. Another good example of A-elements is Ca. The B-elements are based on Ni with many other substitution alternatives like Fe, Ti, Co, Al, etc. The broad range of PCT versatility is evident with the 25^{o}C plateau pressure variable over at least three orders of magnitude depending on the composition. With the exception of $MmNi_5$ itself, hysteresis is quite low for AB_5s. By annealing out the as cast metallurgical composition fluctuations, rather flat plateaux are possible, even with multi component alloys. H- capacity of these hydrides is on a worrisomely low side, not exceeding 1.3% on the plateau basis we are using for definition of the reversible component [6]. Alloy raw material cost is relatively high compared to other alloys of hydriding intermetallics. $CaNi_5$ shows greater potential when it comes to cost and H- content than the Mn or La based alloys. The AB_5 alloys are easy to activate, seldom requiring any heating. They decrepitate to fine powder which is mildly pyrophoric when exposed to air after the first H/D cycle. This is a very relevant factor for safety considerations. Both easy activation and pyrophoricity means AB_5 alloys do not form protective oxide layers if there are trace elements of impurities such as H_2O and O_2 along with H_2 in the system. These impurities do not poison AB_5s

but only act as reactants which slowly reduce capacity. CO is a very strong poison, but regeneration can be achieved by heating to about 100°C and flushing with clean H_2. Intrinsic kinetics of the AB_5s is very good, almost always better than practical engineering heat transfer with regards to purity (absence of CO in the H_2). AB_5 alloy metallurgy is well understood and virtually single phase alloy can be melted into large commercial quantities by vacuum induction melting [6]. AB_5s are subject to dispropornation and this can be reduced by partial substitution of Al or Sn in the B- lattice.

AB_2 compounds: Like AB_5s, AB_2s represent a large and versatile group of hydriding materials with PCT values bordering around ambient temperature range. The A- elements are usually group IV metals e.g. Ti, Zr. The B- elements are usually transition and non transition metals with atomic number from 23- 26 e.g. Fe, Mn, V. etc. A very wide variety of substitution possibilities are possible for both A and B lattices, and this means PCT properties can be fine tuned to a large extent. The AB_2s are based on two related Laves phase crystal structures; the hexagonal prototype and the cubic prototype. PCT properties can be adjusted between pressures of 1- 10 bar and temperature range of 1- 100°C. H- capacity of AB_2 alloys are comparative to AB_5 alloys on a reversible(plateau pressure) basis but are generally higher on a reversible capacity basis. The AB_2s often suffer from less distinct, narrower plateaux, and a residual, essentially "non reversible" heel compared to AB_5s. When larger temperature and pressure range are available, AB_2s tend to show higher capacities than AB_5s. AB_2s offer a better alternative than AB_5s in terms of cost especially if the A- content is Ti. AB_2s are generally more difficult to activate than AB_5s especially for those alloys high in Zr or Mn content. Once activated, H/D kinetics is very high. It is also observed that AB_2s are very sensitive to impurities like CO and H_2O in the H_2. When lanthanide elements are being used in the A- side, AB_2s are prone to dispropornation even after the first cycle. Like the AB_5s, AB_2s decrepitate into fine powders. Alloys high in Zr and Mn are pyrophoric in the activated state whereas those high in Ti and Cr tend not to be. The productions of AB_2s require high metallurgical care.

AB compounds: The first demonstration of reversibility in intermetallic hydrides was done using the AB alloy ZrNi in 1958 by Libowitz. Unfortunately $ZrNi_3$ has a 1 atm desorption temperature of about 300°C and did not present a viable option in terms of practical application. The first practical AB alloy demonstration was with TiFe in 1970 by Reilly and Wiswall at Brookhaven National Laboratory, USA [6]. TiFe alloy and its substitutional modifications remain the most viable AB alloys today. TiFe based AB alloys are based on an ordered body centered cubic

UNIVERSITY of the WESTERN CAPE

structure. They tend to have two plateaux(forming two hydrides) both with reasonable pressures at room temperature. PCT can be modified by partial substitution of the Ti or Fe, for instance with Mn. TiFe shows good volumetric and gravimetric H- capacities competitive with the best AB_5s and AB_2s.Ti/Fe also offers the lowest price, lower on a per unit H_2 storage capacity than any other intermetallic alloy extensively researched. Hysteresis tends to be on the high side. Activation is slow for the TiFe based ABs. Ti/Fe needs to be heated to destroy the natural oxide surface layer. Mn modified TiFe will usually activate slowly at room temperature. In any case it may take a day or two for complete activation to be achieved. As expected, the susceptibility of TiFe alloy to impurities in the H_2 to form oxide layers is very high. On the other hand this alloy exhibits little or no tendency for pyrophoricity because of the formation of Ti- oxides. The melting of TiFe based AB alloys requires care. The metallurgy is made a bit complex because of the tendency of the alloy to pick up oxygen, which over time lowers the reversible capacity. Conventional oxide melting crucibles are not stable enough but arc melting is more advisable. In summary, PCT properties of TiFe are very good, so is H- capacity. Another incentive is the low raw material cost. However, the issues to be addressed if it is to be viable for commercial use are its susceptibility to gaseous impurities and the problems associated with activation.

UNIVERSITY of the
WESTERN CAPE

A_2B compounds

The A_2B family of compounds represents an area of historical activity. Various crystal structures are possible. In one subfamily, A is typically of the Group IV elements Ti, Zr or Hf and B is a transition metal, typically Ni. Another family is based on Mg_2Ni, discovered in the late 1960s by Reilly and Wiswall (USA) [6]. Unfortunately, the A_2Bs offer little in the 0–100^oC, 1–10 atm range, at least with the present state of the art. They are invariably more stable. There has been extensive work on Mg_2Ni for nearly three decades, both from fundamental and applications points of view. H-capacity and cost properties of Mg_2Ni are attractive, but desorption temperatures are too high for most applications. Mg_2Ni is not very amenable to modification of PCT properties by ternary and higher-order substitutions. Numerous attempts to significantly decrease desorption temperatures have not been particularly successful. There have been several successful attempts to increase adsorption and desorption kinetics by surface treated or nanocrystalline and amorphous versions of Mg_2Ni-related alloys (sometimes including catalysts), but the basic hydride thermodynamics have not been improved much.

Based on the above characteristics offered by the different intermetallic compounds, the table below presents a qualitative overview of their attributes.

Table 2. 1:

Qualitative overview of hydride types as to attributes [6]:

Attribute	AB_5	AB_2	A_2B	AB
(i) Versatility	+	+	- / 0	+
(ii) H- capacity	0	+ / 0	+	+/ 0
(iii) PCT	+	+	-	+
(iv) Activation	+	0	0	- / 0
(v) Impurity effect	+	0	0	-
(vi) Cyclic stability	+/ 0/ -	0 /? / -	0 /?	- / 0
(vii) Ease of manufacture	+	0	0	+
(viii)Pyrophoricity	0	-	+	+
(ix) cost	0	+	+	+

Key to table: - good +, neutral 0, poor -, uncertain?

UNIVERSITY of the
WESTERN CAPE

2.4.3. Application of Intermetallic Hydrides according to thermodynamic properties:

Even though it may be outside the scope of this project, it is imperative to briefly highlight the proposed and commercial applications of IMH in terms of properties required. Obviously different properties are desired for different applications and all these properties are tailored under "high" and "low" working temperatures. Therefore before I proceed, a brief overview of low and high temperature IMH is presented.

Low temperature IMH

This type contains hydrides of several classes of intermetallic compounds, e.g AB_5 (A- rare earth metal; B- Ni as a basis, Co, Al, Mn, etc. as alloy additives), AB_2 (A- Ti, Zr; B- Mn, Fe, Cr, etc.) and AB (e.g. TiFe). The most important feature of these materials is the relatively high rate of hydrogen sorption – desorption processes at pressures and temperatures close to "ambient" conditions (1 bar, 20 ^{o}C). The advantage of hydrogen storage in low temperature metal hydrides, apart from their high hydrogen volume density, is a high purity of supplied hydrogen, due to the selectivity of hydrogen adsorption by the hydride forming alloys. Efficient control of hydrogen pressures at the output of MH storage unit, by controlling thermal action onto the MH layer is an additional advantage of the low temperature IMH, allowing for an extension in the performance of the hydrogen storage unit by the function of hydrogen compression. A combination of conventional hydrogen storage methods with the low temperature metal hydrides H storage is considered to be very promising.

UNIVERSITY of the WESTERN CAPE

The main drawback of the low-temperature IMH hydrogen storage is in a rather low weight content of H (typical value is up to 1.5 wt.% for AB_5 and up to 2 wt.% for AB_2 and AB alloys). Moreover, the real values of the weight and volume hydrogen storage capacities are even smaller in the MH hydrogen storage units. Similarly, the power consumption to provide hydrogen release from the MH container is higher than the value of the corresponding heat of the decomposition of IMH. Because of a low heat conductivity of the MH layer and heat losses, the thermal efficiency of the MH devices rarely exceeds 30-35% [19].

Nevertheless, the majority of IMH applications including hydrogen storage units are based on the use of low-temperature IMH, first of all, due to their technological flexibility.

High temperature IMH

This type mainly comprises magnesium-based alloys and intermetallics, which, as compared to the low-temperature hydrides, have larger weight capacity (up to 7.6 wt.% for the magnesium hydride) [33,32]. However, hydrogen absorption – desorption kinetics in these materials is usually slow. Both absorption and desorption processes take place at increased temperatures (250—350 °C). High power consumption for the high temperature MH hydrogen storage is caused by a necessity to maintain elevated temperatures, as well as to stimulate hydride decomposition which heat of formation exceeds the values for the low-temperature MH by more than two times. Nevertheless, this hydrogen storage method can be acceptable for the specific applications where the waste heat with corresponding temperature potential is available.

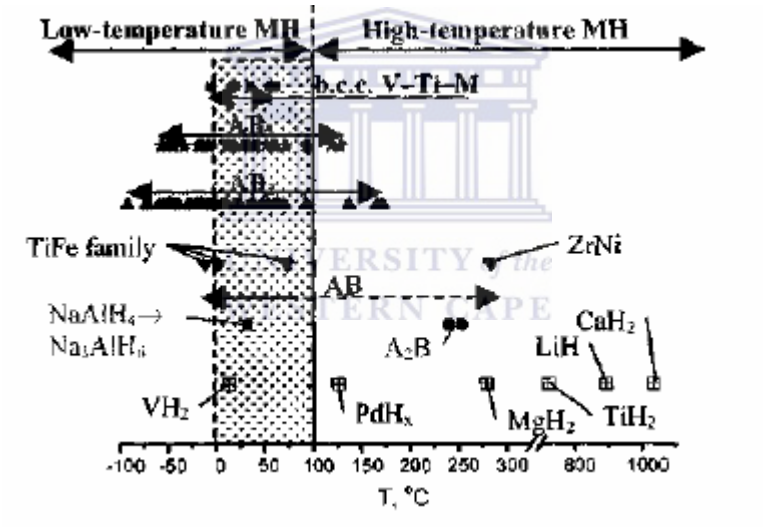

Fig 2.4: Temperatures of hydrogen desorption from the different MH at P =l bar. The shaded area (T =0-100 °C) corresponds to the most common specifications for hydrogen storage systems. [19]

Application in H-storage (stationary and mobile):

Stationary storage usually implies bulk storage and large amounts of alloy, so low alloy cost tends to be an important property. On the other hand *vehicular storage* tends to require high hydrogen weight percent; in fact most existing hydrides fall far short of what is desired in this property. Both kinds of storage desire easy activation to minimize container pressure and temperature requirements for the one-time activation. In both cases, good resistance to gaseous impurities is desirable in case impure H is used or the inevitable accidental introduction of air occurs. In both cases, PCT properties should be roughly in the ambient temperature and pressure area so that waste heat from the environment or vehicle engine (or fuel cell) can be used for endothermic H desorption. Kinetics is somewhat less important for stationary storage because of the relatively slow cycling of stationary storage tanks

Compression:

The compression of gaseous H using thermal swings of hydride beds is an open-ended process and generally requires the alloy to have good impurity resistance (due to impure H pumped) and cyclic stability (high temperatures involved). H/D cycling is relatively fast, so good kinetics and heat transfer and cyclic stability is desired. If rapid cycling can be achieved, then relatively small inventories of alloy are needed and alloy cost becomes secondary to other properties. Good H-capacity is desired so that parasitic heat losses associated with thermal swings are minimized. PCT properties must be tunable to the input and output pressures desired and the input and heat sink temperatures available.

UNIVERSITY of the WESTERN CAPE

Closed thermodynamic systems:

This class of hydride applications includes the following: (1) *heat engines*, where heat is converted to mechanical energy in an expansion engine; (2) *heat storage*, for example solar heat; (3) *heat pumps*, where low-temperature heat is ‘upgraded’ to higher temperature; and (4) *refrigerators*, where heat is converted to refrigeration. Included in heat engines are *actuators* and *temperature sensors*. All of these devices are closed systems, where H2 is a contained ‘working fluid inventory’, so generally impurity resistance is relatively unimportant (assuming the systems are built very cleanly to start with). Most (except (2)) are expected to cycle rapidly and involve relatively high temperatures, so good kinetics and cyclic stability is important. Like in

compressors, good capacity is desirable and PCT must be carefully tuned to the application. In the special case of heat pumps and refrigerators, where two or more different hydrides must be carefully matched to each other, achieving the exact desired PCT properties can be difficult or expensive. To work properly, or at least to maximize overall efficiency, most closed thermodynamic systems demand low hysteresis and low plateau slope.

Metal hydride storage units:

Mainly, commercial MH storage units are intended for laboratory applications providing safe and compact storage of high purity- hydrogen (capacity from 30-40 liters to few m^3, with supply pressure of 1-10 bar). Technological flexibility of the MH units allows adjusting their characteristics to the specific consumer's conditions.

Apart from small scale and medium scale metal hydride hydrogen storage units, several examples of relatively large scale ones are also known. Usually, these units are the intermediate (buffer) storage reservoirs being component parts of hydrogen refueling stations. The units are (75 to 90 m^3 H2 STP) characterized by compactness, safety and easy operation. The largest MH hydrogen storage unit (~15000 m^3 H_2 stored in 100 tons of metal hydride) was produced by GfE Gesellschaft fur Elektrometallurgie mbH which is now part of HERA Hydrogen Storage Systems, GmbH company [19].

UNIVERSITY of the WESTERN CAPE

It is also feasible to use metal hydride storage units in some special mobile applications, where weight storage capacity is not so critical, but safety and compactness are necessary. One example is a zero emission technological transport, like tractor or forklift. The latter approach is of special interest because here MH hydrogen storage can be mounted as a counter balance. It should be noted that in the majority of reviews, the values of weight and volume hydrogen sorption capacities of the metal hydride hydrogen storage method are presented as the maximum capacities of the bulk IMH material. In the real MH storage units these parameters are lower. It is observed that the volumetric efficiency of hydrogen storage in the real MH unit does not practically correlate with the scale of the unit, but as a rule, does not exceed 40-50% of the total volumetric H density in the IMH material. As for the weight of the efficiency, it is observed that there is a tendency of its increase with the unit scale. Moreover, for the low-scale units (up to ~500 liters H2) this effect is more pronounced. In any case, 70-75% is the upper limit for the weight efficiency of the MH hydrogen storage systems [19].

There exist several reasons reducing the hydrogen storage capacity of the MH units below the capacity of the IMH material. First, the useful storage capacity of the unit is determined not by the total, but by the reversible hydrogen capacity of the material, i.e. by the quantity of hydrogen that can be reversibly absorbed/ desorbed in the course of the unit operation. This parameter depends on both the properties of the used IMH (mainly on PCT characteristics of the corresponding system with hydrogen gas) and also on working pressure and temperature range. Another factor reducing the weight hydrogen capacity of the MH storage units is material consumption of the container. This factor is also important in the large scale units where apart from the material itself, the presence of special heat transfer elements for improvement of heat transfer in the IMH is necessary. The usage of lighter design materials allows reducing in some extent the losses in the weight capacity of the system. However this effect is mainly for low-scale units.

The main reason for reduction in the volumetric hydrogen capacity in the real MH storage units is the upper limit of safe packing density of the IMH loaded into the container. It is obligatory to avoid the damage of the swelling effect of the IMH material in the course of hydrogen absorption. This limit depends on the value of the volume increase of the metal matrix under hydrogenation.

Taking into account the above mentioned, it can be concluded that MH hydrogen storage units having a conventional layout (rigid container with the internal heat exchanger or without it, where the IMH powder is loaded) will have the volumetric hydrogen storage capacity not higher than 50% and the weight of no more than 75% of the total capacity of the IMH. According to our estimation, it corresponds to the storage of gaseous hydrogen under the pressure 400- 800 bar. But the real pressure of the hydrogen gas inside MH hydrogen storage unit usually does not exceed several bars, what is important are the precautions of safety and the absence of the expensive cost of hydrogen compression. Moreover, the improvement of the design of MH containers (usage of light materials, non-traditional layout, etc) can improve weight and volumetric indices of MH hydrogen storage units [19].

UNIVERSITY of the WESTERN CAPE

Other applications:

There are a number of lesser-known hydride applications: *liquid H control* and *boil-off capture*, *cryocooling*, *chemical catalysis*, *ammonia synthesis*, *methane synthesis*, *diamond synthesis* [6, 7], *permanent magnet production* and others too numerous to detail here. The biggest commercial application is the *nickel metal hydride* (*NiMH*) *battery* [34-36].

Conclusion:

Based on the above highlighted characteristics, it is our opinion that intermetallic hydrides form a basis for multi-functional applications allowing combining several options, for example in hydrogen storage, purification and controlled supply to consumers provided by a single device. It has been recorded as an example that the metal hydride system intended for hydrogen recovery from ammonia purge gas can give off up to 50% H_2 with a purity of 99.999% and a storage and transportation capacity of 200Nm^3 H^2 in four metal hydride containers and supply to a factory [19].

UNIVERSITY of the
WESTERN CAPE

2.5. Carbon nanotubes as novel material for hydrogen storage:

Gas-on-solid adsorption is an inherently safe and potentially high-energy density hydrogen storage method. The hydrogen storage properties of high surface area ‘‘activated’’ carbons have been extensively studied. However, activated carbons are ineffective in storing hydrogen because only a small fraction of the pores in the typically wide pore-size distribution are small enough to interact strongly with hydrogen molecules at room temperatures and moderate pressures. Recently, many carbon nanostructure absorbents have been produced, including graphite nanofibers and carbon nanotubes.

Carbon nanotubes can be divided essentially into two categories; Single-walled nanotubes and Multi-walled nanotubes. Ideally, Single-walled nanotubes are made of a perfect graphene sheet, i.e. a polyaromatic mono-atomic layer made of a hexagonal display of sp2 hybridized carbon atoms rolled up into a cylinder and closed by two caps (semi-fullerenes).The internal diameter of these structures can vary between 0.4 and 2.5nm and the length ranges from few microns to several millimeters. On the other hand, Multi-walled nanotubes are concentric single-walled nanotubes with increasing diameter and coaxially disposed. The number of walls present can vary from two (double wall nanotubes) to several tens, so the external diameter can reach up to 100nm. The concentric walls are regularly spaced by 0.34nm [37-41]. It is important to take note of the fact that residual metallic particles coming from the production process remain in the inner cavity of multi-walled nanotubes [25, 42]. Since nanotubes are chemically stable and have a low mass density, many published experimental studies for hydrogen storage on carbon nanotubes have attracted much attention. Many investigations have been made both theoretically and experimentally, such as investigating their cycling characteristics, discharge capacity, and electrochemical properties. The amazing mechanical and electronic properties of nanotubes stem in their quasi-one dimensional (1D) structure and the graphite-like arrangement of the carbon atoms in the shells. Thus, the nanotubes possess high Young modulus and tensile strength, which makes them auspicious for composite materials with improved mechanical properties. Nanotubes can be metallic or semi-conducting depending on their structural parameters [15, 43-45].

Extensive research has shown that carbon nanotubes are capable of absorbing high wt% of hydrogen, up to 3% at ambient temperatures and pressures [46].Thus, high H_2 storage capacities could be achieved at relatively low temperatures and low pressures as compared to absorption on other carbon materials. In the Proceedings of the 1994 Hydrogen Program Review of the United States DOE, microbalance data was presented which demonstrated gravimetric hydrogen storage densities of up to 8.4 wt% at 82 K and 570 torr on samples containing carbon nanotubes [10].

UNIVERSITY of the WESTERN CAPE

This substantial uptake at low hydrogen pressures demonstrated the strong interaction between hydrogen and these materials. The adsorption energies on carbon nanotubes were estimated to be a factor of 2-3 times higher than the maximum that has been observed for hydrogen absorption on conventional activated carbons. These were the first results which demonstrated the existence of stable adsorbed hydrogen on any type of carbon at temperatures in excess of 285 K [10]. Studies have been carried out to elucidate the mechanism of H_2 adsorption on CNTs. This type of work is critical to the growing community that has been attempting to understand how CNTs interact with hydrogen. There is considerable debate over the issue in the scientific community, and it is important to obtain a deeper understanding so that;

* Accurate theoretical models and predictions may be developed,
* Specific CNT diameters may be targeted for synthesis, and
* Capacities and performance characteristics may be optimized.

We assume that the interaction between H_2 and nanotubes is mid-way between conventional Van der Waals adsorption and chemical bond formation. A detailed understanding of the mechanism coupled with a high degree of control during synthesis should allow useful hydrogen adsorbents to be designed and constructed.

UNIVERSITY of the
WESTERN CAPE

2.5.1. Methods of synthesis of carbon nanotubes:

Till date only three viable methods of synthesis of carbon nanotubes have been published. These are (i) arc discharge. (ii) Laser ablation (iii) catalytic chemical vapor deposition. The Multi-walled nanotubes were first discovered in the soot of the arc-discharge method by Iijima [47]. This method has been used long before that in the production of carbon fibers and fullerenes. It took two years for Iijima, Ichihashi and Bethune [45, 48] to synthesize Single-walled nanotubes by use of metal catalysts in the arc-discharge method in 1993. A significant progress was achieved by laser-ablation synthesis of bundles of aligned SWNTs with small diameter distribution by Smalley and co-workers [49]. Catalytic growth of nanotubes by the chemical vapor decomposition (CVD) method was first used by Yacaman and co [50]. The industrial application of the carbon nanotubes requires the development of techniques for large-scale production of defect-free nanotubes. In this section, the nanotube production methods will be outlined in historical order.

UNIVERSITY of the
WESTERN CAPE

Arc discharge method:

In 1991, Iijima [47] reported the preparation of a new type of finite carbon structures consisting of needle-like tubes. The tubes were produced using an arc-discharge evaporation method similar to that used for the fullerene synthesis. The carbon needles, ranging from 4 to 30 nm in diameter and up to 1 mm in length, were grown on the negative end of the carbon electrode used for the direct current (dc) arc-discharge evaporation of carbon in an argon-filled vessel (100Torr).Transmission electron microscopy (TEM) revealed that each of the needles comprised coaxial tubes of graphitic sheets, ranging in number from 2 to about 50, later called multi-walled carbon nanotubes. On each of the tubes the carbon-atom hexagons were arranged in a helical fashion around the needle axis. The helical pitch varied from needle to needle and from tube to tube within a single bundle. The tips of the needles were usually closed by curved, polygonal, or cone-shaped caps. A growth model was proposed in which the individual tubes have spiral growth steps at the tube ends. The TEM study of the growth morphology of the carbon microtubules synthesized by arc discharge revealed that there were many variations in shape, especially near the tube tips. A topological model was constructed in which pentagons and heptagons played a key role in the tube-tip shapes. Iijima and co [45] proposed a model for an

open-ended growth, in which the carbon atoms are captured by the dangling bonds, and a layer-by-layer growth, in which the nanotubes thickens.

The nucleation of positive (pentagons) and negative (heptagons) disinclinations on open-tube ends results in changes of growth directions, producing different morphologies.

Large-scale synthesis of multi-walled nanotubes by a variant of the standard arc-discharge technique was reported by Ebbesen and Ajayan [51]. The TEM analysis revealed that the samples consisted of nanotubes of two or more concentric carbon shells. The nanotubes had diameters between 2 and 20 nm, and lengths of several micrometers. The tube tips were usually capped with pentagons. In 1993, Iijima and Ichihashi [45] and Bethune et al [48] almost simultaneously reported the arc-discharge and catalyst-assisted synthesis of SWNTs. The use of the three components—argon, iron and methane, was critical for the synthesis of SWNTs. The TEM analysis of the obtained specimens revealed the presence of SWNT threads, which were curved and tangled together to form bundles. The nanotubes had diameters of ~1 nm with a broad diameter distribution between 0.7 and 1.65 nm. In the arc-discharge synthesis of nanotubes, Bethune et al [48] used as anodes, thin electrodes with bored holes which were filled with a mixture of pure powdered metals (Fe, Ni or Co) and graphite. The electrodes were vaporized with a current of 95–105 A in 100–500 Torr of He. The TEM analysis of the obtained specimens showed that only cobalt-catalyzed nanotubes had single- atomic-layer walls with uniform diameters of 1.2 – 0.1 nm. Large quantities of SWNTs were generated by the arc-discharge technique by Journet et al [52]. By scanning electron microscopy (SEM), the deposited material was seen to consist of large amounts (~80%) of entangled carbon ropes. The high-resolution TEM images showed that the ropes had diameters from 5 to 20 nm. The tube diameters were around 1.4 nm with average separations of ~1.7 nm. The X-ray diffraction (XRD) patterns showed periodic arrangement of the tubes in the ropes. This led to the conclusion that a unique growth mechanism is evident which does not depend on the details of the experimental conditions, but which depends much more on the kinetics of carbon condensation in a non-equilibrium situation.

UNIVERSITY of the WESTERN CAPE

Laser ablation:

In 1996, Smalley and co-workers produced high yields (>70%) of SWNTs by laser-ablation (vaporization) of graphite rods with small amounts of Ni and Co at 1200 ^{o}C [49]. The x-ray diffraction and TEM showed that the synthesized nanotubes were remarkably uniform in diameters and that they formed ropes (or bundles) 5–20 nm in diameter and tens to hundreds of

micrometers long. The ropes formed a two-dimensional (2D) triangular lattice with lattice constant a = 1.7 nm through Van der Waals bonding [49]. The ropes were metallic and it was argued that a particular tube might be the dominant component. The growth of the nanotubes was explained by a ‘‘scooter’’ mechanism. In this mechanism a single Ni or Co atom chemisorbs onto the open edge of a nanotube. The metal atom must have sufficiently high electro negativity as to prevent formation of fullerenes and it must be highly effective in catalyzing the nanotube growth. The metal atom circulates (‘‘scoots’’) around the open-end of the tube and absorbs small carbon molecules and converts them into graphite-like sheet. The tube grows until too many catalyst atoms aggregate on the end of the nanotube. The large particles either detach or become over-coated with sufficient carbon to poison the catalysis. This allows the tube to terminate with a fullerene-like tip or with a catalyst particle. It was argued that the scooter mechanism favors the growth of armchair type nanotubes of most probable type, which corresponds to the experimental observations.

Both arc-discharge and laser-ablation techniques have the advantage of high (>70%) yields of SWNTs and the drawbacks that (1) they rely on evaporation of carbon atoms from solid targets at temperatures >3000 ^{o}C and (2) the nanotubes are tangled which makes difficult the purification and application of the samples [15]. The laser-ablation prepared samples usually contain >70% nearly endless, highly tangled ropes of SWNTs along with nanoscale impurities. A procedure of purification of the as-grown sample before cutting the nanotube was proposed by Liu et al [53]. The purification method consists of refluxing in 2.6 M nitric acid and re-suspending the nanotubes in pH 10 water with surfactant followed by filtration with a cross-flow filtration system. Passing the resultant purified SWNT suspension through a polytetrafluoroethylene filter produced a freestanding mat of tangled SWNT ropes—a ‘‘bucky paper’’. Several cutting techniques were proposed, the most efficient of which was prolonged sonification of the nitric acid-purified SWNT rope material in a mixture of concentrated sulfuric and nitric acids at 40 ^{o}C.

UNIVERSITY of the WESTERN CAPE

Catalytic chemical vapor deposition:

CVD was used for the first time by Yacaman et al in 1993 [15], and in 1994, Ivanov and co-workers [54] used it to grow multi-walled nanotubes. The CVD technique has been subsequently improved and optimized. Generally, the CVD process includes catalyst-assisted decomposition of hydrocarbons, usually ethylene or acetylene, in a tube reactor at 550–750 ^{o}C and growth of carbon nanotubes over the catalyst upon cooling the system. Best results are obtained with Fe, Ni or Co nano-particles as catalyst. The same catalysts are found optimal in the arc-discharge and

laser ablation techniques, which is in favor of a common nanotube growth mechanism. It was argued that the nanotubes grow out of the catalyst nano-particle embedded in the pores by tip growth or base growth depending on the contact force between the catalyst particles and the substrate. Large-scale synthesis of aligned carbon nanotubes was achieved by the CVD technique and iron as catalyst by Li et al [38]. A substrate containing iron nano-particles embedded in meso-porous silica was placed in the reaction chamber. A mixture of 9% acetylene in nitrogen was introduced in the chamber at a flow rate of 110cm^3/min. Carbon nanotubes were formed on the substrate containing the iron nano particles by deposition of carbon atoms obtained by decomposition of acetylene at 700 ^oC. The samples were examined by SEM and energy-dispersive X-ray diffraction (EDX). The SEM image of the obtained thin films showed that nanotubes grew continuously from the bottom to the top of the film in lengths between 50 and 100 mm. The nanotubes were multi-walled with outer diameters of ~30 nm and consisting of ~40 shells, and formed arrays with nanotube spacing of~100 nm, consistent with the spacing between the pores on the substrate. It could not be determined which one of the two so far proposed growth mechanisms—tip growth or base growth, was realized.

Porous silicon wafer was used in a CVD method to grow a regular array of multi-walled nanotubes. The porous silicon was obtained by electrochemical etching of heavily doped n^+ type Si wafers. The substrates were patterned with Fe films by electron beam evaporation through shallow masks with squared openings and side length 10–250 mm at pitch distances of 50–200 mm. On each tube the carbon atoms are arranged in a helical fashion along the tube axis. The diameters of these MWNT range from a few to a few tens of nanometers and their length is of the order of 1μm. The TEM images showed that the nanotubes had diameters of 16 nm formed on top of the patterned iron squares on the substrate. The CVD process was performed in a tube reactor at 700 ^oC in flowing argon, the carbon feedstock was ethylene.

High-quality SWNTs could be grown on silicon wafers patterned with micro-meter scale islands of catalytic material by the CVD technique by Kong et al [55]. Methane was used as carbon feedstock, high reaction temperatures in the range of 850–1000 ^oC were necessary to form small diameter SWNTs. The optimal choice of catalyst was a Fe/Mo species supported on a sol–gel derived alumina-silica multi component material. The TEM images revealed an abundance of individual and bundled SWNT. The SEM images showed that the SWNTs were of high quality with diameter distribution between 0.7 and 5 nm with a peak at 1.7 nm. The high yield of nanotubes (~47%) in this CVD method was found to be due to the increased metal–support interactions which favored base-mode nanotube growth. On the other hand, catalysts with weaker

UNIVERSITY of the WESTERN CAPE

metal support interactions lead to aggregation of metal nano particles and reduced nanotube yield and purity.

Conclusion:

In comparison with the other synthesis methods of carbon nanotubes, chemical vapor deposition appears to be the most promising. This can be adduced from the simplicity of the process, the alterability of synthesis parameters for CNT growth and of course the very high yield of pure CNT.

2.5.2. Carbon nanotubes hydrogen absorption properties:

Carbon is well known as one of the better adsorbents of gases. This property is due to the ability of this material to exist in a very fine powdered form with highly porous structure and the existence of particular interactions between carbon atoms and gas molecules. During recent decades, many improvements have been accomplished to obtain microporous and ultra microporous carbonaceous materials having very high absorbing properties for the most current gases. In line with these results carbon nanotubes have emerged as favorites. The process responsible for hydrogen absorption in carbon materials at moderate temperature is based on weak attraction forces between absorbate and absorbent [56- 57]. The amount of gas adsorbed represents the additive amount of gas which can be introduced in a given volume with respect to the amount of gas occupying an equivalent volume at the same temperature and pressure in the absence of absorption. At a given temperature, the amount of gas adsorbed is only a function of the pressure and is released (desorbed) when pressure decreases; meaning the phenomenon is reversible with pressure. The correspondent units are: mole per gram (mole g^{-1}) or gram per gram (g g^{-1}) or, now the most used, weight % (wt %), rarely, it is expressed in atom/atom, i.e. atom of hydrogen per atom of carbon [16].

UNIVERSITY of the
WESTERN CAPE

The amount of hydrogen physisorbed on carbon nanotubes depends almost linearly on the specific surface area, both at low temperature and at room temperature, and is independent of the type of carbon nanostructure [16]. Therefore the hydrogen absorption process is based on the local interaction between the hydrogen molecule and the surface. As a consequence, promising materials for hydrogen adsorption are nanostructures with high surface area and micro pore density. The linear relation between the pore volume and the storage capacity demonstrates that carbon materials ideal for hydrogen storage should possess a high micro porosity with a small pore dimension [24].

While at room temperature the highest measured storage value that has been reproduced in different laboratories is less than 1 wt% even at high hydrogen pressure, at 77 K the possibility to store up to 10% wt% of hydrogen has been recorded [46]. Future investigations should concentrate on new materials with very high surface area in order to achieve successful storage capacities not only at low temperature but also in ambient conditions. The carbon nanotube samples are characterized by specific surface area (SSA) and by their equilibrium and dynamic

absorption properties. The SSA is calculated from the N_2 adsorption isotherm using the Brunauer-Emmett-Teller (BET) method. N_2 is used as reference gas because H_2 and N_2 undergo a similar sorption mechanism on carbon nanotubes (physisorption).The surface area is observed to be directly proportional to the carbon content of the sample [16]. Results of scientific literature suggest that the surface of the catalyst and the carbon impurities make minor contributions to the measured surface. Moreover, both the outer and the inner surfaces of the nanotubes are accessible for nitrogen adsorption in the studied preparations. The amount of N_2 absorbed is proportional to the pressure, demonstrating the energetic homogeneity of the of N_2 absorption sites, which can be explained with Henry's law. At low absorption coverage the equilibrium and dynamic sorption properties of the nanotubes are strongly affected by the surface functional groups. It is noticeable that the possibility of controlling microscopic parameters such as the nanotube diameters and lengths will enable to control material macroscopic properties such as gas absorption [24]. It is important to notice that different factors can influence the gas absorption. Among these factors, we can cite the specific area of the materials, method used to synthesize the nanotubes, the method used in order to open the tubes, the intercalation of heteroatoms in order to increase the gas uptake and the purification of the absorbent before any absorption measurements. Despite the importance of the hydrogen adsorption capacity of nanotubes for a reliable storage, the bulk density of the nanotubes has to be taken into account. Indeed, the amount of hydrogen stored is directly proportional to the absorption expressed in weight % and consequently, to the bulk density of the absorbent. This bulk density is dependent on synthesis amounts and parameters. The next step should be the measurement of hydrogen absorption in purified and opened carbon nanotubes in order to enable gas absorption both inside and outside the compacted bundles of carbon nanotubes. It is important also to note that hydrogen absorption can be optimized in carbon nanotubes by ensuring suitable nanotube diameters (during synthesis) and adequate spacing between nanotubes in the bundles.

UNIVERSITY of the WESTERN CAPE

Considering some articles published so far, carbon nanotubes seem to be good candidates for the hydrogen storage process. However, some questions persist; in the future, some explanations are still needed for all scientists who are interested in the hydrogen storage by absorption in carbon nanotubes. In particular, as concerns the surface properties of these absorbent materials; the chemical treatment during or after the carbon nanotubes synthesis; the mechanical treatment made on the tubes in order to open their extremities and enable the gas adsorption inside the tubes and the accuracy of the volumetric and the gravimetric measurement methods should be mentioned.

2.6. Composite hydrogen storage materials based on Intermetallic hydrides:

Research on gaseous and liquid methods to inexpensively store hydrogen in a safe, compact and lightweight package has been ongoing for more than a decade. The U.S.A Department of Energy (DOE) Hydrogen, Fuel Cells & Infrastructure Technologies programme, has been instrumental in developing state-of-the-art compressed hydrogen tanks. However, the future focus will be on solid-state materials that will enable the storage of hydrogen at low pressure. Solid-state storage refers to the storage of hydrogen in metal hydrides, chemical storage materials and nanostructured materials. This method of hydrogen storage offers perhaps the best opportunities for meeting the requirements for onboard storage (6.6 wt %). In these materials, hydrogen can be stored both physically and chemically according to the DOE classification. Such storage may be achieved by absorption on high surface area materials like carbon nanotubes; adsorption into metal hydrides such as intermetallic hydrides; and hydrogen binding in chemical compounds. Despite tremendous advances in recent years, no approach currently meets the storage density and/or charge-discharge requirements. However, in addition to limits in hydrogen availability, other issues need to be considered as new hydrogen storage materials are developed and characterized, such as the increase in wt.% storage capacity of the material, the ease of activation, sensitivity to gas impurities, rate of hydrogen absorption/desorption, heat transfer, cyclic stability, and physical properties (e.g., volume change and decrepitation).

UNIVERSITY of the WESTERN CAPE

As mentioned earlier, needed breakthroughs in hydrogen storage technology will require revolutionary new materials to meet the hydrogen storage requirements, and not simple, incremental improvements in current technologies. These breakthroughs require fundamental research to develop and examine new materials and obtain an atomic- and molecular-level understanding of the physical and chemical processes involved in hydrogen storage and release. The knowledge gained from this research will allow the tailored design and synthesis of new materials that will meet the requirements for efficient hydrogen storage. Combining different intermetallic hydrogen storage materials with suitable “dopants”, will introduce new catalytic and thermodynamic properties into the hydrogen storage materials, and thus new classes of hybrid hydrogen storage materials can be developed. For example, a core material could be selected because of its thermodynamic properties, and the mantle could be chosen for its catalytic activity. The combination of functional materials in a layered fashion could open up completely new routes for optimizing the overall performance of such a sorption material. Research on nanostructured hydrides may also provide insight into the mechanisms responsible for the

recently reported improvements in storage and kinetics of hydrides when dopants are added to these materials. Similarly, improvements in the lifetimes of hydride-based storage materials may be possible if we examine nanostructured materials to elucidate the mechanisms for associated degradation processes and sensitivity to impurities. This knowledge is expected to allow the directed design of new, higher-efficiency, recyclable hydride-based materials.

The two basic properties, which make IMH attractive for hydrogen storage and device application, are their high and reversible hydrogen storage capacity per mole of compound, and the high energy per unit volume [14].

Some critical short comings hinder the practical application of these IMH. They have not yet been solved completely. To improve the chances for a wider application of IMH in the existing and future hydrogen industry, the following property areas will need to be seriously addressed [59]:

- Develop IMH with a much greater weight percent capacity at ambient temperature.
- Develop much lover cost IMH alloys.
- Improve resistance to surface damages by impurities, through nano-engineering of the surface of the IMH.
- Learn to reduce or prevent IMH disproportionation.
- Improve the ease of alloy activation.
- Develop measures to eliminate the pyrophoric properties of fine hydride powders.

UNIVERSITY of the WESTERN CAPE

The different families of IMH compounds are classified according to their crystal structures. A comprehensive inventory of the IMH can be found in recent review articles [6, 7, 60-61], but we will briefly comment on the main properties of the commercially available, and highly recommended IMH for hydrogen storage applications. All of them have positive and negative attributes for effective hydrogen storage. A qualitative summary of the thermodynamic properties (Pressure-Composition-Temperature or PCT properties) and other relevant properties of the intermetallic alloys (activation, impurity effects, cyclic stability) are given in *Table 2.1* of this review (see above).

The summary is based on the literature surveys carried out in this Chapter. It is necessary to remember that the important point to note is that there are no ideal alloys that can store hydrogen. The AB_5, AB_2 and AB intermetallic compounds offer the best options for near room –temperature PCT properties, with the AB_2 and AB compounds offering the best combination of good capacity and lowest raw material cost. In our further research, the main focus will be on these types of alloys. The above mentioned problems with the IMH can be addressed by nano-engineering the desired qualities into the IMH chosen, and through the development of composite hydride

forming materials and subsequent study of their hydrogen storage potential for numerous applications.

According to authors involved in similar research, the creation of materials based on modern technological advancements in metal hydride chemistry holds great potential. To improve the hydrogen sorption properties of the IMH, researchers have recommended approaches aimed at:

- Changing the bulk properties of the materials chosen.
- Modifying the surface characteristics of the materials chosen.

For the nano-engineering of these composite materials, a “layer by layer” modification technique is proposed. According to our analysis of the above mentioned problems for the storage of hydrogen in IMH, the following approaches in alleviating these shortfalls are recommended by researchers in this field.

2.6.1. Approaches for increasing of weight capacity of hydrogen adsorption in Intermetallic compounds:

As a result of extensive research, it has been observed that high temperature metal hydrides of group II usually exhibit a relatively high hydrogen storage capacity but then require high temperatures to adsorb and desorb hydrogen; in other words they show clumsy reaction kinetics. On the other hand, low temperature metal hydrides of the Ti-Fe group do not possess a comparatively high storage capacity but they react with hydrogen at temperatures close to ambient conditions. This has led to research in the possibility of fusing together both high and low temperature metal hydrides; in other to ensure the high wt. % storage capacity on the one hand and favorable reaction conditions on the other hand. The composite should possess rapid H-absorption rate, high H-capacity, low working temperature, as well as superior oxidation-resistance. Among the known metals and alloys with potential use in hydrogen storage, magnesium has attracted much interest for its high hydrogen capacity and the very low cost. Recently, this tendency has increased, because it has become clear that the poor hydriding kinetics and high working temperature of Mg could be improved significantly by means of partial substitution, surface treatment or composite formation. Mg–TiFe could be enhanced several times to several 10s of times in comparison with that of pure magnesium. However, in the traditional mechanical milling (MM), which is operated under argon atmosphere, the high ductility of pure Mg impedes a high-degree dispersion of the catalytic phase, which further restricts the full realization of the catalytic function. This problem could be overcome successfully by employing a catalytic reaction ball milling (CRBM) method or by milling the Mg hydride directly [62].

UNIVERSITY of the WESTERN CAPE

In most cases, hydrogen forms a solid solution and the pressure plateau disappears in the studied metallic glass–hydrogen systems, thus depriving the amorphous H-storage material from the possibility of an independent application. Recently, the improved hydriding characteristics exhibited by the alloy containing nano-crystalline and amorphous phases has attracted much interest as an amorphous structure. It is generally accepted that the amorphous region plays an important role in enhancing the hydrogenation performance of the material. High density of active particles and high corrosion-resistance, if associated with relatively high thermal stability, will imply the possible use of some amorphous alloys as an ideal composite phase for improving the hydrogenation behavior of Mg. Amorphous TiFe has been prepared by mechanical milling and chosen to study the catalytic function of the amorphous phase on the hydrogenation of Mg [62].

The hydriding properties of the composite are measured at several temperatures and under different hydrogen pressures using a conventional volumetric method. The topography and morphology of the composite particles are characterized using scanning electron microscopy (SEM) and transmission electron microscopy (TEM). Energy dispersive X-ray analysis (EDX) is used for elemental analysis of the selected micro-area. In situ activation of the material and a highly homogeneous dispersion of the composite phase could be achieved in CRBM. According to the phase transformation revealed by XRD analysis, it was reasonably deduced that the composition is accomplished in the initial stage of CRBM. Then under the action of the catalytic phase-amorphous Ti-Fe and mechanical driving force, Mg hydride begins to form. The instantaneous high-energy collision of steel balls provides the essential condition for the formation of the high pressure phase γ-MgH. During RBM, only small amounts of α-Fe and nanostructured Ti-Fe is detected, the amorphous Fe-Ti remains stable as a whole.

The data presented in [62] clearly indicates that among the TiFe composites synthesized by ball milling in hydrogen atmosphere, Mg (5 wt.)% TiFe had the maximum adsorption capacity of 5.80 wt.% at 300 °C and 5.12 wt.% at 200 °C. It is well known that crystalline Fe-Ti and Mg–Fe-Ti are very difficult to activate. However, for the Mg–TiFe (amorphous) composite, no activation treatment was needed for rapid H-absorption even after exposure in the air for 10 days. Unambiguously, this should be attributed to the existence of amorphous Ti-Fe. The 'windows' for dissociating hydrogen molecules and the "passageways" for diffusion of hydrogen atoms were not destroyed in the oxygen environment.

UNIVERSITY of the WESTERN CAPE

For an even more remarkable increase in weight percent at ambient temperature we propose adopting a method to synthesize carbon nanotubes (CNT) on the surface of intermetallic compounds using a chemical vapor deposition method. The modification of the IMC surface with CNT also offers the opportunity to reduce the working temperature of alloys [42]. The preparation of various inorganic composite materials has been in the focus of materials science since decades. In most cases the new substances show peculiar, surprisingly novel properties. Special interest has been devoted recently to carbon based composites. The change in the composition of a binary composite may shift some substantial properties of the material. Apparently, by choosing the right carbon source, it is possible to tailor the fundamental properties of carbon-containing composites. Morphological parameters we could change by design are: (i) macroscopic morphology (ii) specific surface area (iii) characteristic pore size (iv) surface fractal dimension and (v) pore system homogeneity

The hydrogen storage capability of pure carbon nanotubes is widely reported to be <2 wt % by different laboratories [63-64]. In combination with transition metals, hydrogen storage capacities of more than 6 wt % can be reached as shown unintentionally by Dillon et al [65]. An intended combination of carbon nanotubes and metal hydrides as new storage materials—with nanotubes grown directly on, for example, Ti/Fe -could lead to very high hydrogen storage capacities. With the combination of the properties of the metal-containing part and the carbon nanotubes in a carbon nanotube/metal oxide composite (CMC), the purification process can be avoided.

The synthesis of the carbon nanotube composite materials proceeds by decomposition of hydrocarbons, that is, methane, acetylene, pentane or octane to form the carbon nanotubes. Preliminary experiments are intended to successfully produce Ti/Fe particles with carbon nanotubes on the surface, and magnesium nano-particles on the nanotubes. Further research will focus on optimizing the magnesium loading, determining the hydrogen sorption characteristics of this novel composite, the hydrogen storage capacity, and nano-engineering the composite to tailor its stability and hydrogen storage properties for practical commercial applications.

2.6.2. Approaches for eliminating the impurity effect in the intermetallic hydride:

Impurity effects are a result of the interaction of gaseous impurities, present in the hydrogen, with the IMC alloy surface. Because the adsorption and desorption of hydrogen is highly dependent on surface structure, surface poisoning can have a very dramatic effect on hydrogen sorption properties. These gaseous impurities include methyl mercaptan (CH_3SH), hydrogen sulfide (H_2S), carbon monoxide (CO), carbon dioxide (CO_2), oxygen (O_2), ammonia (NH_3), methane (CH_4), nitrogen (N_2), etc [66]. For improved resistance of the composite material to impurities, we have adopted the surface modification methods recommended in literature.

For a metal covered with surface layers such as oxide/hydroxide or metallic coatings, the following additional steps should be considered; the H_2 dissociation on the layer and the penetration of H into the surface layer and H permeation through the layer. The H_2 molecular permeation may take place for the layers with porous structures. Hydride phases tend to form at the layer/metal interface because of the preferential precipitation of hydride at incoherent sites such as misfits and dislocations. Surface oxide and hydroxide layers become less active with increasing temperature because these layers become thinner or disintegrated by the diffusion of O atoms from the oxide layers into the metal, resulting in accelerated reaction rates of the H_2 adsorption. On the other hand, a metallic coating with Pd or a fluorinated surface layer [67-68] effectively protects the metal surface from the attack of contaminations such as oxidation, hydroxidation and CO adsorption, leading to high H_2 reactivity.

UNIVERSITY of the WESTERN CAPE

The fluorination of the surface of intermetallic compounds is effective in protecting the surface against contaminations. In fact, fluorinated AB_5 could be readily activated even after 6 months air exposure [27]. However, the kinetic data reported so far for this effect are not yet consistent with each other. This inconsistency seems to come from different methods of fluorination and resulting different structures of the fluorinated layers. Therefore, different reaction mechanisms may be anticipated for the surfaces modified by different fluorination methods. A standard and highly effective fluorination process is achieved by soaking the alloy samples into a 100% hydrofluoric acid (HF) solution for 3 h at 293 K, and then the samples dried in a 10^5 Pa N_2 gas flow at 393 K for 3 h [69].The modified surfaces are analyzed using AES (Auger electron spectroscopy) with respect to the surface composition. AES analysis of the formed fluorinated layers showed a thickness of about 50-80 nm. However, the fluorination effect on reactivity of the alloy with H_2 molecules in terms of adsorption becomes quite different according to the chemical composition of the alloy surface [69].

The surface modification of hydrogen storage alloys consisting of copper coating on the alloy surface has been shown to increase resistance to impurity, exhibit longer cycle life and show high rate discharge ability compared with the unmodified alloy. The $CuSO_4$ solution is used as modification reagent and HF is used as catalyst. A brief presentation of the process, as proposed, is as follows [27]; the hydrogen storage alloy is sieved and only particle size between 300 and 400 mesh is used. Then the alloy powder (12 g) is immersed in the solution (200 ml) of CuSO4 and HF. The amount of CuSO4 is varied from 3 to 20 wt% (in copper with respect to the alloy weight), and the amount of HF in the solution is changed from 0.15 to 1 ml. For simplicity and convenience, the optimal value of one variable is searched while the other variable is fixed at a standard condition (5 wt% of $CuSO_4$ and 0.25 ml HF, room temperature). The time for completion of reaction is defined as when the PH value of the solution reached saturation. After reaction finishes, the alloy power is washed with distilled water and methanol and then dried in vacuum at 50 ◦C. With the help of HF, the oxide film on alloy surface is removed and copper coating is easier to deposit, however care has to be taken as HF shows strong corrosive capability. It can be seen that the lower the amount of HF, the less the precipitated copper on the alloy surface. When the amount of HF is too small, the precipitated copper on the alloy surface is very sparse and mostly concentrated on high energy sites such as sharp edges and grain boundaries, resulting in a non-uniform copper coating. The reason for this phenomenon may be that the lower amount of HF does not have enough corrosive capability to remove all the oxide film, thus the activity of alloy surface is relatively low, and it is not easy for copper to deposit on the alloy surface. However, if too much HF is added, the alloy surface is severely eroded and peeled off, and the precipitated copper is also little. The reason for this may be that too much HF has too strong corrosive capability, and the eroding of the alloy surface continues even after completion of copper coating. Thus it is important to determine an optimal amount of HF adding to the solution. It is also observed that the copper coating becomes thicker and less uniform when the amount of copper coating increases. As the copper coating is between 3 and 5 wt%, the alloy surface is covered uniformly by copper particles, making the copper coating thin enough for hydrogen to adsorb and diffuse, resulting in better electrochemical properties. When the amount of copper exceeds 10 wt%, the copper coating became thicker and more asymmetric. When the amount of copper deposition reaches 20 wt.%, the coating is too dense and almost covers the alloy surface completely, making it difficult for hydrogen to adsorb and diffuse. And the waste of cost is too much when the copper amount is excessively large [27].

UNIVERSITY of the WESTERN CAPE

2.6.3. Approaches for improving the activation kinetics of intermetallic hydrides:

The activation of the metal hydride alloys is a key role in the sorption process, since it defines the rate of the reaction of hydrogen with the metals and the incorporation of hydrogen into the bulk structure of the metal. This activation typically involves either high pressure or elevated temperature, or both.

During the activation different processes occur [69] such as reduction of surface oxides, protonation of the surface oxide, etc. Recent surface studies confirmed that electron transfer between the surface and H_2 molecules is crucial for the occurrence of the H_2 dissociation. The dissociation of covalent molecules such as H_2 and O_2 is a result of the interaction between the H_2 anti-bonding orbitals and the lobe-shaped orbitals of the d-electrons of metals. Thus, the ready dissociation of H_2 molecules on the metal surface is crucial for the initial activation of metals [69]. In the past years, great efforts have been made by many researchers to improve the activation of IMH. For example alloying with a third element (Al, La, Ta) to partially substitute A or B in IMH alloys, chemical treatment with acid and alkaline [69-71].

For IMH it also been demonstrated that the presence of amorphous palladium coatings improve the cycle life time of alloys. Partial substitution by catalytically active palladium for Fe is effective for lowering the activation temperature of intermetallic Ti/Fe alloy [6, 72]. Pd is a typical f.c.c. metal which can absorb a large amount of hydrogen. Mechanical grinding a small amount of palladium with the hydrogen storage alloys can lower the activation pressures to sub-atmospheric level at room temperature and significantly increase hydrogen adsorption/desorption rates without changing the PCT behaviors. The addition of palladium helps the disassociation of molecular hydrogen, and the mechanism of the treatment on the activation and hydrogen adsorption/desorption of the alloys can be explained by hydrogen spillover for the adsorption process and reverse hydrogen spillover for the desorption process. The palladium treatment favors the dissociation and recombination, therefore hydrogen spillover and reverse spillover increase the rates of adsorption and desorption. In the adsorption process, the hydrogen atoms dissociated by palladium are spilt-over to the alloy's surface and get adsorbed by the alloy, and in the desorption process, reverse hydrogen spillover takes effect; hydrogen atoms diffuse to the palladium particle by surface diffusion and recombine as molecular hydrogen on the palladium surface. Hence, palladium treatment enhances both the adsorption and desorption of hydrogen storage alloys.

UNIVERSITY of the WESTERN CAPE

For multiple cycles, the hydrogen storage medium must also be resistant to deactivation. The deactivation of the hydrogen storage alloys is caused by the oxidation of the alloy's surface. For hydrogen to enter the alloy and form metal hydride, molecular hydrogen first must dissociate into hydrogen atoms. Fresh and clean hydrogen storage alloy surfaces can readily dissociate molecular hydrogen. However, when the alloys are exposed to air, oxides are formed on the alloy surface, and the possibility that molecular hydrogen can be disassociated into hydrogen atoms is greatly reduced, this leads to the deactivation of the alloy. Pt group metals are well known catalysts for dissociation of molecular hydrogen, and they have been used to improve the hydrogen storage performance of the alloys by electroless plating, mechanical grinding to nano-size and ion beam sputter deposition to the surfaces of the alloy. This treatment also results in high durability of hydrogen storage and activation after air exposure. The ready activation behavior and fast adsorption/ desorption rates can be retained even after more than 2 years air exposure [67].

It is also reported that pre-treatment of intermetallic compounds in alkaline hydroxide solutions like NaOH, LiOH and KOH have a positive effect on the initial activation kinetics. The presence of alkaline elements on the surface of the alloy appears instrumental to the dissociation of H_2 and H_2O. The surface becomes modified and subsequent H_2 absorption reaction in the gas phase commences in spite of the fact that the surface is covered by hydroxide. The ease in initial activation can be attributed to alkaline elements in the surface oxide which ensures that electron transfer from the surface of the alloy to H_2 is relatively fast. A standard procedure for this kind of pretreatment is as follows; the powder sample is oxidized for about 30 days at 1 bar in air. The samples for the H_2 gas phase reaction are soaked in 3 M or 6 M alkaline hydroxides for 3hrs and then dried in air. In order to reduce the hydroxide layer formed, the dried sample samples are thoroughly rinsed in fresh distilled water at room temperature. The initial activation of the samples for gas phase reactions is then measured using a Sievert type apparatus [70].

On the other hand, carbon nanotubes doped with palladium have been shown to have an increased hydrogen storage capacity (approximately three times greater) and exhibited faster initial hydrogen adsorption kinetics when compared with pristine samples. The compensation of the individual hydrogen storage capacity of the metal nano-particles suggests that the enhancement of storage capacity in metal doped CNT is a result of the spill-over phenomena. Additionally, the re-adsorption studies using previously adsorbed samples indicated that metal nano-particles spill the hydrogen predominantly on to the low energy physisorption binding sites, such as the external wall or groove sites on the carbon nanotubes [18]. The results suggest that metal doped CNT can

UNIVERSITY of the WESTERN CAPE

be envisaged as a more pragmatic solution for hydrogen storage as far as the storage capacity and adsorption kinetics are concerned.

UNIVERSITY of the
WESTERN CAPE

2.6.4. Approaches for elimination of problems relating to pyrophoricity and decrepitation

To overcome the problems of sensitivity and the pyrophoric nature of the nano-sized intermetallic hydrides, and to obtain a high reactivity for the hydrogen sorption process, the surface modification should involve a coating with stable inorganic compounds. A new surface treatment method, which employs a flouride ion containing aqueous solution, was successfully applied to intermetallic hydrides [73].

As a consequence of the large volume increase upon hydrogenation, intermetallic compounds break into small particles in a process called decrepitation. This phenomenon is related to embrittlement, cracking, and reduction of the grain particle size. Cracking of the original grain leads to particle size below 10 μm. One of the advantages of this phenomenon is the improvement of the reaction rate with cycling due to the increasing active surface area but it also activates corrosion by the renewal of the fresh surfaces. Solutions to these type problems are not of utmost priority in this particular project and details can be obtained in literature [71].

UNIVERSITY of the
WESTERN CAPE

2.7. Summary

Based on the identified short comings of solid-state hydrogen storage materials which include but are not limited to:

- Thermodynamic problems.
- Slow kinetics (uptake and release).
- Low storage capacity.
- Low gravimetric and volumetric densities (not light in weight and conservative in space).
- Cycle lifetime for hydrogen sorption.
- Mechanical strength and durability.
- Safety under normal use and acceptable risk under abnormal conditions

We have chosen to modify an intermetallic alloy of the AB family (Ti/Fe) because of its low cost, availability and most importantly reactivity with hydrogen at reasonably low temperature and pressure close to ambient conditions. Having concluded this, it is imperative to note (from *Table 2.1*) that this alloy presents other inherent short comings including comparatively low weight % capacity, difficulty in activation and low resistance to impurities in H_2. The main aim is to employ scientific approaches for improvement of this alloy for future commercial application in hydrogen storage.

UNIVERSITY of the WESTERN CAPE

From (*2.6*) we see that a "layer by layer" synthesis of a novel material can change the bulk properties and modify the surface characteristics of the materials.
It is necessary to understand the fundamental atomic processes in the hydrogen sorption process, the role of surface structure and surface catalysts in the hydrogen storage process, the role of hydrogen promoted mass transport on phase transformations, and thermo-physical properties of the potential hydrogen storage materials. All of these parameters can be altered through the deliberate introduction of various moieties; the hydrogen storage materials can be engineered on a nano-scale level to have the desired properties.

The first step in the synthesis of these new hydrogen storage materials is the control of the particle and the grain size. Reducing the particle size and the grain size into the nano-regime can enhance many desirable properties [74, 75]. Methods for controlling the particle size and grain size by ball milling of the starting alloy will be explored by altering milling parameters like

speed, time, diameter of balls used, number of balls used, mass of sample used, reverse or non reverse technique, atmosphere of milling (ambient, dry, wet) and adding specific surface moieties to enhance the hydrogen adsorption properties (carbon nanotubes). It should also be noted that the synergy effect of physical and chemical methods of H storage allows a prospective scenario allowing to suit different applications. We intend to optimize the conditions of carbon nanotube synthesis on the surface of the intermetallic alloy and at the same time improve the quality of yielded carbon nanotubes by altering the hydrocarbon pyrolisis parameters including flow rate, hydrocarbon source, temperature and time of synthesis; to get the best possible combination.

By combining different materials with suitable catalytic and thermodynamic properties, new classes of hybrid hydrogen storage materials can be developed. By altering the materials on the nano-scale, the research may also provide insight into the mechanisms responsible for the recently reported improvements in storage and kinetics of hydrides when dopants are added to these materials. Similarly, improvements in the lifetimes of hydride-based storage materials may be possible if we examine nanostructured materials to elucidate the mechanisms for associated degradation processes and sensitivity to impurities. This approach is expected to allow the directed design of new, higher-efficiency, recyclable hydride-based materials. Characterization of synthesized materials will be by SEM, TEM, XRD, TGA, BET and Sievert's apparatus.

UNIVERSITY of the
WESTERN CAPE

Chapter 3

3.1. Research materials and methodology:

All materials and methods used in preparation of this low temperature hydrogen storage composite are listed in this section. The characterization of physico-chemical properties of the separate layers in this composite is imperative in order to envisage the properties brought to bear on the composite. This presents the reference point for optimization of experimental procedures and application of standard protocol for characterization of the composite.

As reviewed in *chapter 2*, the physical and chemical properties of these materials change drastically upon decreasing their particle size to the nanometer regime thereby necessitating the need to understand and measure the enhanced properties. The inherent properties of the bulk materials have already been elaborated in *chapter 2*.

As well as the materials and methods used, the workings of the various characterization techniques employed for analysis of these materials are elaborated.

UNIVERSITY of the
WESTERN CAPE

3.1.1 Materials:

All materials used and suppliers are listed below

Table 3.1:

Material	**Supplier**
Iron-Titanium powder (60:40 wt%)-40mesh	Alfa Aeser
Liquefied Petroleum Gas (LPG) (C_3H_8, C_4H_{10})	Afrox (South Africa)
Palladium (II) chloride (99.9%)	Aldrich Chemicals.
Tin (II) chloride dihydrate	Aldrich Chemicals
Hydrochloric acid, 37%, A.C.S reagent	Aldrich Chemicals
Mg acetylacetonate dihydrate (98%)	Aldrich Chemicals

Mg bis (2,2,6,6- tetramethyl-3,5-heptanedionate) monohydrate (97%)	Aldrich Chemicals
Retsch planetary ball mill (PM 100)	Monitoring and Control (Pty) Ltd
Pyro-therm furnace	Market Harborough, U.K
Titanium hydride	Aldrich Chemicals

3.1.2: Methods of synthesis:

The composite material for hydrogen storage was synthesized using the methodologies outlined in the subsequent sections. Some of the techniques have been adapted from literature for the purpose of this investigation, whereas other techniques are novel and have been developed by us.

(i) Mechano-chemical pre-treatment of commercial Ti/Fe alloy by ball milling

The ball milling pretreatment was carried on commercially obtained Iron-titanium powder (60:40 wt%, -40 mesh, Alfa Aesar) in a Retsch planetary ball mill with a tungsten carbide jar of weight (6.1kg) and tungsten balls of diameters 2cm and 3cm. The size of balls affected the milling productivity. Generally, big sized balls are useful as the weight of the bearings imparts more striking energy on the powders. However, increasing the ball size increases the space between the bearings and this situation causes delays in breaking the powders in the mechanical milling process. While the size of the ball increases, the strike power of the balls also increases so the deformation of powders and the flatness rate increase more than the small balls but the space between the balls are more than the small ones so this could affect the period of powder breaking. This phenomenon is subject to further study.

The milling atmosphere was dry. The powder to ball ratio in all experiments was maintained at 1:20. There must be enough space for the movement of balls and powders freely because of the milling among the powders and the strike power over these powders. If there is not enough space, bearing does not act freely in the milling chamber and the power over the powders will decrease.

Rotation speed was oscillated between 100 rpm, 200 rpm and 350 rpm. Rotation speed was maintained at a maximum of 350 rpm because for higher speed, excessive heat and vibrations were observed.

UNIVERSITY of the WESTERN CAPE

(ii) *Modification of the surface of Ti/Fe alloy with carbon nanotubes by LPG pyrolysis for composite material preparation*

Based on a model experiment of synthesis of carbon nanotubes on nickel and cobalt substrates using LPG as a carbon source which is elaborated in *chapter 4.2.1*, a similar deposition technique was adopted for the surface modification of pre-treated and as is iron-titanium alloy.

Pre-treated and as is iron-titanium powder was used. In a typical experiment, 5.0g of the powder was weighed into a glazed porcelain sample boat, the boat was loaded into the CVD system, and the CVD system was flushed with nitrogen for 10 minutes. Under a nitrogen flow, the temperature was ramped up to 800^{o}C, once stabilized, the nitrogen flow was terminated and the LPG flow was initiated for 10, 30, 60 and 120 minutes. Different deposition time regimes are shown from (*4.2.1*) in the subsequent chapter to influence the quantity and quality of synthesized nanotubes. After the time had elapsed, the LPG flow was terminated and the samples were cooled under a nitrogen flow to 150^{o}C and collected in a vial for characterization.

UNIVERSITY of the WESTERN CAPE

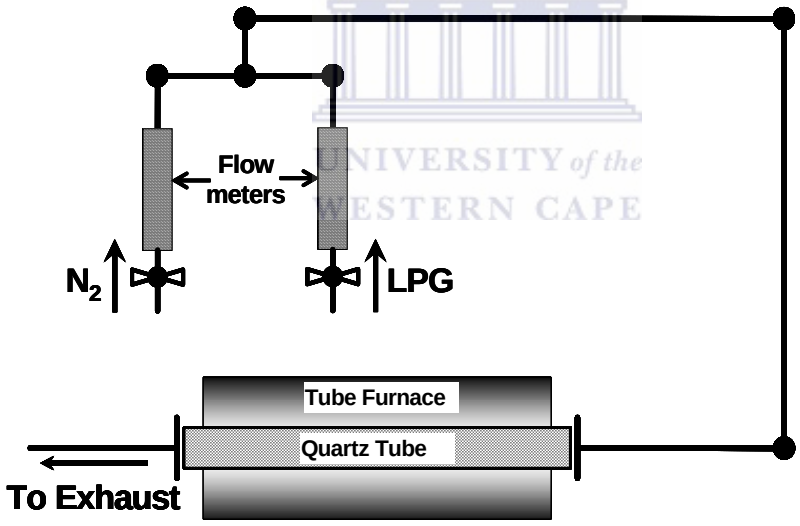

Fig 3.1: Schematic diagram of the CVD set-up for carbon nanotube synthesis using LPG

(iii) *Deposition of palladium layer to improve activation kinetics of composite*

Palladium was deposited on the surface of the nanotube-alloy composite using electroless deposition method. The nanotube-alloy (Ti/Fe-CNT) composite surface was activated by stirring 1.00g in 5.0mL of a palladium-tin colloidal solution for 45 minutes. The colloidal solution was then decanted, and the activated composite was rinsed with three 10.0mL aliquots of a 10% hydrochloric acid solution, and three 10.0mL aliquots of de-ionized water. 10.0mL of a 0.5g/L of palladium (II) chloride and 10.0mL of 25% ammonium hydroxide were mixed in a separate container, and then added to the activated composite; to initiate palladium deposition 2.0mL of a 99% hydrazine solution was added to the mixture. The mixture was left stirring overnight, and then the powder was recovered by filtering and thoroughly washing the powder over a 0.45 micrometer nylon membrane.

UNIVERSITY of the
WESTERN CAPE

(iv) *Deposition of magnesium layer to increase hydrogen weight capacity of composite*

1.000g of the Ti/Fe + CNT+ Pd composite was added to a mixture of 0.1006g Mg bis (2, 2, 6, 6-tetramethyl -3, 5- heptanedione monohydrate and 0.0500g Mg acetylacetonate in a sonication cell. The sonication of the slurry with the high-intensity ultrasound radiation was carried out for 3 hours by direct immersion of the sonication cell in a bath sonicator under a flow of an argon/hydrogen mixture as a reducing agent (90:10) %. The substrate was then washed thoroughly in 200ml acetone, filtered and dried in vacuum.

3.2. Structural characterization of composite materials:

3.2.1. X-ray diffractometry:

X-ray diffractometry (XRD) is a potent means of studying the crystallinity and atomic structure of materials and will elucidate phase changes in the composite and particularly amorphization of the core material after mechano-chemical pre-treatment. It is generally regarded as an all important standard in characterization of materials. It is extensively used in the determination of Bravais lattice types and unit cell dimensions. The dimensions of x-ray wavelengths are in the same order as nano-particle sizes, hence its application in this study. XRD allows for the study of crystal anisotropy and the correlation between structural features and observed chemical properties [76]. XRD analysis can be used in conjunction with known chemical information to establish a structure-chemical relationship in surface sensitive reactions.

The dynamics of XRD show that crystalline solids are bombarded with a collimated x-ray beam which causes crystal plane atoms, serving as diffraction gratings to diffract x-rays in numerous angles. Each set of crystal planes (*hkl*) with inter-planar spacing (d_{hkl}) can give rise to diffraction at only one angle. The diffractions are defined from Braggs' law ($n\lambda = 2d \sin \theta$), where the intensities of diffracted x-rays are measured and plotted against corresponding Bragg angles (2θ) to produce diffractographs. The intensities of diffraction peaks are proportional to the densities or abundance of the corresponding crystal facets in the material lattice. Diffractographs are unique for different materials and can therefore qualitatively be used for material identification. XRD can also be used quantitatively for the determination of average particle size by use of the Scherrer equation, given as:

$$D = 0.9\lambda / \beta \cos \theta$$

Where D = particle size; 0.9 = shape factor; λ = x-ray wavelength; β = peak-width at half peak-height (radians); θ = angle of reflection [77-78].

In this analysis, un-treated, pre-treated intermetallic alloy and composite materials were studied. The measurements were performed using the filtered Cu-Kα_1 radiation (λ=1.540598 Å) and

Debye-Scherrer geometry of the sample holder. Exposition time was 10 seconds per point, range of the 2θ Bragg angles was of 20 to 90 degrees, with the scanning interval 0.1 degree.

The results were processed by the simplified Rietveld profile analysis using Powder Cell software (version 2.4). Reference data for the constituent phases of the core as produced intermetallide are presented in Table 3.2

Table 3.2 Reference data for the constituent phases of the commercial alloy

Phase	Structure description	Lattice periods, Å			Ref.
		a	*b*	*c*	
$TiFe_2$	Space group $P6_3/mmc$ (# 194) Ti in 4f (x=1/3; y=2/3; z=0.064; occupancy 1) Fe1 in 2a (x=0; y=0; z=0; occupancy 1) Fe2 in 6h (x=0.829; y=0.658; z=1/4; occupancy 1)	4.785	–	7.799	[95]
TiFe	Space group $Pm\,{-}3m$ (# 221) Ti in 1b (x=1/2; y=1/2; z=1/2; occupancy 1) Fe in 1a (x=0; y=0; z=0; occupancy 1)	2.972	–	–	[96]
$TiFeH_{\sim 1}$	Space group $P222_1$ (# 17) Ti in 2d (x=1/2; y=3/4; z=1/4; occupancy 1) Fe in 2c (x=0; y=0.303; z=1/4; occupancy 1) H1 in 2a (x=0; y=0; z=0; occupancy 0.9) H2 in 2d (x=1/2; y=0.297; z=1/4; occupancy 0.4)	3.088	4.515	4.391	[114]
TiH_2	Space group $Fm\,{-}3m$ (# 225) Ti in 4a (x=0; y=0; z=0; occupancy 1) H in 8c (x=1/4; y=1/4; z=1/4; occupancy 1)	4.5345	–	–	[115]
TiO_x	Space group $Fm\,{-}3m$ (# 225) Ti in 4b (x=1/2; y=1/2; z=1/2; occupancy 1) O in 4a (x=0; y=0; z=0; occupancy 1)	4.1766	–	–	[98]
Ti_4Fe_2O	Space group $Fd\,{-}3m$ (# 227/2) Ti1 in 48f (x=0.44; y=1/8; z=1/8; occupancy 1) Ti2 in 16c (x=0; y=0; z=0; occupancy 1) Fe in 32e (x=0.202; y=0.202; z=0.202; occupancy 1) O in 16d (x=1/2; y=1/2; z=1/2; occupancy 1)	~11.3	–	–	[97]

UNIVERSITY of the WESTERN CAPE

3.2.2 Scanning Electron Microscopy:

Scanning electron microscopy (SEM) is a versatile imaging technique capable of producing three-dimensional profiles of material surfaces. SEM is used in this study to extract quantitative and qualitative information pertaining to agglomerate size/shape, particle morphology and surface appearance of the pristine alloy, pre-treated alloy and composite materials.

The basic operation in SEM involves the interaction of an accelerated highly mono-energetic electron beam originating from a cathode filament with the atoms at a sample surface. The electron beam is focused into a fine probe which is disseminated over the sample surface. The scattered electrons are collected by a detector, modulated and amplified to produce an exact re-construction of the sample surface and particle profile [79-80]

The samples of interest were supported on double-sided conductive carbon tape and mounted on a sample stub. No sputter-coating was required as all the samples were electron-conductive. Samples were fitted in the vacuum chamber of the microscope (Hitachi X-650). Parameters for the SEM analysis are given as follows

UNIVERSITY of the
WESTERN CAPE

Working distance (mm):	15
Accelerating gun filament:	Tungsten
Filament current (μm):	75-80
Accelerating voltage (KeV)	25

In parallel with the SEM studies, the EDS component analysis of the samples was carried out, by analyzing the energy spectra of the secondary X-rays. Both total (averaged along the whole surface) and local (in specified points) analyses were performed.

3.2.3 Transmission Electron Microscopy:

Transmission electron microscopy (TEM) probes the internal structure of solids and gives access to micro-structural detail. TEM is used in the investigation of average particle size, particle shape and particle size distribution of alloy and composite nano particles.
In this investigation, TEM was utilized mainly to examine the carbon nanotube layer in the composite in order to verify actual nanotubes, ascertain their shapes, diameter, length, size distribution, and also agglomeration of the alloy after pre-treatment.

In TEM operation, a narrow electron beam originating from the tungsten filament is concentrated onto ultra-thin sample surfaces using a series of magnetic lenses. The electrons interact with sample atoms while penetrating the thin sample structure leading to the transmittance of electrons and production of secondary electrons. Secondary electrons pass through an aperture to produce an image on a fluorescent screen [81].
TEM samples were prepared by dispersion of a spatula-tip of the catalyst of interest in 5ml methanol solution, followed by sonication of the suspension. One drop of the suspension was deposited on a carbon/Formvar® film coated copper grid. The methanol was allowed to evaporate at room temperature. Samples were mounted in a sample holder which was introduced directly into the shaft of the microscope (LEO EM 912 and Hitachi H-800 EM). Experimental parameters are given as follows:

UNIVERSITY of the WESTERN CAPE

Accelerating voltage (kV):	200
Current (μA)	20
Condenser aperture	1
Objective aperture	3
Exposure time (seconds)	3

3.2.4 Surface area and porosity determination by N_2 physisorption:

It is widely stated in literature (*chapter 2*) that the Brunauer-Emmett-Teller method, in gas absorption was best suited for the determination of total surface area and porosity of catalysts and composite materials. In this investigation, the surface area and porosity of the alloy (pristine and pre-treated) and composite materials could be determined with high sensitivity using an accelerated surface area and porosity analyzer (Micromeritics Tristar). This information can be used to demonstrate how the surface microstructure, surface area and porosity may affect the reactivity of catalysts and the distribution of reagents and products on the catalyst surface. This technique is particularly useful when the surface morphologies of materials are unknown.

The accelerated surface area and porosity analyzer consisted of a mercury manometer, gas-tight burette, and thermostat, liquid N_2-cooled Dewar flask and a high-vacuum oil pump. High pressures and cryogenic temperatures are used to increase the absorption rate onto solid surfaces [82].

In the basic operation, the samples are placed in an evacuated sample holder at constant temperature ~190^{o}C. The sample holder is filled with helium gas to flush contaminating gases from the sample surface and pores. The helium gas is then purged from the system. Evacuated samples are cooled to -196^{o}C in a liquid N_2 bath while the sample holder is filled with ultra-pure N_2 gas. Pressure within the sample holder is monitored over time and then rapidly reduced to reach an equilibrium state where the quantity of gas absorbed onto the surface is equivalent to the quantity of gas removed from the gas phase. By plotting the quantity of N_2 absorbed versus the equilibrium pressure an adsorption isotherm is obtained which together with the BET equation can be used to determine sample surface area. This adsorption isotherm can be defined as the plot of the dependence of the fractional coverage of surface absorbed molecules on pressure at constant temperature. The BET equation can be given as follows:

$$\frac{1}{W[(P_0/P) - 1]} = \frac{1}{W_m C} + \frac{(C-1)}{W_m C}\frac{P}{P_0}$$

Where W is the weight of N_2 adsorbed at a given relative pressure (P/P_0), W_m is the weight of gas producing monolayer coverage and C is a constant related to the heat of adsorption.

3.3 Thermal and Gravimetric characterization of the alloy and composite materials:

Thermal analysis monitors the properties of materials as they change with temperature. Important thermodynamic, kinetic and physical properties can be monitored using thermal analysis. In this investigation, the thermal stability and the H mass capacity of the alloy and composite materials are studied by thermogravimetry.

TGA involves the continuous weighing of solids using a thermo-balance, while they are heated at a constant rate. Samples are generally heated in inert environments, in this case (10% H_2, balance Argon) and undergo increases in kinetic motion resulting in physical and chemical changes which result in the thermal decomposition of solids to form detectable products. The output signal is a thermogram which is a plot of weight change as a function of increasing temperature. Weight changes can be credited to thermal events such as phase transition, melting, volatilization, thermal decomposition, sublimation, oxidation or dehydration. Information on thermal decomposition range, sample composition and thermal stability range of alloys and composites can be obtained by TGA.

The morphology of nano-materials leads to thermal behavior that deviates from that of the bulk materials [83]. This deviation is manifested in a detectable particle size effect in TGA. Thermal decomposition temperatures of solids decrease with a decrease in particle size due to a relationship where thermal conductivity increases with a decrease in particle size.

TGA was conducted using a simultaneous thermal analyzer (Rheometric Scientific STA 1500) and a 10%H_2, balance Argon atmosphere. Samples were ramped from 25^{o}C to 450^{o}C at 5 ^{o}C/min heating rate. Sample weight was maintained at ~5mg.

UNIVERSITY of the WESTERN CAPE

3.4 Volumetric characterization of core alloy:

Volumetric investigation of the composite materials was done using the Sieverts type apparatus. This specialized apparatus is a set-up for measurement of sorption properties of solid materials. In other words, it is intended for the precise volumetric measurements of quantity of hydrogen adsorbed or desorbed by a hydrogen storage material (hydride forming alloy, carbon nanomaterials, composite, etc.) depending on time, applied hydrogen pressure and sample temperature. In particular, the following about hydrogen sorption performances of the materials can be obtained using the Setup:

- Hydrogen absorption and desorption capacities.
- Pressure –Composition – Temperature (PCT) relations in the system "material – hydrogen gas"
- Hydrogen adsorption / desorption kinetics.

Precise kinetic measurements can be done only assuming that special additional measures are taken to provide the uniform temperature in the sample bed. Otherwise only estimates of the dynamic H sorption performances of the sample having specified geometry, weight and packing density in the specified reactor can be obtained.

UNIVERSITY of the
WESTERN CAPE

The Setup is characterized by the following main performances:

- Volume of the sample of the material under study, cm^3 ~ 0.5
- Range of the sample temperatures, ^oC……-196…+500
- Range of hydrogen pressures, bar (absolute)……0…160
- Accuracy in the determination of the quantity of the absorbed H_2, cm^3*bar STP, at ambient temperature 20…30^oC, not worse……1.5

The principal of operation and layout is in the determination of the quantity of hydrogen adsorbed by (or desorbed from) a sample of a hydrogen storage material of the known weight, starting from the pressure change in the closed volumetric system of the known volume.

The Setup is manually-operated. Data acquisition is provided automatically.

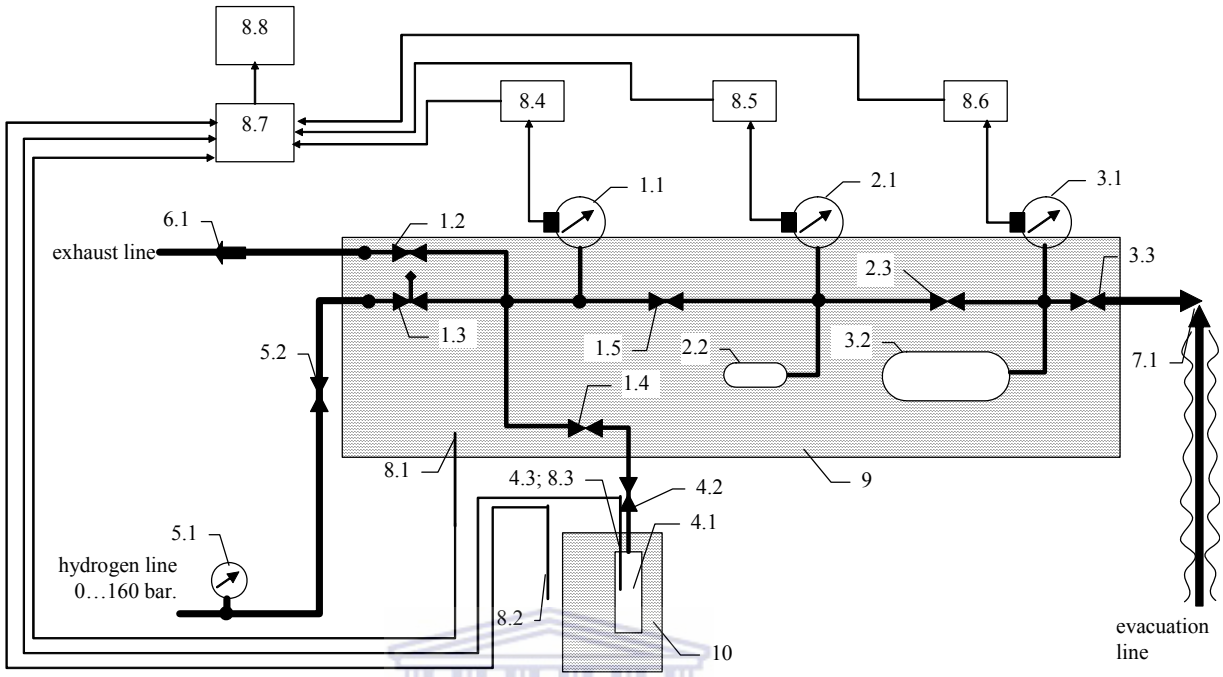

Fig 3.2: Schematic diagram of the Sieverts apparatus at SAIAMC.

UNIVERSITY of the
WESTERN CAPE

The schematic diagram of the set-up is presented in the (*Fig3.2*) above. The set-up includes the following gas/measurements scheme:

1. **High-pressure collector:**
   - **1.1. Pressure sensor 160 bar FS**
   - **1.2. Exhaust valve**
   - **1.3. H_2 input valve**
   - **1.4. Reactor valve**
   - **1.5. Medium-pressure connection valve**
2. **Medium-pressure collector:**
   - **2.1. Pressure sensor 16 bar FS**
   - **2.2. Buffer cylinder 75 cm^3**
   - **2.3. Low-pressure connection valve**
3. **Low-pressure collector:**
   - **3.1. Pressure sensor 2.5 bar FS**
   - **3.2. Buffer cylinder 500 cm^3**
   - **3.3. Evacuation valve**
4. **Reactor assembly**
   - **4.1. Reactor body**
   - **4.2. Gas connection line with locking valve**
   - **4.3. Thermocouple**
5. **H_2 supply line:**
   - **5.1. Manometer 160 bar FS**
   - **5.2. H_2 supply valve**

6. **Exhaust line:**
   - 6.1. **Check valve**
7. **Evacuation line**
   - 7.1. **Vacuum valve**
8. **Data acquisition system**
   - 8.1. **Thermistor measuring bath temperature**
   - 8.2. **Thermistor measuring room temperature**
   - 8.3. **Thermocouple measuring sample temperature**
   - 8.4. **160 bar pressure indicator / transmitter**
   - 8.5. **16 bar pressure indicator / transmitter**
   - 8.6. **2.5 bar pressure indicator / transmitter**
   - 8.7. **34970A data acquisition / switch unit**
   - 8.8. **PC**
9. **Bath**
10. **Thermostat / furnace**

3.5. Synopsis of main points:

Characterization studies were initiated by the investigation of structural properties using the fundamental characterization techniques, namely scanning and transmission electron microscopy and x-ray diffractometry. A couple of other analytical techniques were employed in this investigation. These techniques addressed the minimum set of physico-chemical properties identified in the literature review. Structural and chemical information and the characterization techniques used in their determination can be summarized as follows:

- Crystal structure, crystallinity and particle size of the alloy (untreated and pretreated) could qualitatively be studied using XRD.
- Topography, surface micro and macro structure, length of carbon nanotubes could qualitatively be studied using SEM.
- Alloy particle size, particle distribution, dispersion/agglomeration of pre-treated alloy and diameter of carbon nanotubes could be studied using TEM.
- Total surface area and porosity of composite materials could quantitatively be studied using BET N_2 physisorption.
- Hydrogen gravimetric capacity and thermal stability of the alloy and composites could quantitatively be studied by TGA.
- Hydrogen volumetric capacity and adsorption/desorption kinetics of the alloy could be quantitatively studied using the Sievert's type apparatus.

UNIVERSITY of the
WESTERN CAPE

Methodologies for pretreatment of the commercial Ti/Fe alloy and surface modification with carbon nanotubes have been comprehensively described. Techniques for layer by layer deposition of nano-binary metal hydrides on the composite for enhanced physico-chemical properties were also detailed.

Experimental tasks for the nano-engineering of this composite low temperature hydrogen storage material based on Ti/Fe alloy were identified and implemented after a holistic literature review in *chapter 2*. The results of above highlighted experimental tasks as well as efficacy of characterization tools employed in this chapter are presented in *chapter 4*.

Chapter 4

4.1. Use of ball milling technique for mechano-chemical pre-treatment of Ti/Fe alloy:

Nano-crystalline materials (i.e. polycrystalline metals, alloys and compounds with particle size within the nanometer range) exhibit unusual and promising physical, chemical, and mechanical properties [84-87]. A decade ago, high energy ball milling and mechanical alloying of powder mixtures, were reported to be efficient techniques for the preparation of nano-crystalline metals and alloys. Indeed, as a mechanical processing technique, ball milling is effective for the production of micrometer size particles made of nano-size grains. High energy ball milling is also a way of producing chemical reactions (mechano-chemistry), changing the reactivity of solids (mechanical activation) and a way of inducing phase transformations [85]. This complexity still avoids establishing the necessary theoretical background for the prediction of non equilibrium phase transitions under milling process. However, understanding of the mechanical activation to stress mode dependence, mentioned above, should be very valuable in optimizing the activation process, the subsequent treatment and microstructure of the final materials. Among all non equilibrium preparation methods, mechanical milling has become a popular technique because of its simplicity, relative inexpensive equipment and applicability to most intermetallic compounds.

The influence of mechanical milling on kinetics and thermodynamic H-properties of AB_5 based alloys have been reported in literature [85]. Short milling process yields non-homogeneous, micro-structural (wide distribution of nano-crystallite sizes and amorphous phase) morphological alloy powders. The short-milled alloy exhibits extra H-trapping sites in amorphous domains as detected by thermal desorption [85].

The hydrogen storage capacity, the number of times the storage can be done reversibly, and the kinetics of hydrogen adsorption/desorption are intimately linked to the alloy microstructure. Powder particles having nano-structured features have some definite advantages. Effectiveness of ball milling in promoting hydrogen adsorption in metals results from several factors; (i) the formation of a large amount of oxide-free surface; (ii) the rapid reduction in grain size; (iii) the introduction of significant lattice defects in the grains. During ball milling, the refinement of the powder particles, availability of large surface area, formation of new fresh surfaces, and variable defects such as dislocations, vacancies and microcracks, all contribute to trapping gas in the milled powder through physisorption, chemisorption and dissociative chemisorption [86]

UNIVERSITY of the WESTERN CAPE

The hydrogen adsorption alloy Ti/Fe requires activation treatment before use, because their surfaces have been covered by oxide layers, absorbed gases, moisture and so on which impede hydrogen adsorption. The activation treatment is hitherto usually performed by a number of heating-cooling cycles in a hydrogen atmosphere or in a vacuum [87]. Although the mechanism of the activation is not as yet fully understood, the proposed mechanisms are divided roughly into two groups. The first one is that the activation treatment of Ti/Fe gives rise to Fe-rich clusters close to its surface and these clusters catalyze the dissociation of hydrogen gas. The other is that the activation treatment leads to structural and morphological changes of the powder, i.e. generation of new surfaces by cracking. On the other hand, in powder metallurgy, it is well known that fresh surfaces are mechanically created by milling. Consequently, if the alloy is milled and then hydrogenated without exposure to the air, hydrogen is expected to be readily adsorbed [88].

Milling is done in a closed vial because it has been shown that milling in an open vial would lead to quick agglomeration of the particles, which invariably would hinder gas diffusion in the material. Different structural evolution for the sample milled in an open vial and in a closed vial should be attributed to the difference of the local temperature and/or pressure during milling. This is in addition to the fact that in an open vial, the alloy surface is more susceptible to oxidation thereby forming oxide layers that would also hinder gas diffusion.

We have employed the dry-milling technique in this particular project for various salient reasons. There is a considerable body of knowledge on the explosion characteristics of micron-scale powders (particle sizes ranging from about 10 to 500 μm).Consistent with easier ignition is the fact that some nano-powders are pyrophoric, that is they spontaneously ignite when exposed to air. An example of a pyrophoric nano-powder is iron [89].

The moisture content of the dust will affect the ease of ignition and its ability to sustain an explosion. Increasing the moisture content increases the ignition energy, for some dusts the increase can be exponential, and reduces the explosion violence (the water vapor produced acting as an inert heat sink). The presence of a flammable solvent in the dust will have the opposite effect, lowering the ignition energy and possibly increasing the explosion violence [89].

It has also been observed that cracked and irregular (amorphous) surfaces are more favorable for hydrogen adsorption [89]. Dry milling offers us the best option to collapse the crystalline structure of the alloy due to the abrasiveness of the ball to powder contact; because the presence of liquid in the milling media seems to be a significant factor in decreasing losses in the crystallinity of the sample, e.g., by preventing local temperature from increasing and by leading to a partial re-crystallization of the amorphized regions [90].

UNIVERSITY of the WESTERN CAPE

4.1.1. Influence of rotation speed and ball size on agglomeration of Fe/Ti particles:

For the samples milled with 100 rpm speed, the synthesized powder was observed to be finely dispersed in the medium, regardless of the ball size used or the time of milling (even though for the purpose of consistency of results a time matrix of between 15 minutes, 30 minutes, 60 minutes and 90 minutes was adhered to. Even at 90 minutes this speed was however not efficient for complete deformation of powder as observed visually. The treated sample was similar in structure and grain size to the pristine material as shown by the various characterization techniques. The assumption for this result is that the kinetic energy of the balls in contact with the powder is too low to effect much lattice disorder or damage. It is important to note that the extent of fracturing and cold-welding of the alloy is directly proportional to the amount of energy exerted in the vial.

For the samples milled with 200 rpm speed, the results were very similar to that of the samples milled with 100 rpm. Considerable difference in structure and particle size only became evident after 60 minutes of milling as shown by different characterization techniques. However a higher surface area for each sample milled with 200 rpm than the corresponding samples in the matrix for the samples milled with 100 rpm indicates that there has obviously been better degradation of the alloy powder. The crystallinity of original powder, however, remains unchanged as shown by XRD analysis. The explanation could be that the reaction that has taken place is mechanical grinding (which does not significantly change the grain size of the material, but only reduces the powder size and breaks up the oxide layers) but not necessarily powerful high-energy milling (which can lead not only to nano-crystalline structure, but also to amorphization). Although there are thinner powder particles, fracturing and cold welding of the grain structure is apparently absent in this experiment.

For the samples milled with 350 rpm speed, considerable deformation of the powder takes place after short milling time (15 minutes), regardless of the ball diameter however the bigger balls (3cm) showed an increased impact on powder deformation. At 90 minutes however an agglomeration of the powder is observed. This happens precisely between 60 and 90 minutes because at 60 minutes the powder particles are well dispersed in the medium. An explanation for this is extensive fracturing and cold welding of the particles by this high energy reaction which precipitates larger grain sizes when the grains are pulverized to their small amorphous sizes and start clamping together. The formation of larger aggregates that are composed of small

amorphous particles is probably caused by the compression of material between balls and walls of vessel as well as between balls themselves during the milling.

We regard our optimum milling time as the time when the grains are pulverized to their minutest and yet remain separately and uniformly dispersed in the milling medium. Here the cold welding interfaces do not possess enough force of attraction to latch the smaller particles unto the slightly larger particles (agglomeration). This lattice deformations and subsequent creation of fresh surfaces (highest surface area) offers the optimum gas diffusion options.

Table 4.1 shows the effect of milling parameters on the surface area of the pre-treated alloy.

Table 4.1: Influence of ball diameter on surface area of alloy:

Sample numbers	Time (minutes)	Speed (rpm)	Ball size (cm)	Surface area (m^2/g)	Agglomeration
(unmilled)	-	-	-	0.0389	-
1	15	100	2	0.1039	-
2	15	100	3	0.1721	-
3	30	100	2	0.1250	-
4	30	100	3	0.1982	-
5	60	100	2	0.1402	-
6	60	100	3	0.2111	-
7	90	100	2	0.1500	-
8	90	100	3	0.2284	-
9	15	200	2	0.1355	-
10	15	200	3	0.1957	-
11	30	200	2	0.1563	-
12	30	200	3	0.2111	-
13	60	200	2	0.1852	-
14	60	200	3	0.2301	-
15	90	200	2	0.1910	-
16	90	200	3	0.2580	-

UNIVERSITY of the WESTERN CAPE

17	15	350	2	0.7633	-
18	15	350	3	1.2566	-
19	30	350	2	1.1623	-
20	30	350	3	1.9995	-
21	60	350	2	1.1923	-
22	60	350	3	2.0289	-
23	90	350	2	1.1923	+
24	90	350	3	2.0275	+

Here, we observe a consistent increase in surface area for all the milled samples with increase in milling time and ball size. There is a slight decrease between 60 and 90 minutes for the 350 rpm-3cm balls, an explanation for this could be that the agglomeration observed within this milling time is accountable for the slight decrease since the powder particles are beginning to stick together thereby blocking the fresh surfaces that have been created. However, the powder milled for 60 minutes- 350 rpm with 3 cm balls offers us the highest surface area.

UNIVERSITY of the WESTERN CAPE

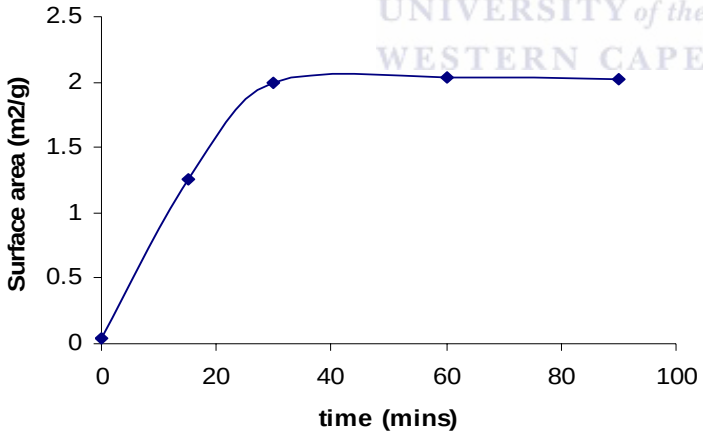

Fig 4.1: Influence of milling time on the samples milled with 3cm balls at 350 rpm.

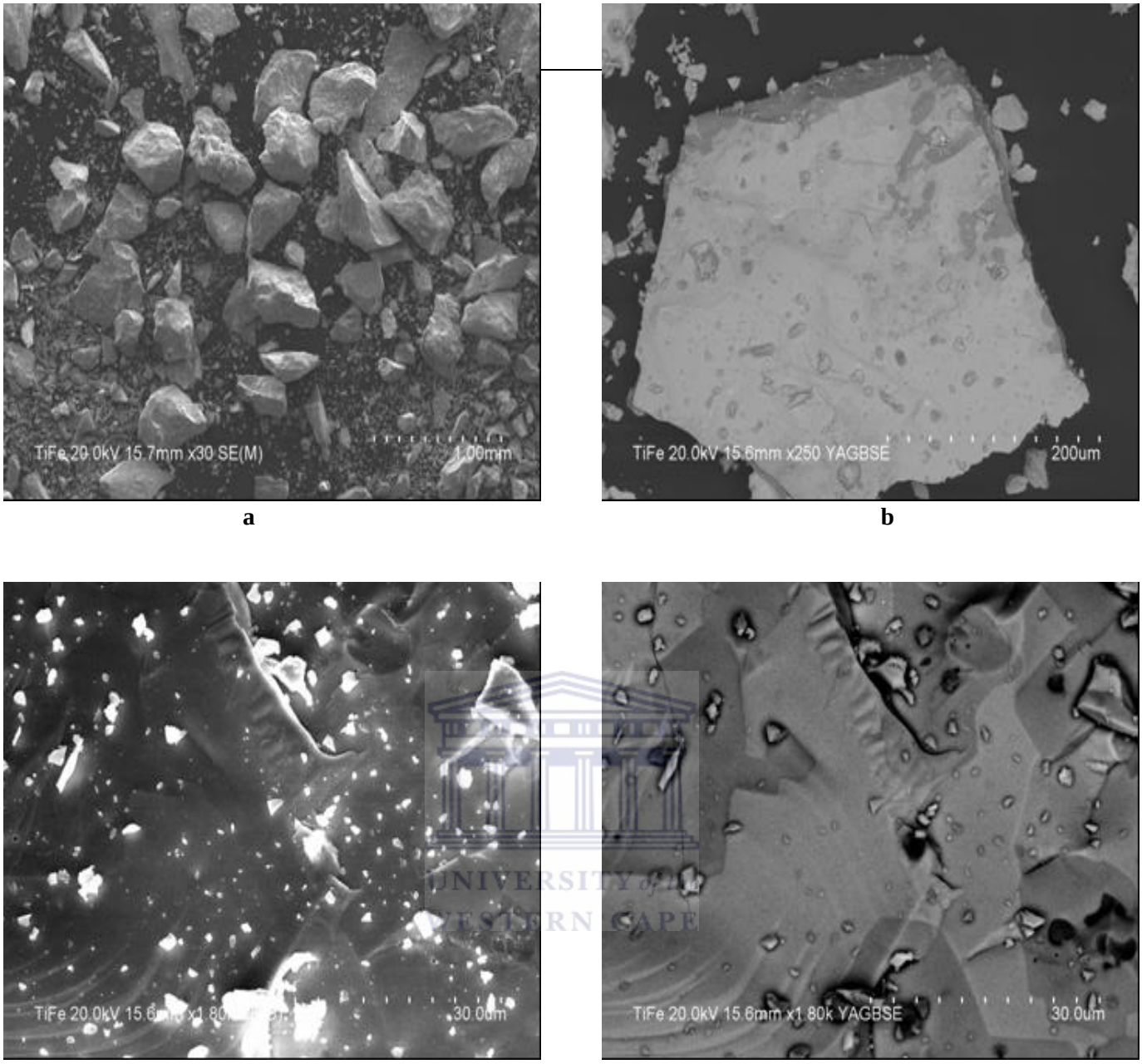

Figure 4.2: SEM images of the pristine Ti/Fe sample:

The SEM images of the Ti/Fe sample are shown in Figure (a–d). As it can be seen from the low-magnification image (Figure a), the Ti/Fe powder mainly consists of rather big isotropic particles, 200 to 500 μm in the cross direction. The typical particle is shown in Figure b; and the pictures (c and d). It has to be noted that for this sample in the studied series; "jumps" of the particles indicating their charging in the course of the measurements were sometimes observed. This, together with bright spots on SE images at high magnifications (Figure c), testifies that the

surface of Ti/Fe particles is covered by a thick enough dielectric, most probably, oxide layer. It correlates with our data on hydrogenation behavior of this material, according to which it is very difficult to be activated: even after 3 activation cycles including heating to 450– 500^{o} C in oil-free vacuum better than 10^{-5} mbar followed by exposition in 99.99999% purity hydrogen at *P*~30 bar and room temperature, the hydrogen sorption capacity does not exceed the value H/ Ti/Fe=0.35, i.e. about 18% of the maximum value reported in the literature, hence the need for mechano-chemical pre-treatment and surface modification of this alloy. The high-magnification YAGBSE image (Figure d) clearly shows that the sample has two phases; the impurity phase can be seen as dark-grey cavities in the light-grey matrix

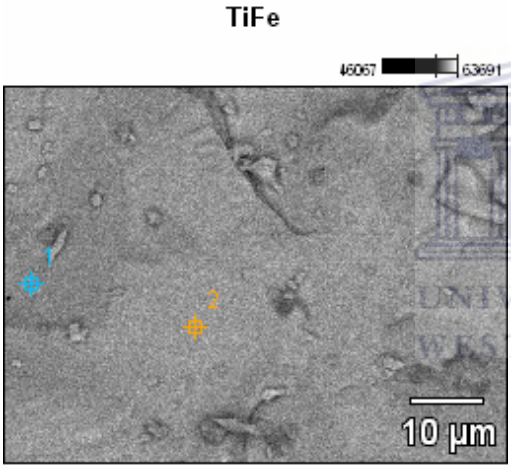

UNIVERSITY of the
WESTERN CAPE

Figure 4.3: Secondary X-ray image of the Ti/Fe sample (the same region and magnification as for Figure.3d). The points correspond to the regions from where the local EDS data were collected (1 – impurity phase, 2 – matrix phase)

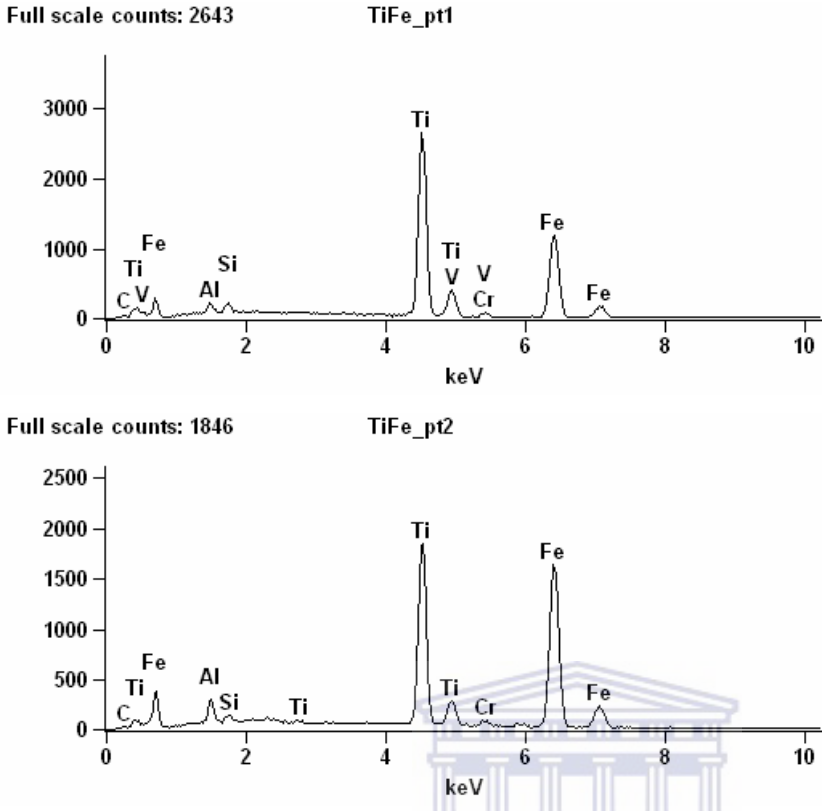

Figure 4.4: Energy spectra of secondary X-rays collected from points 1 (a) and 2 (b) of the Ti/Fe sample.

UNIVERSITY of the
WESTERN CAPE

Table 4.2: Quantitative EDS data from points 1 (a) and 2 (b) of Ti/Fe sample

	Al-K	Si-K	Ti-K	V-K	Cr-K	Fe-L
TiFe_pt1	1123	1309	36187	522	514	2709
TiFe_pt2	1902	693	25884		704	3997

Weight %

	Al-K	Si-K	Ti-K	V-K	Cr-K	Fe-L
TiFe_pt1	1.54	1.33	38.58	0.64	0.71	57.20
TiFe_pt2	2.71	0.74	27.20		0.92	68.44

Atom %

	Al-K	Si-K	Ti-K	V-K	Cr-K	Fe-L
TiFe_pt1	2.92	2.42	41.08	0.64	0.70	52.25
TiFe_pt2	5.18	1.35	29.30		0.91	63.26

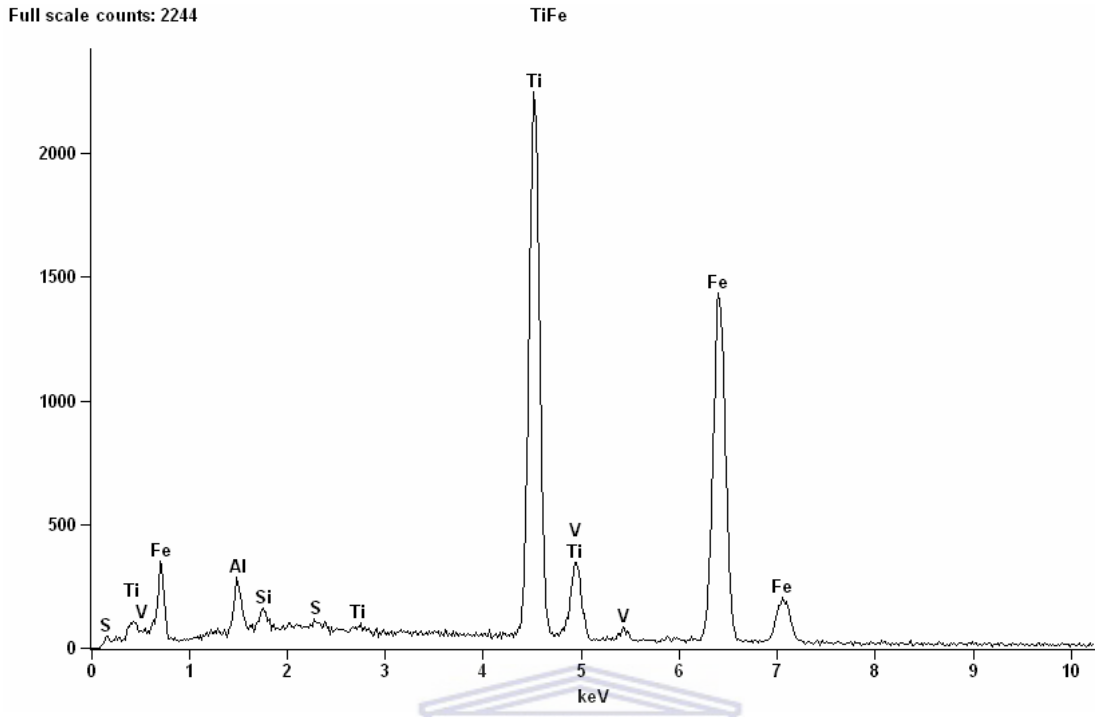

Figure 4.5: Energy spectra of secondary X-rays collected from the total surface of the Ti/Fe sample.

UNIVERSITY of the
WESTERN CAPE

Table 4.3: Quantitative EDS data for the total surface of Ti/Fe sample

Element Line	Net Counts	Weight %	Atom %
Al-K	1708	2.37	4.51
Si-K	832	0.86	1.57
S-K	335	0.28	0.44
Ti-K	30155	31.70	33.92
V-K	870	1.04	1.04
Fe-L	3446	63.95	58.51
Total		100.00	100.00

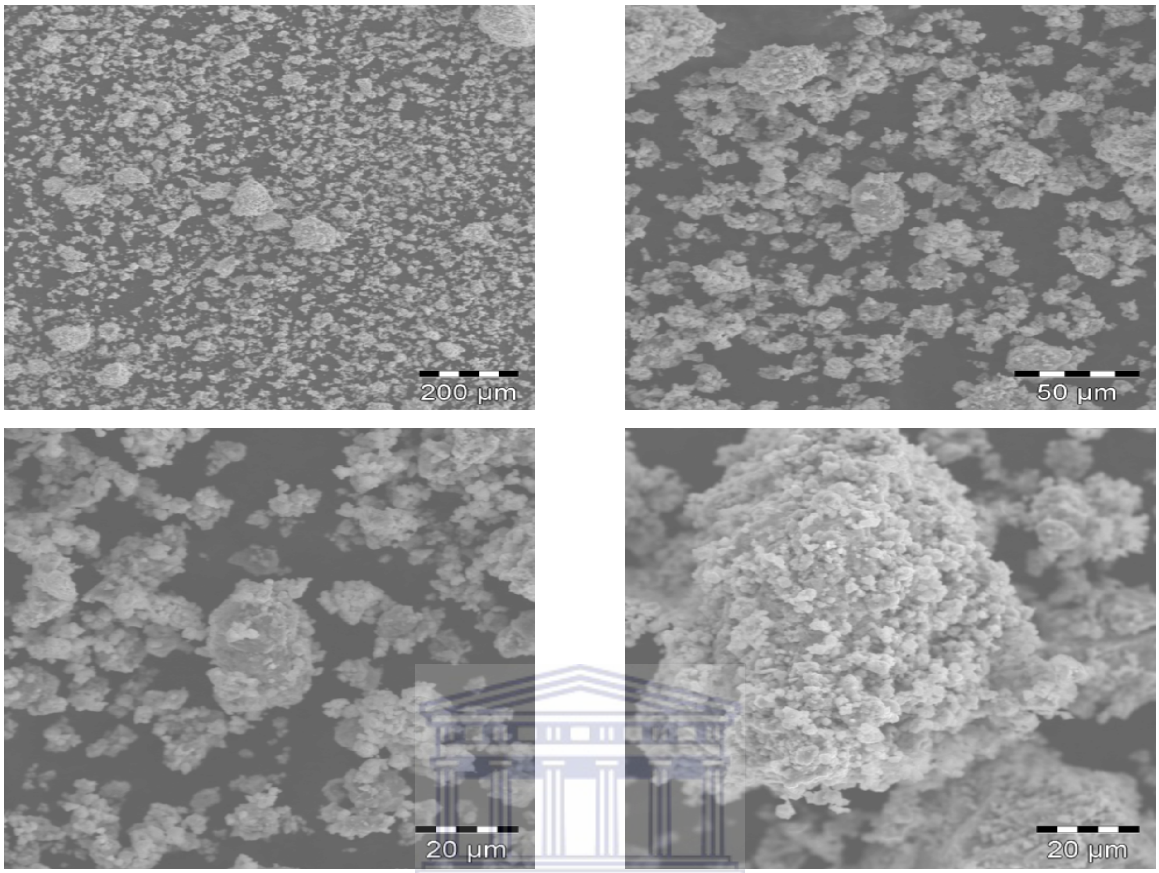

Fig 4.6: SEM images of Ti/Fe ball milled after 60 minutes with 3cm balls at 350 rpm.

UNIVERSITY of the
WESTERN CAPE

As observed, the average size of the particles has been reduced to the region of 1 – 10 µm. The typical pretreated particles are shown from different magnifications in figure a, b, c and d.

4.1.2. Crystallinity change in Ti/Fe alloy after ball milling:

The full possibilities of high-energy ball-milling applications are still to be discovered. Recently, it was used to completely modify the morphology of different metastable aluminas and to transform them into the thermodynamically stable α-form [92]. Therefore, one may expect that the technique could also be used to gradually collapse Iron-Titanium crystalline structures turning them into amorphous materials. It seems probable that during such a process partially destroyed crystallites may expose part of their internal pore structure. Assuming that the active sites may partially survive such a treatment, they should enhance catalytic activity of Iron-Titanium alloy, because partially opened pores and smaller dimensions of broken crystallites would facilitate access to the sites, lowering considerably both geometrical and diffusion limitations.

It was observed from the time matrix (15, 30, 60, and 90) minutes that only samples milled with 3 cm balls showed considerable crystallinity loss even though SEM images show that particle size reduction has taken place, and that the surface of the particles appear to be predominantly smooth for all other milled samples. XRD for all samples was performed in the $0^o - 90^o$ range of 2θ scale with step of measurements 0.1^o. The lines with visible intensity were obtained only in $35^o - 55^o$ range. The XRD patterns for samples after 15, 30, 60 and 90 minutes of ball milling are shown in *Figure 4.8* below. The intensive and wide reflections were observed in the XRD pattern only after 15 minutes of milling. After only 60 minutes of milling, a very broad peak is obtained, suggesting that the powder has become amorphous. It was found that the amorphization rate obtained by the milling of crystalline pre-alloys can be fitted with an exponential relaxation function [93]:

UNIVERSITY of the WESTERN CAPE

This is due to the fact that relaxation proceeds from a stable crystalline state into a new metastable equilibrium. This is not the case when starting from elemental powders, because the amorphization mechanism is superimposed by the mixing of the various elements.

No reasonable change was observed in the broadened peaks between 60 and 90 minutes. X-ray amorphous powder with a high yield was achieved after only 60 minutes of milling without a milling agent. This is much faster than that usually reported in literature starting from elemental powders of similar composition and milling with a planetary ball mill. This is not very surprising because rapid amorphization was also reported in [93-94], where amorphization started from various intermetallic compounds instead of elemental powders.

The indexed XRD pattern of the as-delivered Ti–Fe alloy is presented in Fig 4.7; results of the Rietveld refinement are also shown in Table 4.4. As it can be seen, the studied sample is multiphase, and the major phase (more than 60 vol.%) is the $TiFe_2$ hexagonal Laves phase (C14),

rather than TiFe intermetallic compound (CsCl structure type) whose amount in the alloy was estimated as lower than 5 vol.%. In addition, the sample contains the significant amount of the oxygen-stabilised Ti_4Fe_2O intermetallide (interstitial η-phase, structure derivative from Ti_2Ni type), as well as the cubic titanium suboxide TiO_x having the NaCl-type structure.

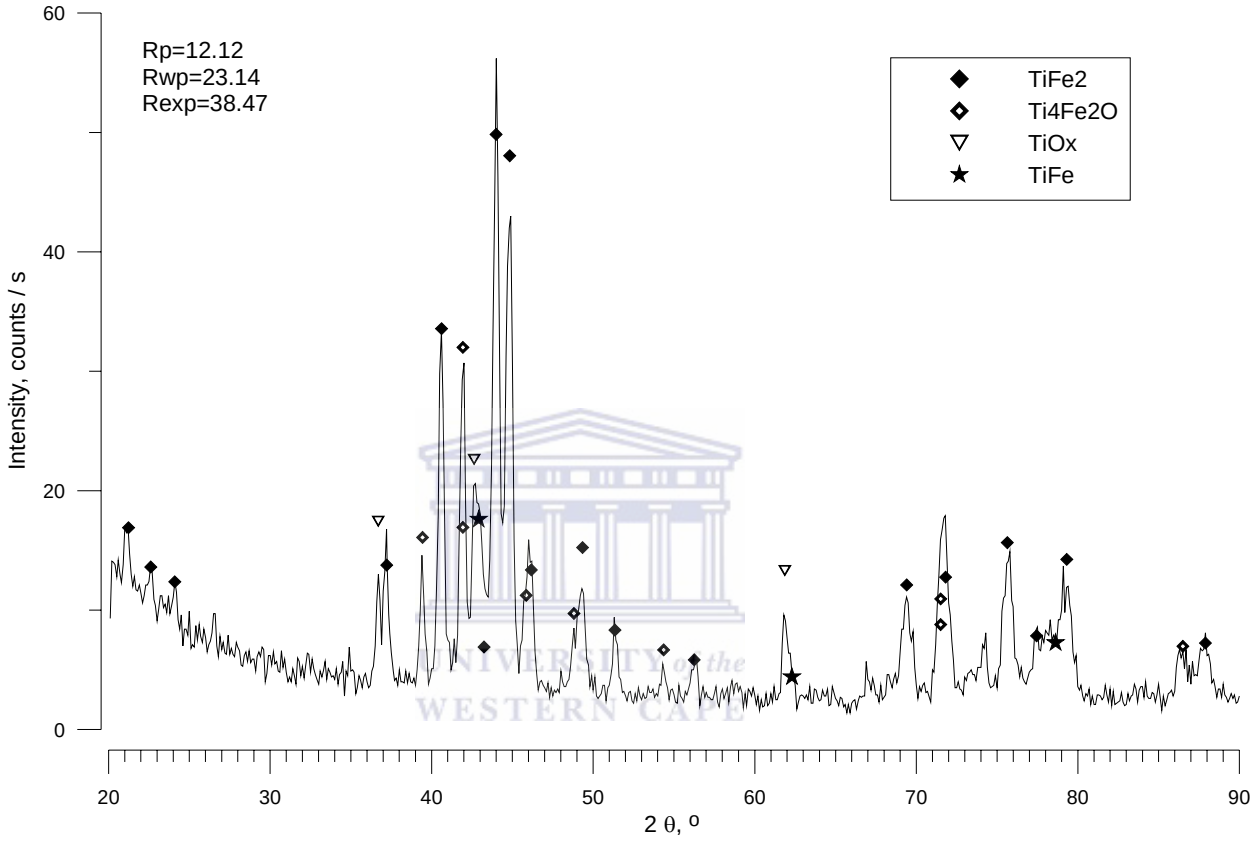

Figure 4.7: XRD pattern of the as-delivered Ti/Fe sample

Table 4.4 Results of the Rietveld refinement of the as-delivered T/iFe sample (Figure 4.7):

Phase	Lattice periods, Å		Estimated quantity, vol.%
	a	*c*	
$TiFe_2$	4.8277	7.8582	62.70
Ti_4Fe_2O	11.1852	–	20.78
TiO_x	4.2385	–	11.72
TiFe	2.9774	–	4.80

The lattice periods of the $TiFe_2$ phase are in a satisfactory correspondence with the reference data (*a*=4.785 Å, *c*=7.799 Å [95]) exceeding them, both for *a* and *c*, not more than 0.8%. The

deviation of lattice period of TiFe from the corresponding reference data (2.972 Å [96]) is rather small (+0.3%). For the oxygen-containing phases the deviations of the lattice periods from the reference data are bigger: –1% for Ti_4Fe_2O (a~11.3 Å [97]) and +1.4% for TiO_x (a=4.1766 Å [98])

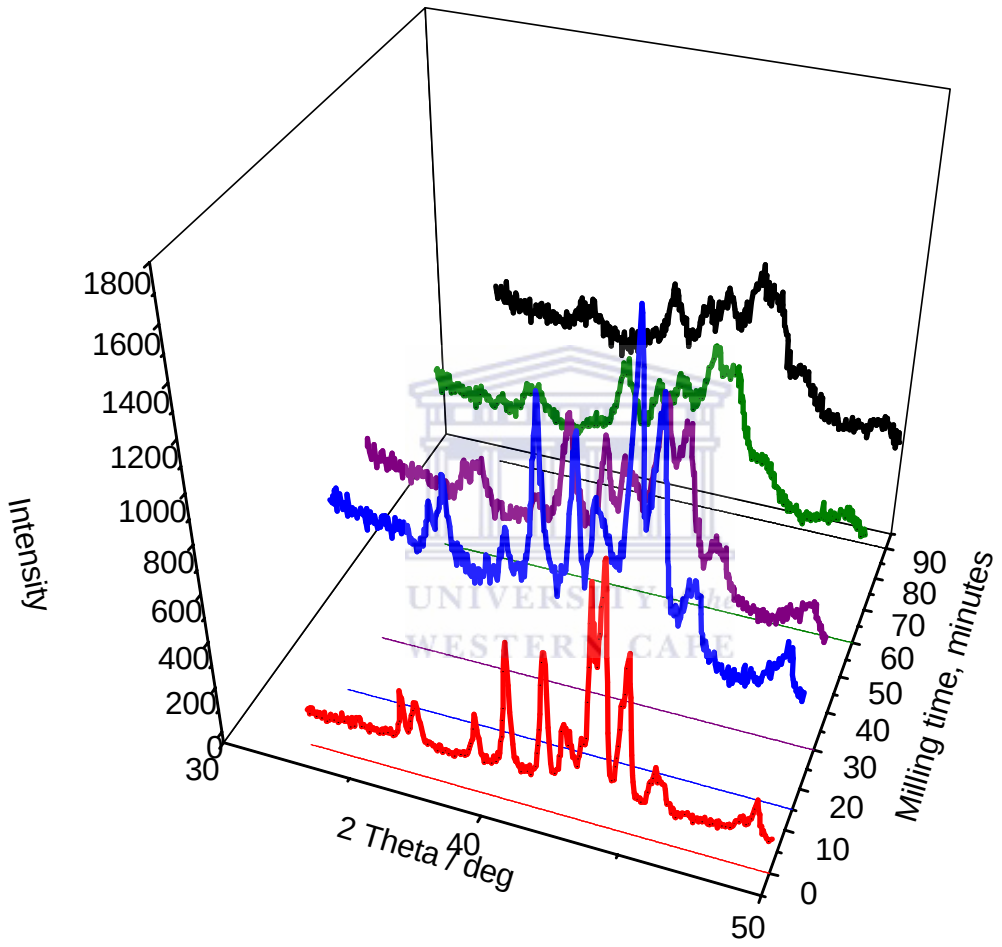

Fig 4.8: X-ray diffractographs showing broadening of the intensity peaks of Ti/Fe alloy with extended milling time for samples milled with 3cm balls at 350 rpm.

As mentioned above, there is considerable collapse of the crystals after 15 minutes implying that the amorphization has commenced. It is also seen that at 60 minutes, there is complete broadening of the peaks and not much further differences are seen at 90 minutes.

4.2. Development of carbon nanotube growth technique for the surface modification of Ti/Fe alloys:

Different techniques (laser ablation, arc discharge and chemical vapour deposition) have been used in literature for surface modification of metal catalysts [15] but due to availability of materials for experimental set-up, ease of set-up, production of high quality and purity of carbon nanotubes on large area substrates compared to other techniques and commercial reproducibility, we adopted the chemical vapour deposition of carbon nanotubes. While the first two techniques are appropriate for large-scale production of CNTs, they cannot be used for self-assembly on surfaces. CVD appears to be the method of choice for direct deposition on specific structures and substrates [99]. The synthesis of CNTs (multiple-walled) by CVD involves the catalytic decomposition of a carbon precursor (e.g. hydrocarbons) on nano-structured transition metal catalyst like Ti, Co, Ni, or Fe. Carbon nanotube growth mechanisms involve the dissociation of these hydrocarbons catalyzed by transition metals, and saturation of carbon on the metal nano-particle. Carbon precipitates from the saturated metal nano-particles and forms nanotubes. The nanotube structure is favored because it has no dangling bonds and forms a low energy system. Typical CVD temperatures for nanotube growth vary between 600 and 1000 ^{o}C. The process is sensitive to the catalyst structuring, as well as to the reaction conditions. Nanotubes synthesized by CVD are known to be longer than those obtained by other processes. It is also possible to grow dense arrays of aligned CNTs by CVD [99]. The rate of deposition of CNTs depends on process/reaction conditions, the catalyst, and the precursor. During large-scale CNT self-assembly, where the CNTs are grown in a large structure, the gas phase composition of the carbon source varies as active free radicals and intermediates and at high temperature react with the precursor and among them. Kinetic models can be used to interpret precursor decomposition, intermediates, free radical formation, by-product generation and in identifying the reaction pathways. As the growth is catalyst-assisted, it becomes evident that the catalyst is instrumental for controlling the properties of the nanotube. The catalyst particle size influences strongly the nanotube diameter, and the density of particles determines in turn the spacing between nanotubes. Key parameters can thus be directly controlled by the catalyst, while the CVD process itself can be monitored to tailor the length of the structures [100]. Different structure of CNTs exhibit different properties, for example, pure CNTs display the properties of the semiconductor or conductor depending on their diameter and chirality, but nitrogen-flushed CNTs are conductor, independent of their diameter and chirality. From the papers reported on nitrogen-flushed CNTs, the nitrogen-flushed CNTs are bamboo-structure, i.e. there are some interlinking carbons sheets

UNIVERSITY of the WESTERN CAPE

in CNTs. Simultaneously, the reported results show that the bamboo-structured CNTs are synthesized as long as the reaction gases contain nitrogenous gas or the nitrogenous precursor are employed during preparation of CNTs, these indicate that nitrogen plays an important role in the process of formation of the bamboo-structured CNTs [101].

4.2.1. Implementation of LPG pyrolysis for growing carbon nanotubes on the surface of Ni and Co substrates (model experiment):

Novel experiments have been carried out in the South African Institute of Advanced Materials Chemistry (SAIAMC) to investigate the possibility of synthesizing carbon nanotubes on nickel and cobalt substrates using a multiple composition gas. The carbon source used was liquefied petroleum gas (LPG), and one of the advantages is, in this method developed, the use of hydrogen to pre-treat the catalysts or control the growth of the carbon nanotubes is not required. Carbon nanotubes were grown in a horizontally aligned tube furnace. The catalysts used were nickel foils, cobalt foils or nickel porous membrane measuring 0.5cm x 0.5cm. In Some cases the cobalt or nickel foil was covered with an electroless deposit of the respective metal. The deposition temperatures used were 600°C, 800°C, and 1000°C. In a typical experiment the catalyst was weighed and then loaded into an alumina tube with a length of approximately 5cm and a diameter of 1cm. The alumina tube was then placed within a quartz tube located inside the tube furnace. The system was then flushed with nitrogen for 10 minutes, and then the furnace temperature was ramped up to the desired temperature. Once the temperature had stabilized, the nitrogen flow was terminated and the LPG flow was initiated, after 30 minutes the LPG flow was terminated and the nitrogen flow re-initiated. After 10 minutes the furnace temperature was reduced and the resulting carbon deposits were cooled under a flow of nitrogen. In addition, similar experiments were carried out using carbon cloth. For the carbon cloth, Ni was chosen as the catalyst for nanotube growth, and two different methods were used to deposit Ni onto the surface of the cloth. The first method used was an electroless deposition method and the second method was a magnetron sputter method. For the nanotube growth experiments, a 4.0cm long by 2.0cm wide piece of carbon cloth, with Ni deposited onto the surface was used. Simply weighing the samples before and after deposition, was a quick way to determine the optimum temperature for the growth of carbon nanotubes. Further extensive characterization proved to be limited at the two non-ideal temperatures (at 600^{o}C and 1000^{o}C) due to the lack or very low amount of deposits found. At 600^{o}C, on both the Ni and Co foils the amount of carbon deposit was less than 1 mg, however visual inspection of the foils after deposition revealed a small amount of black discoloration. SEM examination showed no carbon nanotubes present, but only amorphous carbons. At 1000^{o}C, the deposits on both the Ni, and Co foils were a few milligrams more than at 600^{o}C; however, visual inspection revealed the deposits to consist of grey ‘flakes’ which differed significantly from those at 600^{o}C. SEM examination revealed no carbon nanotubes, only amorphous carbons. SEM examination of the samples at 800^{o}C revealed that the carbon deposits

UNIVERSITY of the WESTERN CAPE

consisted of carbon nanotubes. There was very little amorphous carbon observed in these samples [102].

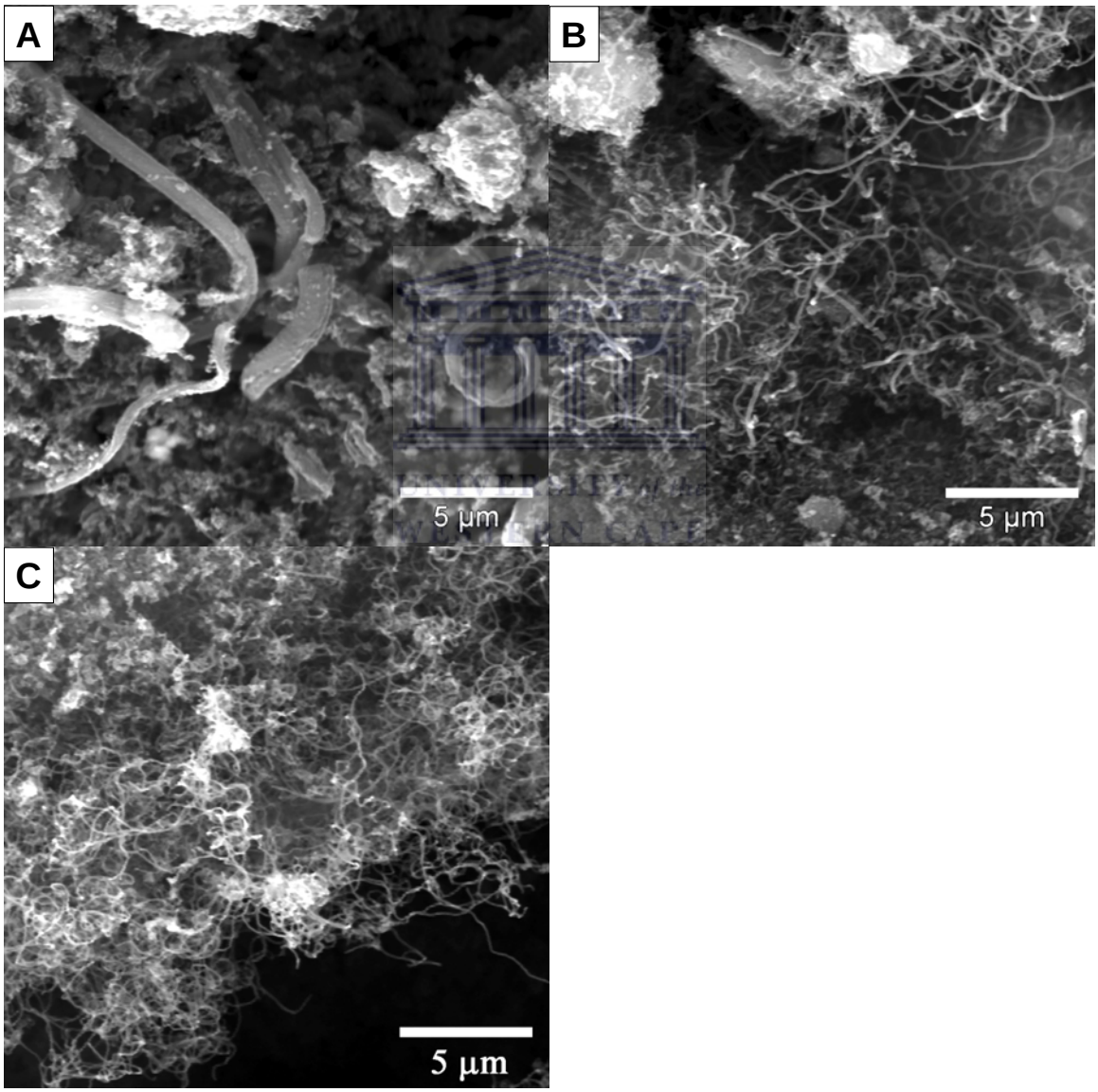

Fig 4.9: SEM images of CNT grown on different substrates at 800^{o}C and 30 minutes LPG deposition time (a) nickel foils (b) cobalt foils (c) nickel porous membrane

4.2.2. Modification of the surface of Ti/Fe alloy with carbon nanotubes by LPG pyrolysis for composite material preparation:

Based on the model experiment of synthesis of carbon nanotubes on nickel and cobalt substrates using LPG as a carbon source, a similar deposition technique was adopted for the surface modification of pre-treated and as is iron-titanium alloy. The primary objective is to use carbon nanotubes as scaffolds for the alloy, adding specific surface moieties to enhance hydrogen storage properties of the material. Carbon nanotubes are well recognized absorbent of gases due to their comparatively high surface area. Besides, CNT possess impressive thermo-conductive properties which will further enhance the hydriding/ dehydriding kinetics of this composite with regards to temperature alterations. It is interesting also to investigate the contribution of carbon nanotubes to the weight % capacity of this hydrogen storage composite, since high wt % capacities have been reported for CNT in low temperatures [103].

Pre-treated and as is iron-titanium powder was used. In a typical experiment, 5.0g of the powder was weighed into a glazed porcelain sample boat, the boat was loaded into the CVD system, and the CVD system was flushed with nitrogen for 10 minutes. Under a nitrogen flow, the temperature was ramped up to 800^{o}C, once stabilized, the nitrogen flow was terminated and the LPG flow was initiated for 10, 30, 60 and 120 minutes. Different deposition time regimes have been shown from (4.2.1) above to influence the quantity and quality of synthesized nanotubes. After the time had elapsed, the LPG flow was terminated and the samples were cooled under a nitrogen flow to 150^{o}C and collected in a vial for characterization.

UNIVERSITY of the WESTERN CAPE

Optimization of pyrolysis parameters for carbon nanotube deposition on Ti/Fe alloy:

Temperature of deposition was maintained at 800^{o}C because the highest yield of pure carbon nanotubes without other carbonaceous deposits was observed. Similar to observations in the model experiment (3.2.1), only amorphous carbon was obtained at 600^{o}C and 1000^{o}C as revealed by SEM examination. Simply weighing the samples before and after deposition, was a quick way to determine the optimum temperature for the growth of carbon nanotubes.

LPG flow rate of 0.35 L/min was applied because this is observed to ensure the most efficient use of the gas (the point at which all the applied gas is used is in the pyrolysis process). This factor is imperative for commercialization of this process because it ensures the feed gas is not wasted by applying a higher gas flow that will not be used in the process. The entire exposed alloy surface was covered with carbon nanotubes at this flow rate as observed by SEM examination.

The most important parameter for this pyrolisis process is seen to be the time of deposition of the gas. Examination of the samples by BET surface area analysis showed an exponential increase in surface area of the composite from 10 to 60 minutes of LPG deposition. After 60 minutes there is no further increase in surface area and it is assumed that the entire alloy surface is saturated with carbon nanotubes. The explanation for this is that the process is self-terminating after complete saturation of the alloy surface and because of a rapid deactivation of the catalysts. Therefore, we determine the optimum deposition time to be 60 minutes.


UNIVERSITY of the
WESTERN CAPE

Structure and morphology of Ti/Fe-CNT composite:

As-produced CNTs are usually contaminated with residual metal catalyst and carbon species such as carbon nanoparticles, fullerenes, carbon nano-onions, and amorphous carbon. Furthermore, it was suggested that metal and carbon impurities in CNTs promote hydrogen chemisorption. In this process, hydrogen is dissociated on the impurities, and the generated hydrogen atoms spill over to the tubes, leading to C-H bond formation [104]. The amount of metal catalyst in the sample of nanotubes has been shown to affect the combustion rate and the onset oxidation temperature [105], however, in the samples prepared using LPG this does not seem to be a factor. The lower the number of defect sites, and the greater the degree of graphitization the more stable nanotubes are to thermal oxidation [106]. The SEM micrographs show unevenly distributed carbon nanotubes on the surface of Ti-Fe particles. This uneven distribution is typical of the sample. The diameters vary typically between 50-300 nm and the length between tens to hundreds of microns. It has been proffered that the size of the alloy particle plays a very potent role in the diameter of the resulting nanotubes i.e. the pore sizes between the alloy particles are roughly equal to the CNT diameter. Beyond this size correlation, only small nano particles are able to catalyze formation of CNT. This can be explained on the one hand by the fact that such very small nano-particles can exhibit peculiar electronic properties and thus catalytic properties due to the

unusually high ratio surface, atom/bulk atom [107]. TEM micrographs reveal well defined tube walls as shown in (*fig 4.13*). Few fringe terminations were observed within the bundles, indicative of well-aligning of individual tubes. Considering the alignment pattern of these nanotubes, hydrogen molecules can be located linearly inside nanotubes or interstitially between them. Catalyst particles are embedded in the tubular structure or at the tips which is related to their growth process, a common feature of tubes synthesized by CVD. The nanotubes are seen to be bamboo-shaped as a result of their continuous curvature. The bamboo structure is reported to be rich in defects such as dislocation and local layer terminals [104]. Here, the imperfection in the tube structure may provide access to interior adsorption sites. High energy sites such as defect sites and graphite particle edges have been proposed to induce hydrogen chemisorption on the tubes.

UNIVERSITY of the
WESTERN CAPE

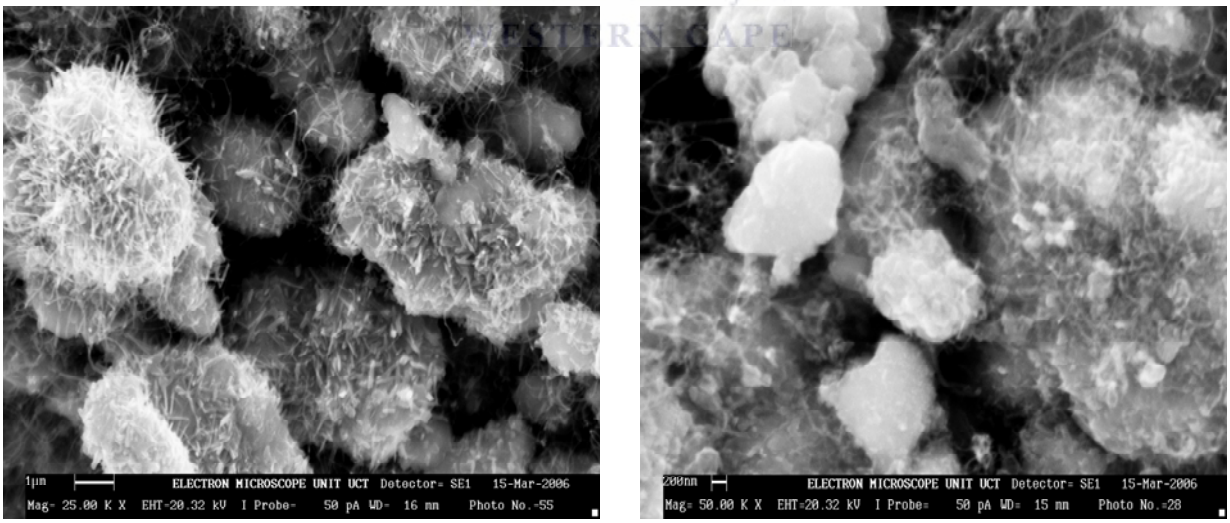

Fig 4.10: SEM image showing LPG deposit on the alloy after 10 minutes for sample ball milled 60 minutes-350 rpm-3cm balls.

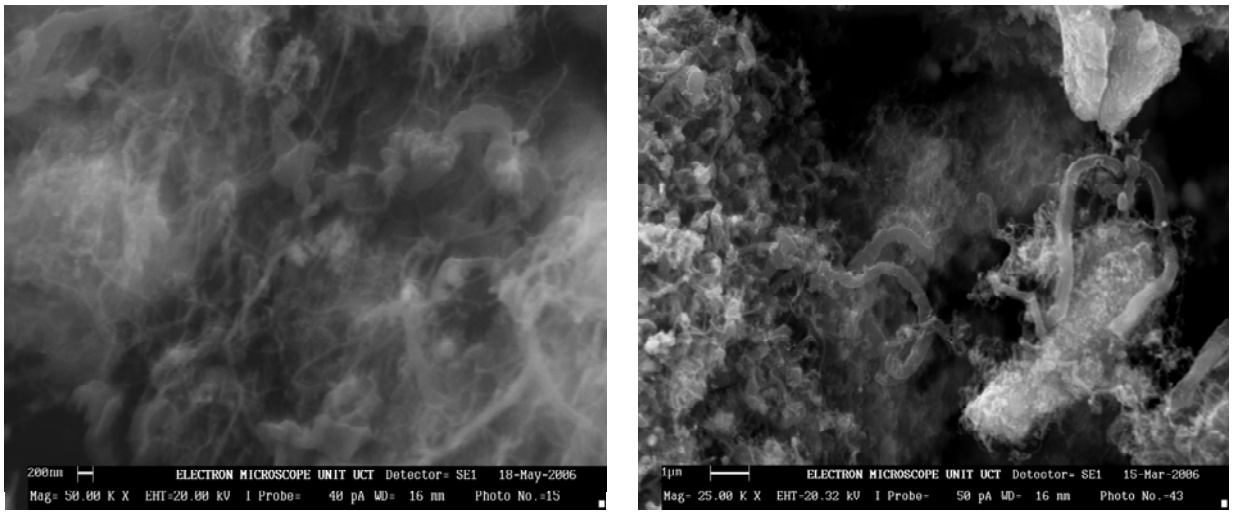

Fig 4.11: SEM image showing LPG deposit on the alloy after 30 minutes for same sample.

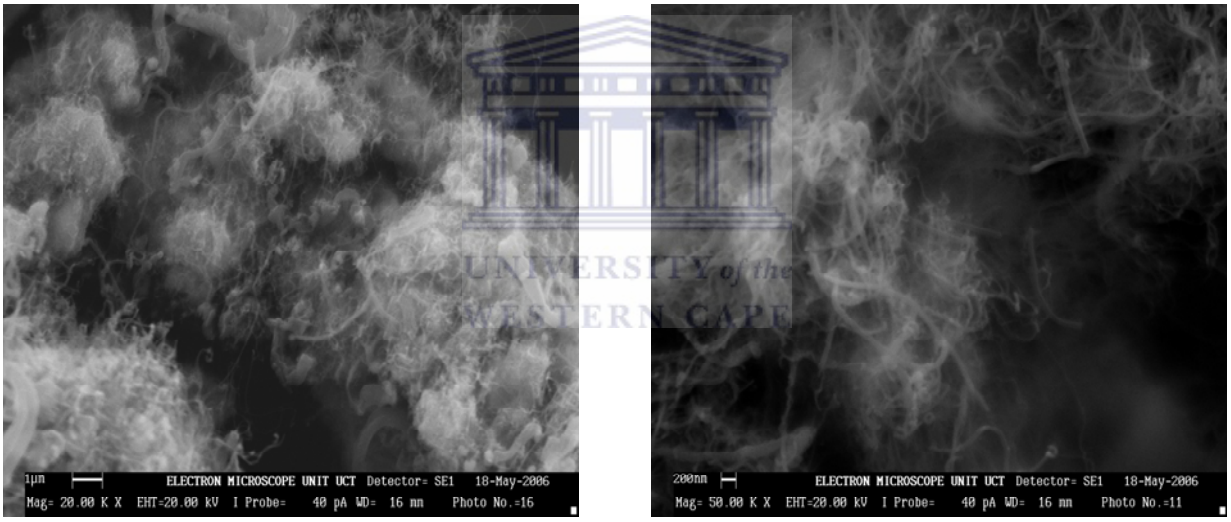

UNIVERSITY of the
WESTERN CAPE

Fig 4.12: SEM image showing LPG deposit on the alloy after 60 minutes for same sample.

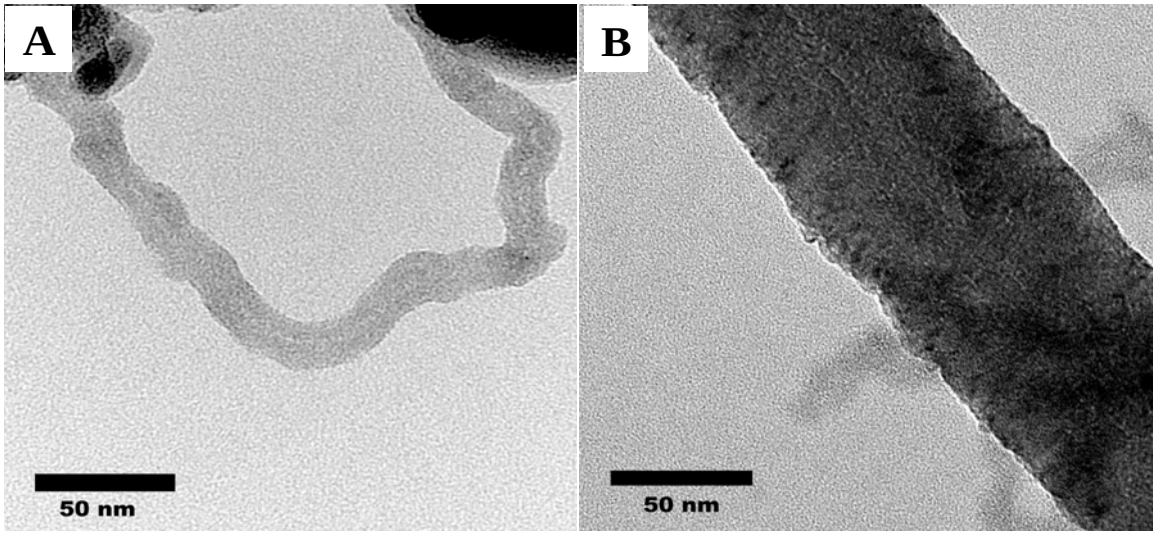

Fig 4.13: TEM images confirming the nanotubes with (a) hollow centre and diameter of ~20 nm and (b) filled centre and diameter of ~70 nm for LPG deposit on the alloy after 60 minutes for same sample.

UNIVERSITY of the
WESTERN CAPE

Influence of CNT deposition on surface area of Ti/Fe-CNT composite:

Carbon nanotubes have been found to possess a wide variety of extremely remarkable properties, most notably high electrical and thermal conductivity, mechanical strength, and catalytic surface area. The specific surface area is an attractive property of carbon nanotubes that is anticipated to improve many applications like hydrogen storage. Using a starting alloy powder with a reasonably high specific surface area favors the nucleation and growth of surface Ti/Fe particles, as opposed to intra-granular particles. Increasing the alloy content also produces more surface Ti/Fe particles, which give more CNTs. However, a too high surface density of Ti/Fe particles favors the coalescence and the formation of encapsulated Ti/Fe particles, which eventually hampers the modification. Very high specific surface areas are observed when using low Ti/Fe contents (~5g). The decrease in surface area for higher alloy mass could be due either to the increasing presence of carbon nano-capsules or to a bundling effect of the nanotubes [108]. The specific surface area of the nano-capsules is equivalent to that of CNTs with the same diameter and number of layers. However, a given catalyst particle produces either a CNT or a nanocapsule and one can consider that the contribution to the surface area in m^2 by the nano-capsule is

negligible compared to that of the CNT which has a very high aspect ratio. Therefore, the contribution of the nano-capsules to the total surface area is likely to be small. Thus, the decrease of surface area is more likely related to the increase of the diameter of the tube bundles. From the values of the surface areas before and after LPG treatment (*Table 4.5* below), we can obtain the contribution to the surface area by the carbon formed by the decomposition of LPG. We have listed the $\Delta S = S_1 - S_0$ values for selected samples in the Table below. The results show that Ti/Fe alloy nano-particles produced by ball milling technique are good agents for generating multi-walled nanotubes with high surface area.

Table 4.5 showing influence of carbon nanotubes on surface area of different samples milled with 3cm balls.

Sample number	Milling time (minutes)	Milling speed (rpm)	Ball size (cm)	Surface area (S_0)	Surface area + CNT (S_1)	% increase (ΔS)
unmilled	-	-	-	0.0389	0.2933	653
1	15	100	3	0.1721	0.9909	475
2	15	200	3	0.1957	5.4151	1134
3	15	350	3	1.2566	7.3254	244
4	60	100	3	0.2111	2.5632	1114
5	60	200	3	0.2301	5.6547	2357
6	60	350	3	2.0289	19.7277	872

Here we observe an exponential increase in the surface area by a factor of 10 for the alloy after carbon nanotubes growth on their surface.

UNIVERSITY of the WESTERN CAPE

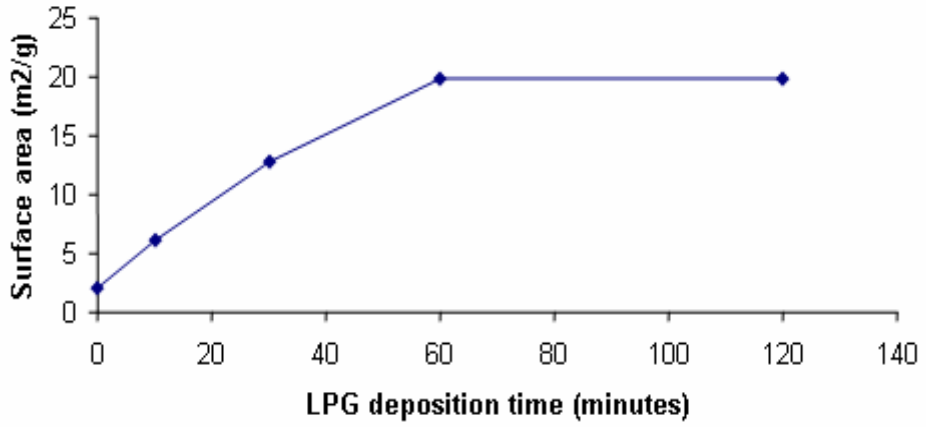

Fig 4.14: LPG deposition time Vs surface area showing increase in surface area of composite from 2.0289 m^2/g to 19.7277 m^2/g with progressive LPG deposition time for samples ball milled for 60 minutes at 350 rpm using 3cm balls.

We conclude from the graph above that increased LPG deposition time increases the carbon nanotube content on the surface of the alloy consequently increasing the surface area of the composite. However there is a lull after 60 minutes of deposition indicating that the surface area of the composite does not increase any further between this time and 120 minutes. An explanation for this is that the process is self terminating after saturation of the catalyst surface by carbon nanotubes. This saturation time is assumed to be 60 minutes.

4.3 Development of methods for surface modification of composite Ti/Fe-CNT material using binary metal hydrides:

Due to inherent short comings surrounding Ti/Fe as a hydrogen storage material (see chapter *2.4.2*), we have developed further surface modification of this composite tailored to address these areas. The composite should possess excellent overall hydrogenation properties: rapid H-absorption/desorption kinetics, high H-capacity, low working temperature, quick activation, as well as superior oxidation resistance. Palladium metal exhibits suitable hydrogen adsorption/desorption temperature (T<400K) but low capacities (~0.6 mass %), while magnesium metal has suitably high capacities (~7.6 mass %) but too high desorption temperature (T>550 K) [13]. To achieve high performance with high absorbing capacity and suitably low desorbing–absorbing temperature, we have proposed to design nano-composite materials, which are made from three kinds of metals/alloys with contrast hydrogen storage properties, and to subtract advantageous hydrogen storage properties in these materials using the cooperative phenomena that hydrogen displays in nano-meter scale. In these situations, we have planned to apply non-traditional and new nano-technology methods for designing high-performance hydrogen storage materials. Nowadays, we are planning to use hydrogen weakly trapped in the defective sites between carbon nanotube layers for H-storage and lowering the desorption temperature as well as increasing overall storage capacity by surface modification due to catalyzing binary metals to be deposited by the techniques developed as follows (a) electroless deposition of palladium on the composite (b) Ultra-sound (sonification) deposition of magnesium on the composite.

UNIVERSITY of the WESTERN CAPE

4.3.1. Deposition of palladium layer to improve activation kinetics of composite:

Electroless palladium coating is one of the methods tested for improving the charge/discharge characteristics of the metal hydride composites. The Pd coating was found to be very effective for increasing both the discharge capacity and the rate capability, and for decreasing the number of cycles required for activating the alloy. The improved performance of the Pd-coated alloy over that of an uncoated alloy was attributed to the catalytic effect of Pd on the charge-transfer step of the hydriding–dehydriding reactions occurring at the composite surface. The catalytic effect of Pd on hydrogen adsorption in mechanically alloyed Mg_2Ni, $LaNi_5$ and Fe/Ti was studied by Zaluski et al [72]. The palladium treatment gave powders ability to adsorb hydrogen at room temperature with no need for any activation cycles. Also, hydrogen adsorption characteristics for the nanocrystalline materials were enhanced, increasing the adsorption rates, even at low temperatures.

During electroless plating, electrons are released by the anodic partial reaction and consumed by the cathodic partial reaction [109]:

$$R^0 \rightarrow R^{2+} + ze^- \quad (1)$$

$$M^{z+} + ze^- \rightarrow M^0 \quad (2)$$

UNIVERSITY of the WESTERN CAPE

Where R is the reducing agent, M is the metal (or composite in this case) and z is the number of electrons transferred.

The nanotube-alloy composite surface was activated by stirring 1.000g in 5.0mL of a palladium-tin colloidal solution for 45 minutes with the tin binding palladium to the surface of the composite via the following reaction:

$$Sn^{2+} + Pd^{2+} \rightarrow Sn^{4+} + Pd^0 \quad (3)$$

The colloidal solution was then decanted, and the activated composite was rinsed with three 10.0mL aliquots of a 10% hydrochloric acid solution, and three 10.0mL aliquots of de-ionized water. 10.0mL of a 0.5g/L of palladium (II) chloride and 10.0mL of 25% ammonium hydroxide were mixed in a separate container, and then added to the activated composite; to initiate

palladium deposition 2.0mL of a 99% hydrazine solution was added to the mixture and palladium reduced via the reaction:

$$2Pd(NH_3)_4^{++} + N_2H_4 + 4OH^- \rightarrow 2Pd^0 + 8NH_3 + N_2 + 4H_2O \quad (4)$$

The mixture was left stirring overnight, and then the powder was recovered by filtering and thoroughly washing the powder over a 0.45 micrometer nylon membrane.

According to the SEM characterization, the feature of the Pd particles on the surface of samples is affected strongly by the plating conditions. Increasing the $PdCl_2$ concentration, the time of plating and warming the plating solution causes the increase in the size of Pd particles and agglomerations of these clusters in some places. The change in HCl concentration causes the change in the number and the size of Pd particles. Palladium metal was successfully deposited on to the nanotube-alloy composite using a hydrazine reduction of a Pd salt technique, and a sono-chemical method with hydrogen gas as reducing agent. SEM and EDS analysis revealed palladium on the nanotubes.

UNIVERSITY of the
WESTERN CAPE

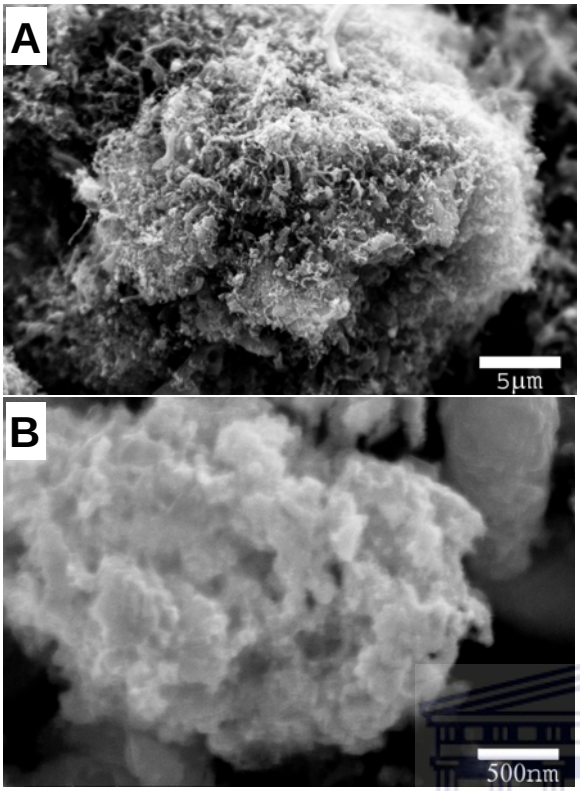

Fig 4.15: Micrograph A is a typical example of the carbon nanotubes grown on the surface of the iron titanium alloy. Micrograph B is an image of the palladium functionalized nanotubes on the alloy. The amount of palladium deposited has completely obscured the nanotubes on the surface of the alloy.

UNIVERSITY of the
WESTERN CAPE

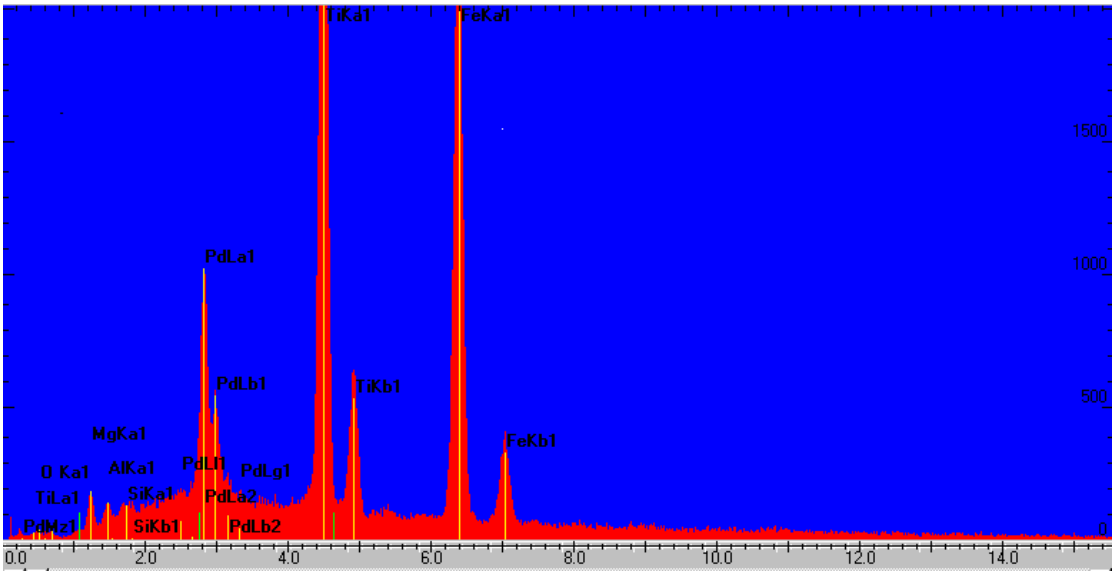

Fig 4.16: EDS peaks showing the presence of palladium deposited on the composite. The smaller peaks are a result of contamination from preparation materials.

4.3.2. Deposition of magnesium layer to increase hydrogen weight capacity of composite:

Among the known metals and alloys with potential use in hydrogen storage, magnesium has attracted much interest for its high hydrogen capacity and very low cost. The combination of its advantageous mechanical properties with low density makes this light metal an interesting material for composite hydrogen storage material synthesis. Recently, this tendency has increased, because it has become clear that the poor hydriding kinetics and high working temperature of Mg could be improved significantly by means of composite formation thus endowing the material with markedly improved overall hydriding properties [62].
Efforts to deposit magnesium from solutions of its simple salts in aprotic solvents failed so far, consequently we have developed a method for ultrasound deposition of magnesium nano-particles on the Ti/Fe-CNT-Pd composite. Aside from their very high surface area, these particles possess chemical and physical properties that are distinct from those of both the bulk phase and individual molecules. Power ultrasound effects chemical changes due to cavitation phenomena involving the formation, growth, and collapse of bubbles [110]. These ultrasonic waves are strong enough to produce oxidation, reduction, dissolution, and decomposition.

1.0000g of the Ti/Fe-CNT-Pd composite was added to a mixture of 0.1000g Mg bis (2, 2, 6, 6-tetramethyl -3, 5- heptanedione monohydrate and 0.05g Mg acetylacetonate in a sonication cell. The sonication of the slurry with the high-intensity ultrasound radiation was carried out for 3 hours by direct immersion of the sonication cell in a bath sonicator under a flow of an argon/hydrogen mixture as a reducing agent (90:10) %.

UNIVERSITY of the WESTERN CAPE

This mechanism of the formation of magnesium nanoparticles takes into consideration that free radical species are generated from water molecules by the absorption of ultrasound (eq 1). This would be the initiation reaction:

$H_2O))))))) H + OH$ (1)

The H radical formed in eq.1 can act as a reducing species
and trigger the reduction (eq.2):

$Mg^{+} + H = Mg^{0} + H^{+}$ (2)

The substrate was then washed thoroughly in 200ml acetone, filtered and dried in vacuum. Three different regions are formed during an aqueous sono-chemical process: (a) the inner environment (gas phase) of the collapsing bubbles, where elevated temperatures (several thousands of degrees) and pressures (hundreds of atmospheres) are produced, causing water to pyrolyze into H and OH radicals; (b) the interfacial region where the temperature is lower than in the gas phase region but still high enough to induce a sono-chemical reaction (a few hundred degrees Celsius); and (c) the bulk solution, which is at ambient temperature. Sono-chemical reactions appear to occur within the interfacial region [110]. The sono-chemical reduction process generates high temperatures and pressures for the reduction of Mg salts to amorphous Mg. An argon/hydrogen mixture produces even more H radicals, thus enhancing the reduction of Mg^{+} under the sono-chemical conditions. The advantage of the process described is that it is simple and efficient and produces a uniform coating of Mg nano-particles on the composite. The period of sonication is only 3 hours.

UNIVERSITY of the
WESTERN CAPE

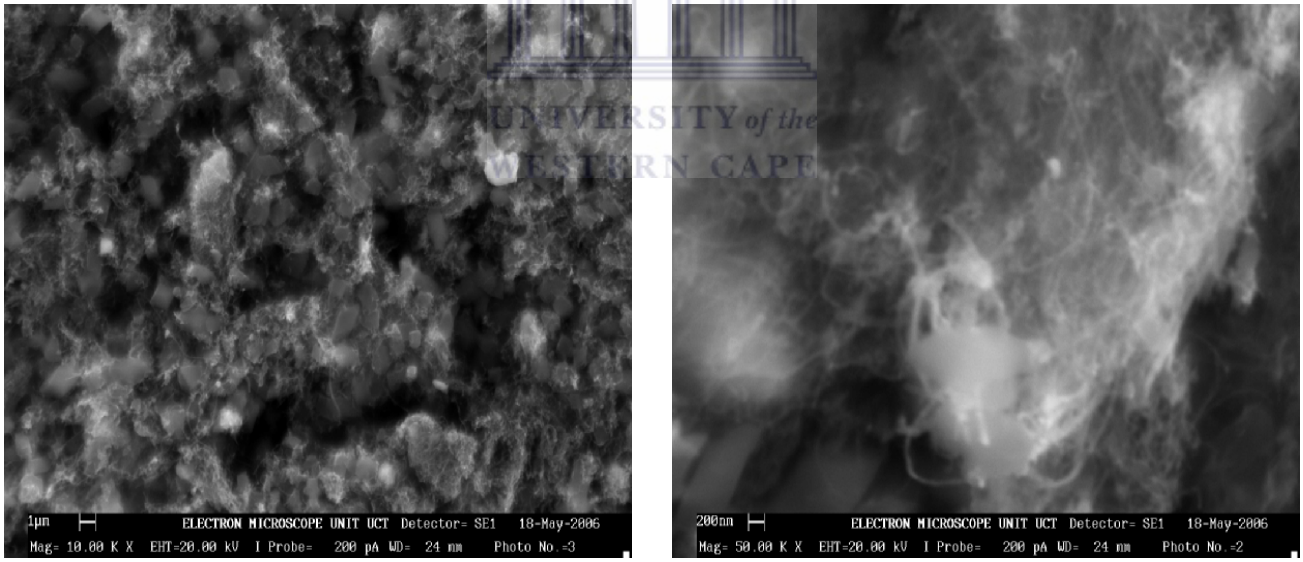

Fig 4.17: SEM images showing magnesium functionalized carbon nanotubes of Fe/Ti alloy

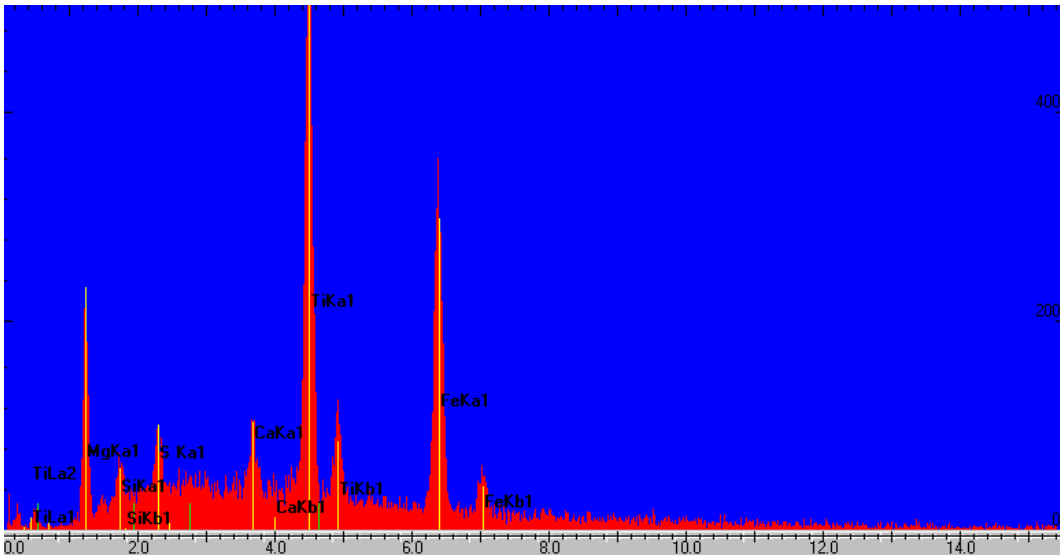

Fig 4.18: EDS peak showing the presence of magnesium deposited on the composite. The smaller peaks are a result of contamination from preparation materials.

UNIVERSITY of the
WESTERN CAPE

4.4. The Investigation of hydrogen storage properties of composite material based on Fe/Ti alloy obtained by layer-by-layer technique:

The analysis methods of the hydrogen storage materials are quantitative. The main parameter under investigation will be hydrogen mass and volume percentage in the material. Analysis of material properties will be based on classical methods.

Direct calorimetric measurement of hydrogen in the material by Thermo- Gravimetric Analysis (TGA):

For analysis of their hydriding properties, 5 mg of the sample was placed in the apparatus concerned without further treatment. The high pressure differential scanning calorimeter (HP-DSC) employed is controlled by a processor, and interfaced to a personal computer. Aluminium oxide pans were used for the sample and reference in the DSC.

The system was then thoroughly flushed free of oxygen by first flowing N_2 through the HP-DSC cell at atmospheric pressure. The cell was isolated and the pressure was allowed to build up to 100 kPa. This procedure also allows the presence of any leaks in the system to be identified and eliminated. The pressure was slowly reduced, ensuring that as it approaches atmospheric, nitrogen gas flow was again started to prevent oxygen getting back into the system. This pressure cycling with nitrogen was carried out twice and at the end of the third cycle, (hydrogen 10%, balance Argon) was then introduced into the system. The same flushing procedure as with nitrogen was employed and finally, the cell was pressurized to 100 kPa of H_2, balance Ar. A heating ramp of $5^oC\ min^{-1}$ from 25^oC to 450^oC was applied. A pressure controller is attached downstream of the HP-DSC to ensure that a constant pressure is maintained throughout the temperature scans. Cooling from 450^oC was carried out in the same H_2, balance Ar atmosphere. In both the heating and cooling stages, the heat flow corresponding to hydrogen desorption / absorption as well as to other events leading to a change in the enthalpy of the sample were recorded. The samples were cycled up to three times. After the final cycle, the samples were taken for thermo-gravimetric analysis (TGA) for the determination of weight loss resulting into the absolute amount of hydrogen stored in the sample. TGA analysis was performed using a Rheometric STA 1500 scientific TGA with a controller linked to a personal computer for data logging and control.

UNIVERSITY of the WESTERN CAPE

Measurement of hydrogen absorption/desorption isotherms using Sievert's-type apparatus:

The method allows quantitatively defining energy parameters (enthalpy and entropy), phase structure and amount of stable adsorption /desorption cycles of a metal hydride. The weighted sample of the material under study was loaded into reactor (m~0.5...1 g). Then the sample was activated by heating up to 450...500 ^{o}C for 1 hour, being simultaneously evacuated (ultimate vacuum better than 10^{-5} mbar). In so doing, the valves 1.2 and 1.3 were closed, and valves 1.4, 1.5, 2.3, 3.3 and 4.2 were opened. Afterwards, the reactor was gradually cooled to room temperature, put in the thermostat 10 at T=25...30 ^{o}C, and the valves 1.4 and 1.5 were closed. Then hydrogen was introduced into the high-pressure collector (by opening and consequent closing of the valves 5.2 and 1.3), at the starting pressure 80 to 120 bar. Hydrogen pressure in the high-pressure collector (measured by the sensor 1.1), as well as temperatures of gas-distributing system (thermistor 8.1), room (thermistor 8.2), and reactor (thermocouple 8.3) were started to be logged. After 3-5 minutes the valve 1.4 was opened, and hydrogen absorption by the sample was monitored.

After completion of the absorption, the valves 1.4 and 3.3 were closed; hydrogen pressure in high-pressure collector was released by opening and consequent closing of the valve 1.2. Then the valve 1.5 was opened followed by the evacuation of gas system including high-, medium- and low-pressure collectors to the vacuum better than 10^{-4} mbar. The experiment for hydrogen desorption into the gas system was started by the opening valve 1.4, in so doing hydrogen pressure in the low-pressure collector (measured by the sensor 3.1), as well as temperatures of gas-distributing system (thermistor 8.1), room (thermistor 8.2), and reactor (thermocouple 8.3) were logged.

UNIVERSITY of the WESTERN CAPE

The determination of hydrogen sorption capacity of materials was based on the calculation of the total amount of gaseous hydrogen in the internal volumes of the gas-distributing system and reactor, starting from the hydrogen pressures, P_i, therein; as well as the temperatures, T_i, of these volumes:

Equation 1

$$n = \sum_i \frac{P_i V_i}{Z(P_i, T_i) R T_i};$$

where n is the total number of moles of H_2 in the volumes V_i taken into account (maintained at the corresponding temperatures, T_i), R=8.3143 J/(mole·K) is the gas constant, and Z is the compression factor of hydrogen gas at the specified pressure P_i and temperature T_i.

Calculating the amount of hydrogen gas before (n_0) and after (n_1) hydrogen absorption / desorption by a sample, one can determine the change of the hydrogen sorption capacity (Δx) of the material as:

Equation 2a

$$\Delta x\left[\mathrm{cm}^3/\mathrm{g\ STP}\right]=\frac{22400\left(n_0-n_1\right)}{m};\ \text{or:}$$

Equation 2b

$$\Delta x\left[\mathrm{H/f.u.}\right]=\frac{2\left(n_0-n_1\right)}{m/FW}.$$

UNIVERSITY of the WESTERN CAPE

The specific form of

Equation 2 is selected depending on required units of Δx, so if it is expressed as the volume of gaseous hydrogen at normal conditions (STP: P=1 bar, T=0°C) per unit of material weight, the

Equation 2a is used (m is sample weight; 22400 cm^3/mole is the molar volume of hydrogen at the above-specified normal conditions). If the capacity is expressed as a number of hydrogen atoms per formula unit (f.u.) of the material, then it is necessary to use

Equation 2b, substituting thereto the value of formula weight (FW) of the material [95].

In the presented notation, $\Delta x>0$ for absorption and $\Delta x<0$ for desorption. Making the series of measurements of Δx, it is possible to determine the absolute hydrogen sorption capacity (x) of the material:

Equation 3

$$x = x_0 + \Delta x .$$

Note that the correct (i.e. free from systematic error) value of the hydrogen sorption capacity can be obtained only when the starting value, x_0, is known. The measurements are usually begun from absorption when a material is in the non-hydrogenated state, x_0=0. After completing the absorption and beginning desorption, starting value x_0=x_f is assumed to be equal to the value x_f finally calculated for the previous absorption experiment.

As it is seen in Figure 4.19, the monitored temperatures include the temperature, T_S, of the sample in the reactor (volume V_S); room temperature, T_R, of the connecting capillary pipeline (volume V_C); and the temperature, T_0, in the thermostated gas-distributing system. The latter includes the volumes, V_{160}, V_{16} and $V_{2.5}$ of the corresponding sections where the sensors, which provide monitoring the pressures P_1 (in V_{160}, 0–160 bar), P_2 (in V_{16}, 0–16 bar) and P_3 (in $V_{2.5}$, 0–2.5 bar), are placed.

In so doing,
Equation 1 can be modified to determine starting (n_0) and actual (n_1) number of H_2 moles in the system:

UNIVERSITY of the
WESTERN CAPE

Equation 4

$$n_0 = \frac{P_0 V_S}{Z(P_0, T_S) R T_S} + P_j \left(\frac{V_C}{Z(P, T_R) R T_R} + \frac{V_j}{Z(P, T_0) R T_0} \right);$$

$$n_1 = P_j \left(\frac{V_S}{Z(P, T_S) R T_S} + \frac{V_C}{Z(P, T_R) R T_R} + \frac{V_j}{Z(P, T_0) R T_0} \right);$$

where P=P_1, V_j=V_{160} for hydrogenation (H absorption); and P=P_3, V_j=V_{160}+V_{16}+$V_{2.5}$ for H desorption. P_0 is equal to the pressure in the reactor before opening reactor valve.

The parameters monitored by the Setup are schematically shown in 4.19

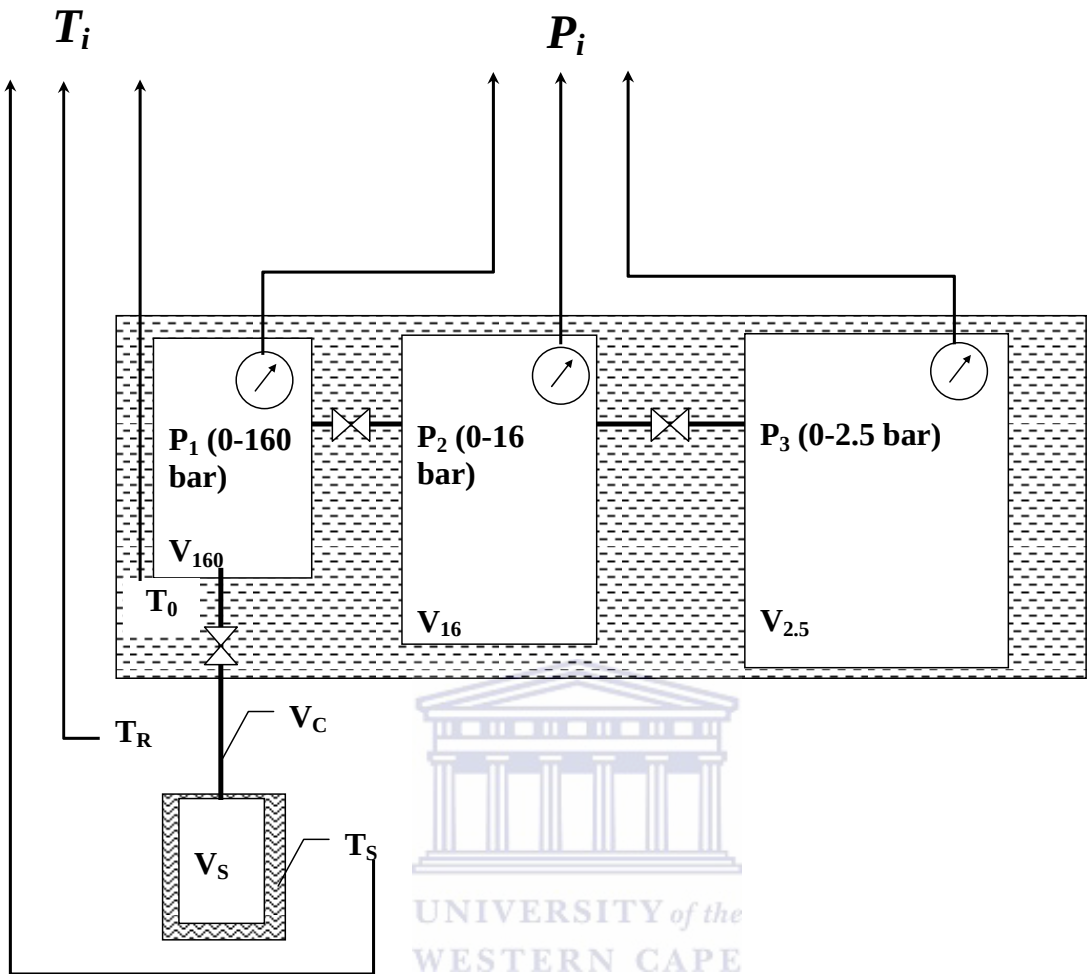

UNIVERSITY of the WESTERN CAPE

Figure 4.19 Schematic representation of parameters monitored by the Set-up.

4.4.1. Thermo-gravimetric study of hydrogen sorption properties of Fe/Ti based composite materials:

Comparative studies were made to identify the differences in hydrogen weight % in the pristine alloy, the modified alloy and the composite materials. Below is absorption/ desorption patterns recorded by the Rheometric STA 1500 scientific TGA.

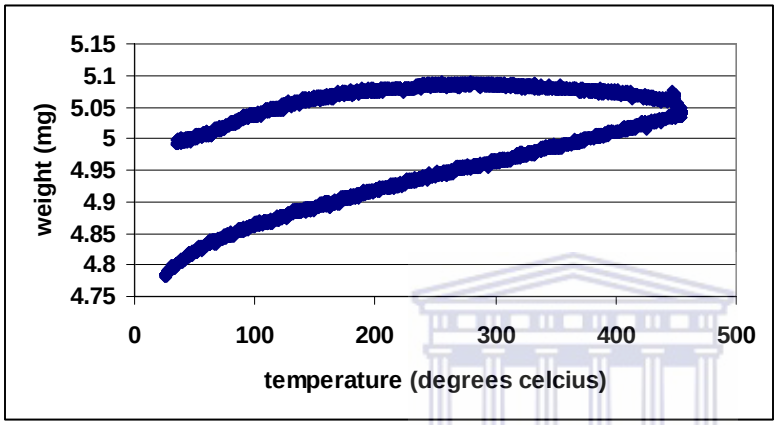

Fig 4.20: TGA absorption/desorption pattern for the unmilled Fe/Ti sample showing an average maximum of ~1.8% wt hydrogen capacity corresponding to known values in literature.

UNIVERSITY of the
WESTERN CAPE

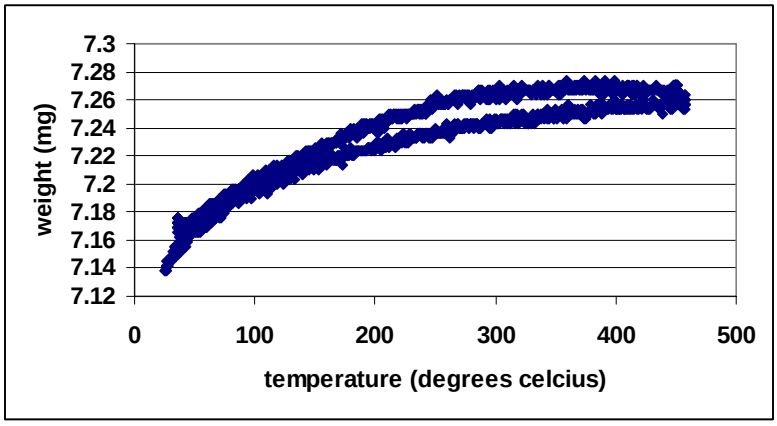

Fig 4.21: TGA absorption/desorption pattern for the sample milled for 60 mins – 3cm balls – 350 rpm showing an average maximum of ~2% wt hydrogen capacity.

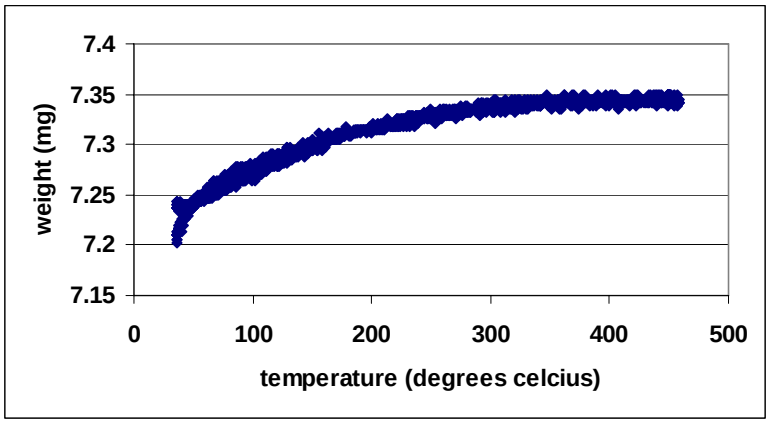

Fig 4.22: TGA absorption/desorption pattern for the sample milled for 60 mins – 3cm balls – 350 rpm + CNT showing an average maximum of ~1.9% wt hydrogen capacity.

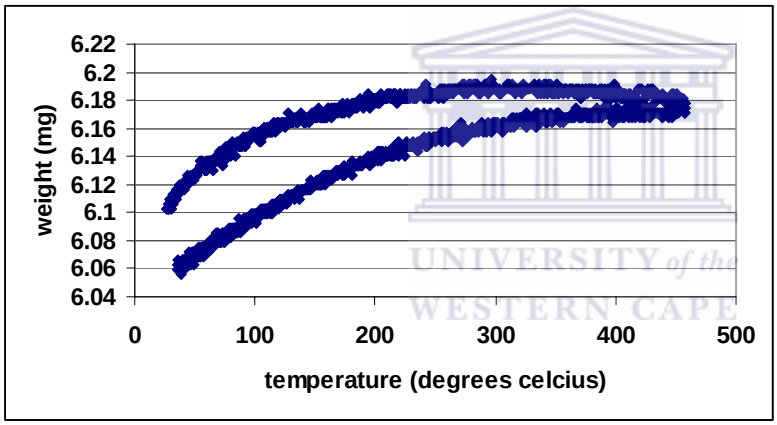

UNIVERSITY of the WESTERN CAPE

Fig 4.23: TGA absorption/desorption pattern for the sample milled for 60 mins – 3cm balls – 350 rpm + CNT + Pd showing an average maximum of ~2.1% wt hydrogen capacity.

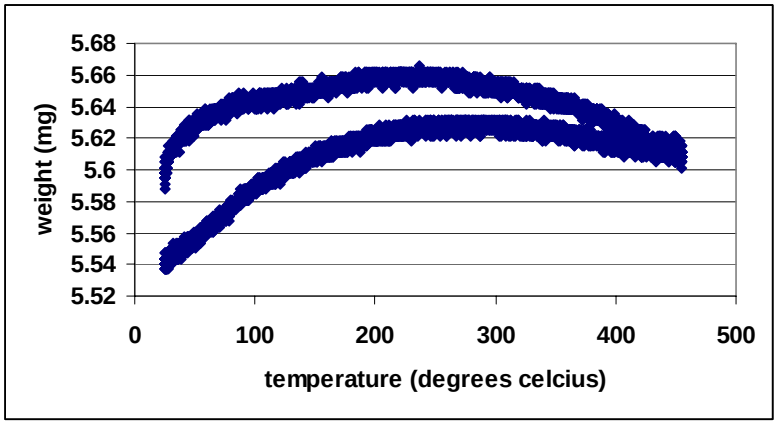

Fig 4.24: TGA absorption/desorption pattern for the sample milled for 60 mins – 3cm balls – 350 rpm + CNT + Pd + Mg showing an average maximum of ~3.35% wt hydrogen capacity.

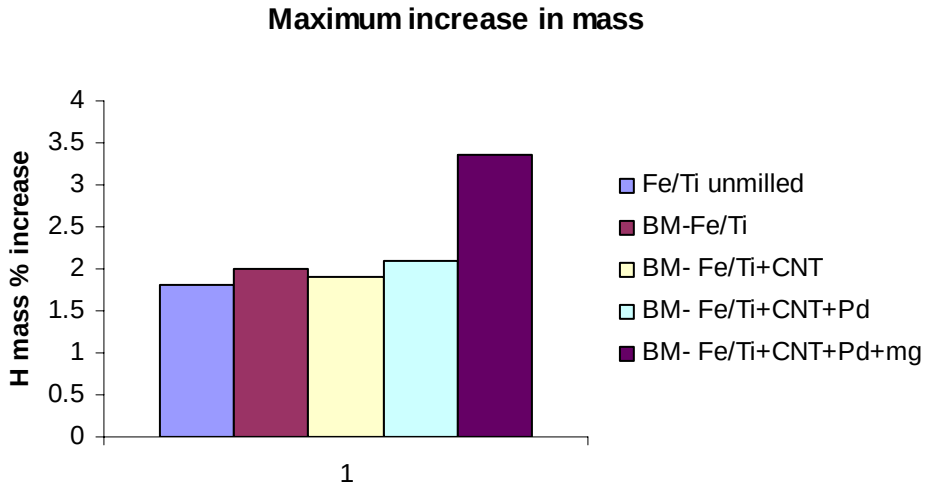

Fig 4.25: Progressive increase in mass % hydrogen capacity in composite layers (BM- ball milled).

UNIVERSITY of the
WESTERN CAPE

From TGA results, a maximum mass capacity of 1.8% was observed for the pristine alloy. After ball milling pre-treatment, a marginal increase to 2% was observed There was no further increase in mass capacity for the carbon nanotube and Ti/Fe composite layer rather a decrease to 1.9 %, however, concomitant to our logic, this layer provided a scaffolding effect for relatively easy deposition of the palladium layer which caused an increase in mass capacity to 2.1%. The most appreciable increase was recorded from the magnesium layer on the composite which caused a rise in mass capacity to 3.35 %.

4.4.2. Volumetric study of Ti/Fe as a core material:

Preliminary experiment was carried out the pristine alloy using the Sievert type apparatus to determine the activation kinetics of the commercial TiFe (Alfa Aesar, 40:60 wt%,-40 mesh) alloy for hydrogen absorption/ desorption. This is because results of the EDS analysis are rather unexpected. Although they indicate that the compositions of the phases approximately correspond to formulae TiFe and $TiFe_2$ (*Table 4.2*) that is in agreement with the Ti–Fe phase diagram [111], the phase TiFe was found as the impurity, and the phase $TiFe_2$ – as the matrix one. It is confirmed by the results of the total analysis (*Table 4.3*) showing that the average composition of the alloy in the studied region is close to $TiFe_2$, as well as by reduced Ti content in the impurity phase (point 1) as compared to TiFe composition. There are possible two reasons of this: (i) – selective oxidation of Ti in near-surface layer followed by segregation of $TiFe_2$ intermetallide; and (ii) – error in charge composition or burning-out of titanium in the course of the alloy preparation. The quantitative XRD analysis is necessary to clear, which reason takes place in fact. However, these results allow understanding the above-mentioned very poor hydrogenation behaviour of the material, since $TiFe_2$ does not absorb noticeable amounts of hydrogen [111].

UNIVERSITY of the
WESTERN CAPE

Hydrogen absorption experiments using the Sievert's type apparatus:

First the reactor assembly was put into the furnace. Then all the gas systems of the set-up were evacuated. After which the reactor was opened and left open through the duration of all series of experiments. The furnace was switched on and temperature set at 500^{o}C (which is set-point for Ti- containing samples). Then we started logging the reaction temperature, noting the value of vacuum to event log at set point temperature. The sample was kept under evacuation at activation temperature for 1 hour and the value of vacuum to event log noted. The furnace was then switched off and the sample left to cool to room temperature under evacuation. After this we stopped logging the reaction temperature and saved the data. The sample was then hydrogenated and the total hydrogen absorption capacity measured. Hydrogen pressure was released from the system by opening the "release" valve and then closing it. The process was repeated severally and only considered complete when the total hydrogen absorption capacity measured was reproduced from cycle to cycle, which was about ten times in this case.

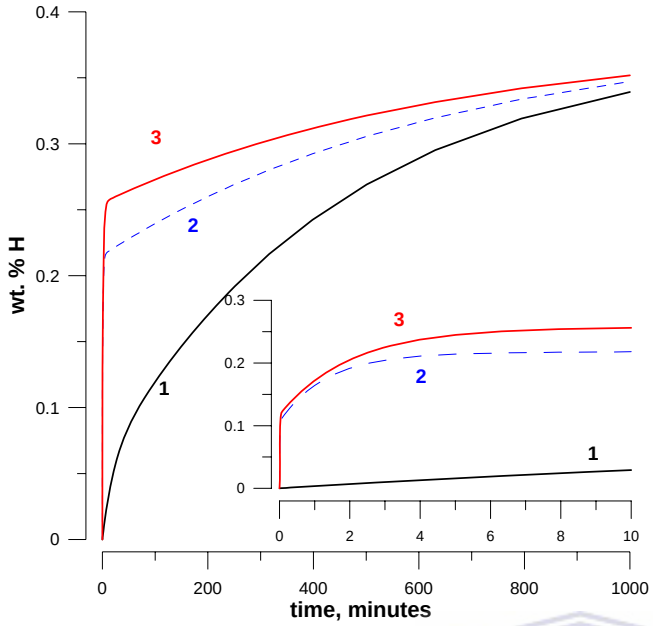

Figure 4.26: Dynamics of hydrogen absorption by the as-delivered Ti/Fe sample. Numbers of curves correspond to the number of cycle including vacuum heating at T=450 °C for 1 hour followed by hydrogen absorption at T=25°C and starting H_2 pressure ~30 bar

UNIVERSITY of the WESTERN CAPE

Hydrogen absorption characteristics of the starting Ti/Fe alloy (Figure 4.26) show that the first hydrogenation cycle (curve 1) is characterised by the poor dynamics: the maximum H sorption capacity was reached in more than 16 hours. However, the repeated vacuum heating significantly accelerates hydrogen absorption, and 90% of maximum H capacity is reached in 5-10 minutes (curve 2). The third cycle also improves dynamics of hydrogen absorption, and becomes reproducible for the following cycles. This behaviour is typical for TiFe which requires several activation cycles to show satisfactory H absorption / desorption performances [112]. However, in all cases the maximum H storage capacity was low, not more than 0.35 wt.%, or about 20% of the reported value for TiFe [112]. According to both XRD and SEM data it is caused by the fact that the intermetallic compound TiFe is evident in the Ti/Fe alloy as a minor phase, while the main phase is a non-hydride-forming $TiFe_2$. Moreover, as it can be seen from Table 4.2, in the minor TiFe phase the significant substitution of Ti with not hydride-forming elements (Al, Si, Cr; ~6 atom% in total) takes place. It could result in the further decrease of the H storage capacity of the Ti/Fe alloy. This highlights the clumsy sorption kinetics and low volume H % capacity of the commercially obtained sample as recorded by Sievert's analysis and the need for pretreatment and further modification.

However, in extraneous research, attempting to correct this anomaly, reducing the "impediment" for hydride formation ($TiFe_2$ phase) could be achieved by the doping of the parent alloy with titanium; the amount of the dopant was estimated from the EDS analysis (Table 4.2-4.3) as 30 wt.% relating to the starting Ti/Fe alloy. Ball milling with TiH_2 was selected to introduce the extra titanium into the alloy, since (i) this procedure is more simple in realisation and less expensive than conventional melting, (ii) it was recently shown [113]that ball milling of TiH_2 with Fe results in the formation of hydrogenated TiFe, and (iii) such a procedure yields the nanoscale particles of the hydride forming alloy, heightening expectations of better activation and kinetic performances as compared with the pristine intermetallide.

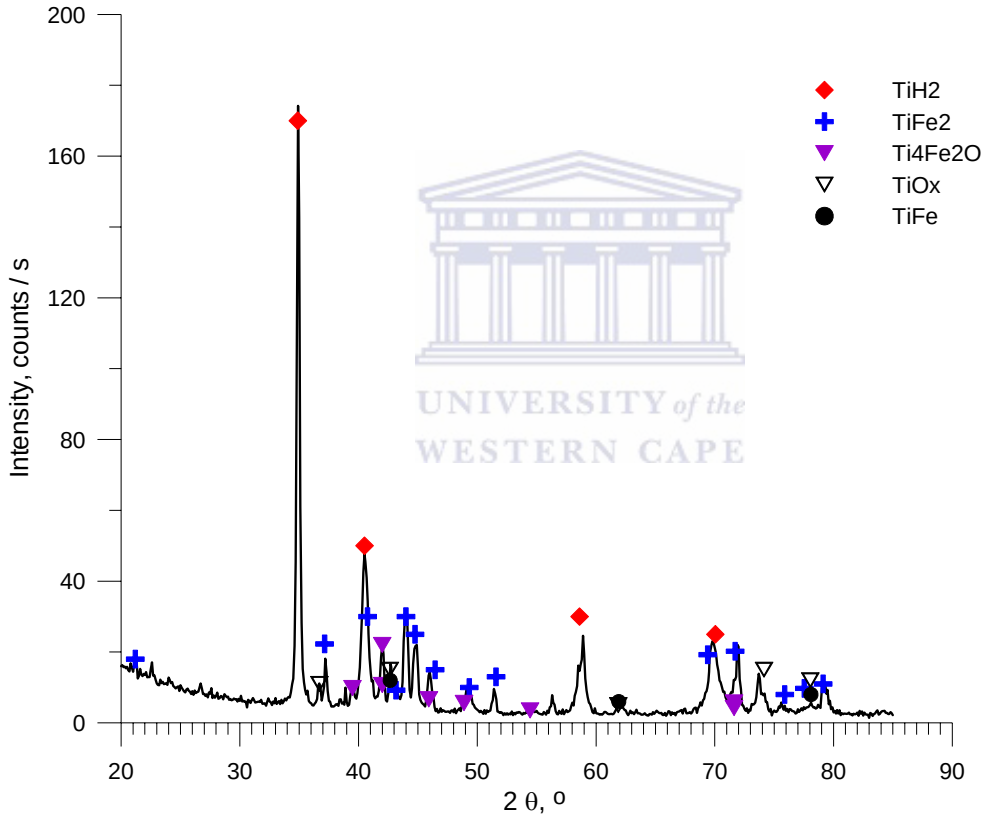

UNIVERSITY of the WESTERN CAPE

Figure 4.27: XRD pattern of the mixture Ti/Fe + 30% TiH_2 before ball-milling

Compared to the patterns of the starting Ti/Fe alloy (Figure 4.7) and its mixture with TiH_2 before ball milling (Figure 4.27), the XRD pattern of the Ti/Fe + TiH_2 mixture ball-milled in argon for one hour (Figure 4.28) shows very weak diffuse peaks testifying that the sample is in the state

close to amorphous one. Nevertheless, the existing peaks do not show the presence of $TiFe_2$ in the ball-milled mixture, moreover the most intensive peaks can be ascribed to TiFe, and to the traces of its monohydride, TiFeH. Such a behaviour is similar to one reported for the phase transformations during ball milling of TiH_2 + Fe mixture [113]. However, in this case the significant amorphization was observed after just 1 hour of milling, ratifying the earlier experiment with as produced Ti/Fe alloy, whereas authors [113] observed this effect only after 2 days of milling. Most probably due to different starting charges, since we already had intermetallic starting alloy Ti/Fe ($TiFe_2$ + TiFe) that was supposed to facilitate the mechanical alloying with TiH_2.

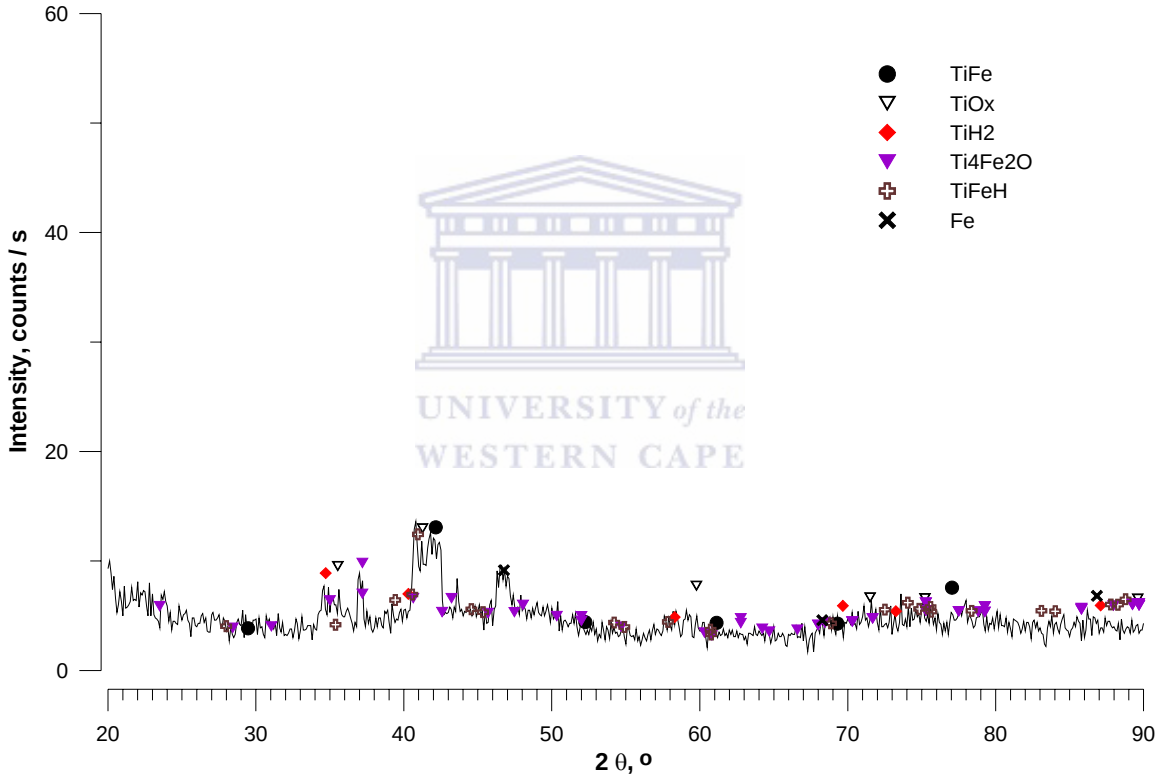

UNIVERSITY of the WESTERN CAPE

Figure 4.28: XRD pattern of the Ti/Fe + 30% TiH_2 sample, ball-milled for 1 hour

Figure 4.29 shows the indexed XRD pattern of the 1 hour ball milled sample Ti/Fe + 30% TiH_2 after 3 cycles including vacuum heating to 450...500 ^{o}C for 1 hour and consequent hydrogenation

at starting hydrogen pressure 30...50 bar and room temperature . In contrast with the ball milled Ti/Fe + 30% TiH_2 (Figure 4.24), the hydrogenated sample shows pronounced crystallinity. This is most probably due to re-crystallization processes in the course of repeated dehydrogenation–hydrogenation.

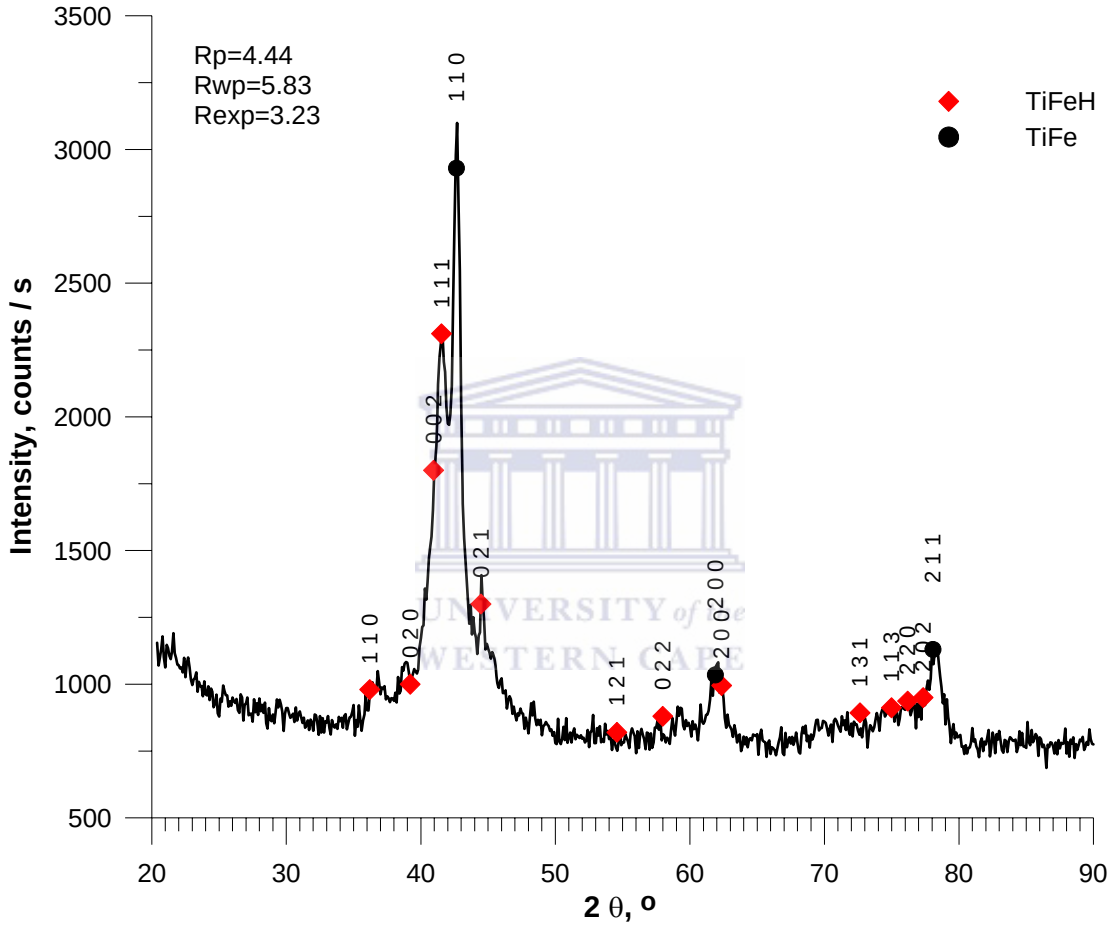

Figure 4.29: XRD pattern of the hydrogenated Ti/Fe + 30% TiH_2 sample, ball-milled for 1 hour

As it can be seen from Table 4.6 below, not all the sample was hydrogenated to TiFeH, about 40 vol.% of the TiFe intermetallide was left unhydrogenated. The lattice periods of TiFeH are in correspondence with literature data [97] showing deviations –3.5% for *a*, +1.7% for *b* and +0.3% for *c*. Despite this, the lattice period of TiFe is 10% higher than was i, Cr, S; see Table 4.2, Table

4.3) in the parent alloy reducing the total H sorption capacity. reported in literature [96] probably caused by hydrogen dissolution in the intermetallide to form α-phase with expanded lattice.

Table 4.6: Results of the Rietveld refinement of the hydrogenated Ti/Fe + 30% TiH_2 sample, ball-milled for 1hour (Figure 4.29).

Phase	Lattice periods, Å			Estimated quantity, vol.%
	a	*b*	*c*	
$TiFeH_{\sim 1}$	2.9757	4.5917	4.4045	58.48
TiFe	2.9961	–	–	41.52

Figure 4.30 below shows the hydrogenation behaviour of the ball-milled sample Ti/Fe + 30% TiH_2 (milling time 1 hour) under the same conditions as the "as-delivered" sample (Figure 4.22). It can be seen that in this case much better activation behaviour and hydrogenation kinetics were observed; 90%hydrogenation takes place in less than 3 minutes, and after the second cycle hydrogenation curves become reproducible. The maximum H concentration is about 0.75 wt.% H that is ~2 times more than for the "as-delivered" Ti/Fe alloy, and the residual hydrogen concentration (P=0.05 bar, T=100 oC) corresponds to H/TiFe ~0.3. However, even for the ball-milled sample the maximum hydrogenation was not observed, and the final product was shown to contain less than 80% of monohydride TiFeH (confirmed by the XRD data in Table 4.5). The most probable reason for this is the presence of impurities of non hydride-forming elements (Al, S, Si, Cr, S; see Table 4.2, Table 4.3) in the parent alloy reducing the total H sorption capacity.

UNIVERSITY of the WESTERN CAPE

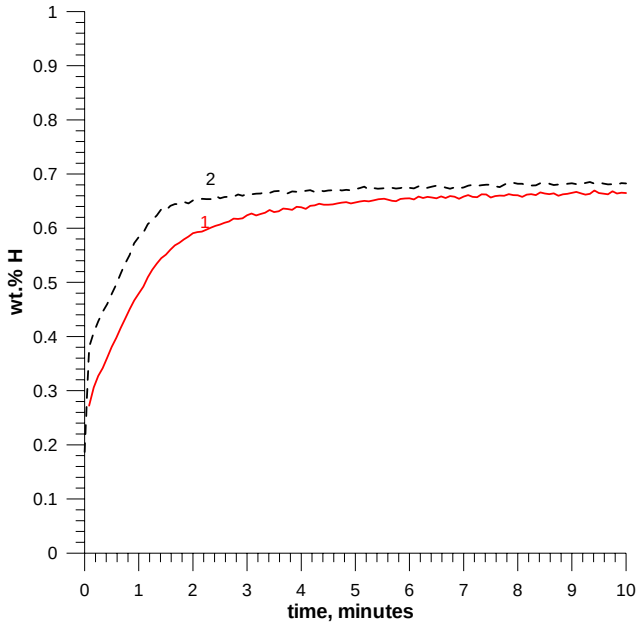

Figure 4.30: Dynamics of hydrogen absorption by the sample Ti/Fe + 30% TiH_2 sample, ball-milled for 1 hour. Numbers of curves correspond to the number of cycle including vacuum heating at T=450 ^oC for 1 hour followed by hydrogen absorption at T=25^oC and starting H_2 pressure ~30 bar.

UNIVERSITY of the
WESTERN CAPE

4.5. Overview of main points:

A mechano-chemical method of pretreatment has been successfully applied on the commercially obtained Ti/Fe through ball milling and parameters have been optimized as follows; milling time – 60 mins, milling speed – 350rpm, ball size- 3cm and the following observations were made (a) This has induced a complete amorphization of the alloy as shown by XRD analysis; (b) The surface area of the alloy has been increased from 0.0389 m^2/g to 2.0289 m^2/g thereby creating fresh surfaces for H adsorption; (c) This treatment has facilitated the surface modification of the alloy by carbon nanotubes, as it has been shown [15] that only nano-size metal particles can catalyze the growth of CNT.

A method of carbon nanotube synthesis on the surface of pre-treated Ti/Fe alloy by chemical vapour deposition using liquefied petroleum gas (LPG), a multi-component and readily available hydrocarbon source, has been employed and investigated. The set-up for this method was ascertained to be quite uncomplicated when compared to other methods of carbon nanotube synthesis (arc discharge and laser ablation). This is expedient for commercial potential. The process has been optimized as follows; flow rate-0.35 L/min, growth temperature-800^oC; gas deposition time- 60 minutes. High quality and purity carbon nanotubes with diameter range of 20-70 nm and length range of ~100 μm have been synthesized as shown by SEM and TEM analysis. These carbon nanotubes have further increased the surface area of the pre-treated alloy from 2.0289 m^2/g to 19.7277 m^2/g, a factor of 10. This is expected to further enhance H diffusion kinetics in this composite; the mechanism responsible for this physico-chemical reaction is still subject to further investigation. Carbon nanotubes have been discovered to possess a scaffolding effect by stabilizing binary metal nano-particles [18]. This process suggests that the metal nano-particles spill hydrogen preferentially to the external walls or groove-sites. The spill-over of hydrogen in carbon nanotubes can be envisaged as an effective method to enhance their hydrogen storage capacities. This conforms ideally with our layer by layer approach for creation of this novel composite material for hydrogen storage.

Methods of surface modification of the Ti/Fe-CNT composite by nano-size binary palladium and magnesium metals via electroless deposition and ultrasound deposition techniques have been explored. These subsequent layers are tailored to enhance activation kinetics and increase H wt% capacity as repeatedly shown in literature review [33-36, 67-69, 72]. Care has been taken to optimize deposition conditions including; deposition rate, composition and concentration of bath

UNIVERSITY of the WESTERN CAPE

constituents and deposition temperature. 10% each of the palladium and magnesium layer in the total mass of the composite have been seen to yield optimum results.

Hydrogen mass% capacity has been increased from ~2% wt in the core commercially obtained Fe/Ti alloy to ~3.35% in the composite material as shown by thermal gravimetric analysis (TGA).

Volumetric hydrogen sorption properties of the starting Ti/Fe alloy were characterised by Sievert's measurements. It was shown that the starting alloy is characterised by poor activation performances and hydrogen storage capacity. The latter does not exceed 20% of the reported value for TiFe. This is caused by the presence of non hydride forming $TiFe_2$ phase, as well as by the contamination of the alloy with non hydride-forming elements (Al, Si, Cr, S). This was addressed in part by milling the as-produced Ti/Fe alloy in 30% TiH_2. This was seen to increase the H storage capacity by a factor of 2, as well as drastically improve the activation behaviour of the alloy.

UNIVERSITY of the
WESTERN CAPE

Chapter 5

Conclusions and Recommendations:

The objective of this study was to develop a novel composite hydrogen storage material with high H wt% storage capacity, high intrinsic safety, appropriate thermodynamics, high mechanical strength, easy activation, reversibility of the system, and fast sorption kinetics based on a well known "low temperature" intermetallic alloy as the core. In the course of achieving this objective, the structural, thermal, chemisorptive and physisorptive attributes of this material on a nano-scale have been evaluated considering that nano-structuring is a potentially promising approach for controlling bond strength, kinetics, and sorption temperatures and pressures. By combining different materials with suitable catalytic and thermodynamic properties, a new class of hybrid hydrogen storage material has been developed. More importantly, the focus was to increase the capacity of hydrogen adsorbed in this material. This goal was achieved with the mechano-chemical pre-treatment of Fe/Ti alloy and surface modification with carbon nanotubes, binary palladium and magnesium metals via a layer-by-layer modification technique. The chemical and mechanical stability of hydrogen storage materials is of great importance because hydrogen storage materials must withstand repeated adsorption and desorption cycles. The layer by layer approach that was used in this project allowed the investigation of the chemical and mechanical stability of the materials as each layer was added. Through this layer by layer approach suitable nano-particles were introduced that are chemically and mechanically stable. The knowledge emanating from this investigation is expected to allow the directed design of new, higher-efficiency, recyclable hydride-based materials in pursuance of the 6.0 wt% goal set forth by the US Department of Energy.

A set of physico-chemical properties governing the applicability of the chosen materials as hydrogen storage materials due to the incentives they offer were identified in a comprehensive literature review. Experimental tasks were formulated to address the short-comings of the core Fe/Ti alloy and a detailed research work plan was designed to address these issues. The novelty of the chosen research work plan was also highlighted.

UNIVERSITY of the WESTERN CAPE

- Fe/Ti surface pre-treatment through ball milling has been optimized as follows; milling time – 60 minutes, milling speed – 350rpm, ball diameter- 3cm.

- Novel experiments yielding carbon nanotubes on nickel, cobalt substrates and carbon cloth using Liquefied Petroleum Gas (LPG) as a hydrocarbon source were carried out. Based on the possibilities discovered, experiments were carried out to modify pre-treated Fe/Ti alloy with carbon nanotubes and the synthesis parameters were optimized as follows; LPG flow rate-0.35 L/min, growth temperature-800^{o}C; LPG deposition time- 60 minutes. High quality and purity carbon nanotubes were synthesized to form a composite.

- An electroless deposition technique was applied to modify the composite with binary palladium nano-particles from a palladium- ammonia complex and the parameters were optimized as follows; concentration of solution- 0.1M per gram of composite; reducing agent- hydrazine; deposition time- 4 hrs 30 minutes.

- A sono-chemical (ultrasound) deposition method was explored for the introduction of binary magnesium nano-particles on the composite from a magnesium- organic complex and the parameters were optimized as follows; concentration of solution- 0.1M per gram of composite; reducing agent- H_2; deposition time- 3 hrs.

UNIVERSITY of the WESTERN CAPE

Standard characterization tools were reviewed and used in the investigation of this material including Transmission Electron Microscope (TEM), Scanning Electron Microscope (SEM), X-ray diffraction (XRD), Brunauer-Emmett-Teller (BET) surface area and porosity analyzer, Thermo-gravimetric analyzer (TGA), and the Sievert-type apparatus.

- SEM and TEM microscopy were used to image down to nanometer sizes, to discern interfaces, surfaces topography and relief, internal structures in the bulk material, cross sections of thin film materials, void structures, and surface film thickness. More importantly these techniques provided crucial details regarding length, diameter and type of carbon nanotubes synthesized in the composite as this was vital to alteration of synthesis parameters to tailor products optimally for hydrogen sorption. EDS showed that aside from the fact that the commercial intermetallic alloy showed non hydride forming $TiFe_2$ as the matrix phase, and hydride forming TiFe as the impurity phase that there was

considerable contamination of S, Cr, Al, Si in the material probably a result of preparation materials used by the manufacturer.

- Structural identification, phase transformations, atomic bonding & strain were determined by X-Ray Diffraction (XRD). Specifically, amorphization of the core alloy was confirmed. There is considerable body of knowledge on the marked improvement of hydrogen sorption properties of metal alloys in the amorphous phase in comparison to their bulk structure because partially opened pores and smaller dimensions of broken crystallites would facilitate access to the sites, lowering considerably both geometrical and diffusion limitations. It was seen from XRD that comparatively short ball milling time (60 minutes) resulted in the formation of the nanoscale / close to amorphous microstructure of the material.

- BET analysis by N_2 physisorption in the Ti/Fe – CNT composite was used to determine the influence of carbon nanotubes on the total surface area of the material. As mentioned earlier, these carbon nanotubes further increased the surface area of the pre-treated alloy by a factor of 10.

UNIVERSITY of the
WESTERN CAPE

- TGA was used to monitor the thermodynamic, kinetic, chemical and physical properties of materials as they change with temperature. The thermal stability of the composite material at temperature range (25^oC - 450^oC) which ratifies its suitability for practical applications and the H mass capacity of the core and composite materials were confirmed by thermo-gravimetry.

- Preliminary volumetric analysis was made using the Sievert's type apparatus, to determine the activation kinetics of the commercially obtained and un-treated core. This characterization technique was imperative so as to justify the need for pre-treatment and further modification. It was ascertained that the high activation temperature and copious cycles required for full activation of this Ti/Fe sample (40:60 wt%, -40 mesh, Alfa Aesar) was probably because although compositions of the phases approximately correspond to formulae Ti/Fe and Ti/Fe_2, the phase Ti/Fe (hydride forming) was found as the impurity, and the phase Ti/Fe_2 (non hydride forming) as the matrix one. This result explains the above-mentioned very poor hydrogenation behavior of the material, since $TiFe_2$ does not absorb noticeable amounts of hydrogen hence the source and metallurgical procedures

used for production of the commercial alloy should be scrutinized before further studies. However, further volumetric studies should be done on the composite since the accuracy of the volumetric techniques is potentially greater when compared to that of the thermo-gravimetric techniques, because large changes in gas pressure are measured rather than small changes in mass. This also explains the discrepancies between the TGA results and that of the Sievert's apparatus. However, this is a time consuming process and will form part of the future work. Some of the more important characteristics to be recorded are kinetics of the sorption processes and cycling stability.

- It was shown that ball milling with TiH_2 significantly improves activation performances, hydrogen absorption kinetics and H storage capacity of the Ti/Fe intermetallic compound.

As a result of the hydrogen mass capacity increase from ~2 wt% in the core Ti/Fe to ~3.35 wt% in developed composite as recorded from TGA, it was established that Ti/Fe is a promising core alloy for development of composite "low temperature" hydrogen storage materials. This presents numerous possibilities in the future study of Ti/Fe as a core for solid-state composite hydrogen storage materials. These include:

UNIVERSITY of the
WESTERN CAPE

- optimizing the core alloy with regards to volumetric H storage capacity and sorption kinetics
- creating a new core by alloying Ti/Fe with promising group V and VI elements which show high H wt % capacities
- modifying these materials via the realized layer by layer technique
- volumetric study of H sorption performances of the materials modified by carbon nanotubes and the influence of additional surface modification (e.g. Pd, Co, Cu coating) of the materials on their H absorption – desorption, impurity resistance and cyclic stability properties.

The developed composites are expected to maintain the chemical and mechanical integrity of the core.

REFERENCES

(1) Zuttel, A.; Schlapbach, L. Hydrogen-storage materials for mobile applications. *Nature*, 414, (2001) 772-782.

(2) Zhou, L. Progress and problems in hydrogen storage methods. *Renewable and Sustainable Energy Reviews*, 9, (2005) 395–408.

(3) Zuttel, A. Hydrogen storage methods and materials. *Naturwissenschaften*, 91, (2004) 157-172.

(4) Fakioglu, E.; Yurum, Y.; Veziroglu, T. N. A review of hydrogen storage systems based on boron and its compounds. *International Journal of Hydrogen Energy*, 29, (2004) 1371-1376.

(5) Nijkamp, M. G.; Raaymakers, J. E. M. J.; van Dillen, A. J.; de Jong, K. P. Hydrogen storage using physisorption - materials demands. *Applied Physics A- Materials Science & Processing*, 72, (2001) 619 – 623.

(6) Sandrock, G. A panoramic overview of hydrogen storage alloys from a gas reaction point of view. *Journal of alloys and compounds*, 293-295, (1999) 877-888.

(7) Dantzer, P. Properties of intermetallic compounds suitable for hydrogen storage applications. *Materials Science and Engineering*, A329–331, (2002) 313–320.

(8) A Multiyear Plan for the Hydrogen R&D Program Rationale, Structure, and Technology Roadmaps.– Office of Power Delivery; Office of Power Technologies; *Energy Efficiency and Renewable Energy*; U.S. Department of Energy; August (1999)– 55 pp.

(9) Skolnik, E.G. Technical assessment and analysis of hydrogen R&D projects – *Proceedings of the 2000 Hydrogen Program Review*, NREL/CP-570-28890.

(10) Hydrogen – the fuel for the future – Produced for the U.S. Department of Energy (DOE) by the *National Renewable Energy Laboratory*, a DOE national laboratory. DOE/GO-10095-099, DE95004024, March (1995)

(11) Chalk, S.; Inouye, L. The President's Hydrogen Initiative: U.S DOE's Approach – *A Paper for the Biennial Asilomar Conference on Energy and Transportation on "The Hydrogen Transition"*, July-August (2003)

(12) Satyapal, S. *Overview of Hydrogen storage activities*, U.S Department of Energy, June 20, (2005)

(13) Fujii, H.; Orimo, S-I. Hydrogen storage properties in nano-structured magnesium and carbon-related materials. *Physica B*, 328, (2003) 77-80.

UNIVERSITY of the WESTERN CAPE

(14) Zaluska, A.; Zaluski, L.; Strom-Olsen J.O. Structure, catalysis and atomic reactions on the nano-scale: a systematic approach to metal hydrides for hydrogen storage. *Appl. Phys.A*, 72, (2001)157-165.

(15) Popov, V.N. Carbon nanotubes: properties and application. *Material Science and Engineering*, R, 43, (2004) 61-102.

(16) Lamari Darkrim, F.; Malbrunot, P.; Tartaglia, G.P. Review of hydrogen storage by adsorption in the carbon nanotubes. *International Journal of Hydrogen Energy*, 27, (2002) 193-202.

(17) Schlapbach, L. Hydrogen as a Fuel and its Storage for Mobility and Transport. *MRS Bulletin*, September (2002).

(18) Zacharia, R.; Kim, Y.K.; Fazle Kibria, A.K.M.; Nahm, K.S. Enhancement of hydrogen storage capacity of carbon nanotubes via spill-over from vanadium and palladium nanoparticles. *Chemical Physics Letters*, 412, (2005) 369–375.

(19) Hamburg, Y.Du.; Dubovkin, N.F. (Eds.), Hydrogen: Properties, Production, Storage, Transportation, Applications. Reference Book, *"Khimia"*, Moscow, (1989).

(20) Sandrock, G. *Hydrogen Implementation Agreement*. Presented at 2005 NORSTORE conference, Hverageroi, Iceland, 2-3 June 2005.

(21) Takagi, H.; Hatori, H;Yamada, Y;Matsuo, S;Shiraishi, M. Hydrogen adsorption of activated carbons with modified surafces. *Journal of alloys and compounds*, 385, (2004) 257-263.

(22) Shindo, K.; Kondo, T.;Sakurai, Y. Dependence of hydrogen storage characteristics of mechanically milled carbon materials in their host structures. *Journal of alloys and compounds*, 372, (2004) 201-207.

(23) Shindo, K.; Kondo, T.;Sakurai, Y. Hydrogen physisorption capacities of mechanically milled activated carbon powders in a H2 atmosphere using a gravimetric method. *Journal of alloys and compounds*, 379, (2004) 252-255.

(24) Zuttel, A.; Nutzendal, Ch.; Sudan, P.; Mauron, Ph.; Emmenegger, Ch.; Rentsch, S.; Schlapbach, L.; Weidenkaff, A.; Kiyobayashi, T. Hydrogen sorption by carbon nanotobes and other carbon nanostructures. *Journal of alloy and compounds*, 330-332, (2002) 676-682.

(25) Serp, P.; Massimiliano, C.; Kalck, P. Carbon nanotubes and nanofibers in catalysis. *Applied Catalysis A*: 253, (2003) 337-358.

(26) Yartys, V.A.; Riabov, A.B.; Denys, R.V.; Sato, M.; Delaplane, R.G. Novel intermetallic hydrides. *Journal of Alloys and Compounds*, 408–412, (2006) 273–279.

UNIVERSITY of the WESTERN CAPE

(27) Deng, C.; Shi, P.; Zheng, S. Effect of surface modification on the electrochemical performances of $LaNi_5$ hydrogen storage alloy in Ni/MH batteries. *Materials Chemistry and Physics*, 98, (2006) 514–518.

(28) Fukai, Y. *The Metal-Hydrogen System - Basic Bulk Properties*. Springer-Verlag, Berlin, 27 (1993) 113-118.

(29) Buchener, H.; Povel, R. The Daimler-Benz Hydride Vehicle Project. *Int. J. Hydrogen Energy*, 7, (1982) 259.

(30) Eberle, U.; Arnold, G.; von Helmolt, R. Hydrogen storage in metal-hydrogen systems and their derivatives. *Journal of Power Sources*, 231,(2005) 551-557.

(31) Schlapbach, L.; Züttel, A.; Gröning, O.; Gröning, P.; Aebi, P. Hydrogen for novel materials and devices. *Appl. Phys*. A 72, (2001)245–253.

(32) Tran, N.E.; Imam, M.A.; Feng, C.R. Evaluation of hydrogen storage characteristics of magnesium-misch metal alloys. *Journal of alloys and compounds*, 359, (2003) 225-229.

(33) Berlouis, L.E.A.; Cabrera, E.; Hall-Barientos, E.; Hall, P.J.; Dodd, S.; Morris, S.; Imam, M.A. A thermal analysis investigation of the hydriding properties of nanocrystalline Mg-Ni based alloys prepared by high energy ball milling. *Journal of alloy and compounds*, 305, (2000) 82-89.

(34) Paillier, J.; Roue, L. Hydrogen electrosorption and structural properties of nanostructured Pd–Mg thin films elaborated by pulsed laser deposition. *Journal of Alloys and Compounds*, 392,(2005) 990-998.

(35) Kishore, S.; Nelson, J.A.; Adair, J.H.; Eklunda, P.C. Hydrogen storage in spherical and platelet palladium nanoparticles. *Journal of Alloys and Compounds*, 389, (2005) 234–242.

(36) Ambrosio, R.H.; Ticianelli, E.A. Studies on the influence of palladium coatings on the electrochemical and structural properties of a metal hydride alloy. *Surface & Coatings Technology*, 197, (2005) 215– 222.

(37) Zhang, H; Chen, Y; Li, S; Fu, X. Hydrogen storage for carbon nanotubes synthesized by the pyrolysis method using lanthanum nickel alloy as catalyst. *Journal of applied physics*, 94, (2003) 301-310.

(38) Li, Y.; Zhang, X.B.; Tao, X.Y.; Xu, J.M.; Huang, W.Z.; Luo, J.H.; Luo, Z.Q.; Li, T.; Liu, F.; Bao, Y.; Geise, H.J. Mass production of high-quality multi-walled carbon nanotube bundles on a Ni/Mo/MgO catalyst. *Carbon*, 43, (2005) 295-301.

(39) Dresselhaus, M.S.; Dresselhaus, G.; Saito, R. Physics of Carbon Nanotubes. *Carbon*, Vol. 33, No. 7, (1995) pp. 883-891.

UNIVERSITY of the WESTERN CAPE

(40) Liu, J.; Fan, S.; Dai, H. Recent Advances in Methods of Forming Carbon Nanotubes. *MRS Bulletin*, April, (2004).

(41) Morales, F.M.; Mendez, D.; Ben, T.; Molina, S.I.; Araujo, D.; Garcıa, R. Structural Study of Micro and Nanotubes Synthesized by Rapid Thermal Chemical Vapor Deposition. *Microchimica Acta*, 145, (2004)129–132.

(42) Shaijumon, M.M.; Ramaprabhu, S. Synthesis of carbon nanotubes by pyrolysis of acetylene using alloy hydride materials as catalysts and their hydrogen adsorption studies. *Chemical Physics Letters*, 374, (2003) 513–520.

(43) Tsarjova, S.Yu.; Zharikov, E.V.; Kovalenko, A.N.; Anoshkin, I.V. Carbon nanostructures formation by catalytic pyrolysis of hydrocarbons. Proceedings of the High Education School. *Electronics*, No.1, (2003) p. 20-24, in Russian.

(44) Kwok, K.; Chiu, K.S.W. Growth of carbon nanotubes by open-air laser-induced chemical vapor deposition. *Carbon*, 43, (2005) 437-446.

(45) Iijima, S.; Ichihashi, T. Single-shell carbon nanotubes of 1-nm diameter. *Nature (London)*, 363, (1993) 603.

(46) Lan, A.; Mukasyan, A. Hydrogen Storage Capacity Characterization of Carbon Nanotubes by a Microgravimetrical Approach. *J. Phys. Chem. B*, 109, (2005) 16011-16016.

(47) Iijima, S. Helical microtubules of graphitic carbon. *Nature (London)*, 354, (1991) 56.

(48) Bethune, D.S.; Kiang, C.H.; de Vries, M.S.; Gorman, G.; Savoy, R.; Vazquez, J.; Beyers, R. Cobalt-catalysed growth of carbon nanotubes with single-atomic-layer walls. *Nature (London)*, 363, (1993) 605.

(49) Thess, A.; Lee, R.; Nikolaev, P.; Dai, H.; Petit, P.; Robert, J.; Xu, C.; Lee, Y.H.; Kim, S.G.; Rinzler, A.G.; Colbert, D.T.; Scuseria, G.E.; Tomane´k, D.; Fischer, J.E.; Smalley, R.E. Crystalline ropes of metallic carbon nanotubes, *Science*, 273, (1996) 483.

(50) Yacaman, M.J.; Yoshida, M.M.; Rendon, L.; Santiesteban, J.G. Catalytic growth of carbon microtubules with fullerene structure, *Applied Physics Letter*, 62, (1993) 202.

(51) Ebbesen, T.W.; Ajayan, P.M. Large-scale synthesis of carbon nanotubes. *Nature (London)*, 358, (1992) 220.

(52) Journet, C.; Maser, W.K.; Bernier, P.; Loiseau, A.; Lamy de la Chapelle, M.; Lefrant, S.; Deniard, P.; Lee, R.; Fischer, J.E Large-scale production of single-walled carbon nanotubes by the electric-arc technique, *Nature (London)*,388, (1997) 756.

UNIVERSITY of the WESTERN CAPE

53) Liu, J.; Rinzler, A.G.; Dai, H.; Hafner, J.H.; Bradley, R.K.; Boul, P.J.; Lu, A.; Iverson, T.; Shelimov, K.; Huffman, C.B.; Rodriguex-Macia, F.; Colbert, D.T.; Smalley, R.E. Fullerene pipes, *Science*, 280, (1998) 1253.

(54) Ivanov, V.; Nagy, J.B.; Lambin, P.; Lucas, A.; Zhang, X.B.; Zhang, X.F.; Bernaerts, D.; Van Tendeloo, G.; Amelinckx, S.; Van Landuyt, J. The study of carbon nanotubules produced by catalytic method, *Chem. Phys. Lett*, 223, (1994) 329.

(55) Kong, J.; Soh, H.T.; Cassell, A.M.; Quate, C.F.; Dai, H. Synthesis of individual single-walled carbon nanotubes on patterned silicon wafers, *Nature (London)*, 395, (1998) 878.

(56) Otvos, Z.; Onyestyak, G.; Valyon, J.; Kiricsi, I.; Konya, Z.; Rees, L.V.C. The dynamics of H_2 and N_2 sorption in carbon nanotubes. *Applied Surface Science*, 238, (2004) 73-76.

(57) Panella, B.; Hirscher, M.; Roth, S. Hydrogen adsorption in different carbon nanostructures. *Carbon*, 43, (2005) 2209-2214.

(58) Akiba, E.; Okada, M. Metallic Hydride 111: Body-Centered-Cubic Solid-Solution alloys. *MRS Bulletin*, September 2002.

(59) Bowman, R.B. Jr.; Fultz, B. Metallic Hydrides 1: Hydrogen Storage and Other Gas-Phase Applications. *MRS Bulletin*, September 2002.

(60) Zuttel, A. Materials for Hydrogen storage. Materials Today, September 2003.

(61) Bodganovic, B.; Sandrock, G. Catalyzed Complex Metal Hydrides. *MRS Bulletin*, September 2002.

(62) Wang, P.; Wang, A.M.; Ding, B.Z.; Hu, Z.Q. Mg–$FeTi_{1.2}$ (amorphous) composite for hydrogen storage. *Journal of Alloys and Compounds*, 334, (2002) 243–248.

(63) Hirscher, M.; Becher, M. Hydrogen Storage in Carbon Nanotubes. – *Journal of Nanoscience and Nanotechnology*, (2003) Vol. 3, No. ½, pp.3-17.

(64) Thomas, G.J.; Guthrie, S.E. Hydrogen storage development. *Proceedings of the 1998 U.S. Hydrogen Program Review* NREL/CP-570-25315.

(65) Dillion, A.C.; Gennet, T.; Alleman, L.; Jones, K.M.; Parilla, P.A.; Heben, M.J. Carbon nanotube materials for hydrogen storage. *Proceedings of the 2000 DOE/NREL Hydrogen program review*, May 8-10, (2000).

(66) Sandrock, G.; Goodel, P.D. Cyclic life of metal hydrides with impure hydrogen: overview and engineering considerations. *Journal of Less-Common Metals*, 104, (1984) 159-173.

(67) Shan, Xi.; Payer, J.H.; Wainwright, J.S. Increased performance of hydrogen storage by Pd-treated $LaNi_{4.7}Al_{0.3}$, $CaNi_5$ and Mg_2Ni.*Journal of Alloys and Compounds*, 88, (2006) 1180-1190.

UNIVERSITY of the
WESTERN CAPE

(68) Sanders J.H.; Tatarchuk, B.J. Buried-interfacial reactivity of palladium-coated Fe_2O_3,/FeTi thin films during vacuum or hydrogen annealing. *J. Phys, Condens. Matter*, 2, (1990) 5809-5818.

(69) Uchida, H. Surface process of H_2 on rare earth based hydrogen storage alloys with various surface modifications. *Int. Journal of Hydrogen Energy*, 24, (1999) 861 – 869.

(70) Uchida, H-H.; Moriai, K.; Aoyama, K.; Kondo, H.; Uchida, H. Effect of alkaline pretreatment on the initial activation of $LaNi_5$ and $LaNi_{2.5}Co_{2.5}$ in the H_2 gas and electrochemical reactions. *Journal of Alloys and Compounds*, 253-254, (1997) 525-528.

(71) Latroche, M. Structural and thermodynamic properties of metallic hydrides used for energy storage. *Journal of Physics and Chemistry of Solids*, 65, (2004) 517–522.

(72) Zaluski, L.; Zaluska, A.; Tessier, P.; Strom-olsen, J.O.; Schulz, R. Catalytic effect of Pd on hydrogen absorption in mechanically alloyed Mg_2Ni, $LaNi_5$ and FeTi. *Journal of Alloys and Compounds*, 217, (1995) 295-300.

(73) Sun, Y-M.; Suda, S. Studies on the fluorination method for improving surface properties and characteristics of AB_5-type hydrides. . *Journal of Alloys and Compounds*, 330-332, (2000) 627-631.

(74) Aoyagi, H.; Aoki, K.; Masumoto, T. Effect of ball milling on the hydrogen absorption absorption properties of FeTi, Mg_2Ni and $LaNi_5$. *Journal of Alloys and Compounds*, 231, (1995) 804-809.

(75) Chen, D.M.; Ichikawa, T; Fujii, H.; Ogita, N.; Udagawa, M.; Kitano, Y.; Tanabe, E. Unusual hydrogen absorption properties in graphite mechanically milled under various hydrogen pressures up to 6 MPa.. *Journal of alloys and compounds*, 385, (2004) 257-263.

(76) Prabhuram, J; Zhao, T.S; Wong, C.W; Guo, J.W. *Journal of Power Sources*, 134, (2004) 555-567.

(77) Lipson, H; Steeple, H. *Interpretation of X-ray Powder Diffraction patterns*. London, Macmillan and Company Ltd, (1970).

(78) Cullity, B.D. *Elements of X-ray Diffraction*, 2nd Edition, Ontario, Addison-Wesley Publishing Company Inc, (1978).

(79) Newbury, D.E.; Joy, D.C.; Echlin, P.; Fiori, C.E.; Goldstein, J.I. *Advanced Scanning Electron Microscopy and X-ray Microanalysis*. New York, Plenum Press, (1986).

(80) Oatley, C.W. *The Scanning Electron Microscope, Part 1: The instrument*, London, Cambridge University Press, (1972).

(81) Fultz, B.; Howe, J.M. *Transmission Electron Microscopy and Diffractometry of Materials*, 2nd Edition, Berlin, Springer-Verlag, (2002).

UNIVERSITY of the
WESTERN CAPE

(82) Webb, P.A.; Orr, C.; Camp, R.W.; Olivier, J.P.; Yunes, Y.S. *Analytical methods in Fine Particle Technology*, Georgia, Micromeritics Instruments Corporation, (1997).

(83) Brown, M.E.; *Introduction to Thermal analysis: Techniques and Applications*, New York, Chapman .and Hall Ltd, (1988).

(84) Pan, X.; Ma, X. Phase transformations in nanocrystalline TiO_2 milled in different milling atmospheres. *Journal of Solid State Chemistry*, 177, (2004) 4098–4103.

(85) Ares, J.R.; Cuevas, F.; Percheron-Guégan, A. Influence of thermal annealing on the hydrogenation properties of mechanically milled AB5-type alloys. *Materials Science and Engineering*, B108, (2004) 76–80.

(86) Small, D.A.; MacKay, G.R.; Dunlap, R.A. Hydriding reactions in ball-milled titanium. *Journal of Alloys and Compounds*, 284, (1999) 312–315.

(87) Jankowska, E.; Jurczyk, M. Electrochemical behaviour of high-energy ball-milled TiFe alloy. *Journal of Alloys and Compounds*, 346, (2002) L1–L3.

(88) Bobet, J-L.; Even, C.; Quenisset, J-M. On the production of ultra-fine titanium hydride powder at room temperature. *Journal of Alloys and Compounds*, 348, (2003) 247–251.

(89) Pritchard, D.K. Explosion hazards associated with nanopowders. *Health & Safety Laboratories*, HSL /2004/ 12.

(90) Akcay, K.; Sirkecioglu, A.; Tather, M.; Tunc Savascı, O.; Erdem-Senatala, A. Wet ball milling of zeolite HY. *Powder Technology*, 142, (2004) 121– 128.

(91) Cetinkaya, C.; Findik, T.; Ozbilen, S. An investigation into the effect of experimental parameters on powder grain size of the mechanically milled 17-4 PH stainless steel powders. *Materials and Design*, 14, (2006) 405.

(92) Zielinski, P.A.; Van Neste, A.; Akolekar, D.B.; Kaliaguine, S. Effect of high-energy ball milling on the structural stability, surface and catalytic properties of small-, medium- and large-pore zeolites. *Microporous Materials*, 5, (1995) 123-133.

(93) Siegrist, M.E.; Siegfried, M.; Loffler, J.F. High-purity amorphous $Zr_{52.5}Cu_{17.9}Ni_{14.6}Al_{10}Ti_5$ powders via mechanical amorphization of crystalline pre-alloys. *Materials Science and Engineering*, A 418, (2006) 236–240.

(94) Gross, Karl J; Chartouni, D; Leroy, E; Zuttel, A; Schlapbach, L. Mechanically milled Mg composites for hydrogen storage: the relationship between morphology and kinetics. *Journal of Alloy and Compounds*, 269, (1998) 259-270.

(95) Bruckner, W.; Kleinstuck, K.; Schulze, G.E.R. – *Phys. Status Solidi*, 23, (1967) 475–480.

(96) van der Kraan, A.M.; Buschow, K.H.J. – *Physica B+C*, 138B, (1986) 55–62.

(97) Rupp, B.; Fischer, P. – *J. Less-Common Met*., 144, (1988) 275–281.

UNIVERSITY of the WESTERN CAPE

(98) Taylor, D. – *Trans. J. Brit. Ceramic Soc*., 83, (1984) 5–9.

(99) Brukh, R.; Mitra, S. Mechanism of carbon nanotube growth by CVD. *Chemical Physics Letters*, 424, (2006) 126–132.

(100) Bonard, J-M. Carbon nanostructures by Hot Filament Chemical Vapor Deposition: Growth, properties, applications. *Thin Solid Films*, 501, (2006) 8 – 14.

(101) Wang, T.; Wang, B. Study on structure change of carbon nanotubes depending on different reaction gases. *Applied Surface Science*, 67, (2006) 109–122.

(102) Ndungu, P.; Onyegbule, N.; Bucher, R.; Nechaev, A.; Linkov, V. The Use of LPG for the Synthesis of Carbon Nanotubes on Various Substrates. New Diamond and Frontier carbon technology, xxx, (2006) xxx-xxx.

(103) Sarkar, A.; Banerjee, R. A quantitative method for characterization of carbon nanotubes for hydrogen storage. *International Journal of Hydrogen Energy*, 29, (2004) 1487 – 1491.

(104) Shen, K.; Xu, H.; Jiang, Y.; Pietra,T. The role of carbon nanotube structure in purification and hydrogen adsorption. *Carbon*, 42, (2004) 2315–2322.

(105) Chen, C-M.; Chen, M.; Peng, Y-W.; Lin, C-H.; Chang, L-W, Chen, C-F. Microwave digestion and acidic treatment procedures for the purification of multi-walled carbon nanotubes. *Diamond & Related Materials*, 14, (2005) 798– 803.

(106) Chen, X.H.; Chen, C.S.; Chen, Q.; Cheng, F.Q.; Zhang, G.; Chen, Z.Z. Non-destructive purification of multi-walled carbon nanotubes produced by catalyzed CVD. *Materials Letters*, 57, (2002) 734– 738.

(107) Dupuis, A-C. The catalyst in the CCVD of carbon nanotubes - a review. *Progress in Materials Science*, 50, (2005) 929–961.

(108) Basca, R.R.; Laurent, C.; Peigney, A.; Basca, W.S.; Vaugien, T.; Rousset,A. High specific surface area carbon nanotubes from catalytic chemical vapor deposition process. *Chemical Physics Letters*, 323, (2000) 566–571.

(109) Paglieri, S.N.; Way, J.D. *Innovations in palladium membrane research*; Separation and Purification methods, 31(1), (2002) 1-169.

(110) Pol, V.G.; Srivastava, D.N.; Palchik, O.; Palchik, V.; Slifkin, M.A.; Weiss, A.M.; Gedanken, A. Sonochemical Deposition of Silver Nanoparticles on Silica Spheres. *Langmuir*, (2002) 18, 3352-3357.

(111) Busch, G.; Schlapbach, L.; Stucki, F.; Fischer, P.; Andresen, A.F. Hydrogen storage in FeTi: surface segregation and its catalytic effect on hydrogenation and structural studies by means of neutron diffraction.– *Int. J. Hydrogen Energy*, Vol 4, (1979) pp 29-39.

UNIVERSITY of the WESTERN CAPE

(112) Kivalo, L.I.; Antonova, M.M.; Skorokhod, V.V. Hydrogen storage in Titanium – Iron intermetallide. – Preprint 6-83, *Institute for Problems of Materials Science, Kiev*, 1983. – 46 pp.

(113) Novikova, A.A.; Agladze, O.V.; Tarasov, B.P. Structure transformations during the milling of Fe +TiH_2 mixture. – *Russ. J. Inorg. Chem.*, 45, (8) (2000) 1288 – 1292.

(114) Schefer, J.; Fischer, P.; Halg, W.; Stucki, F.; Schlapbach, L; Andresen, A.F – *Mater. Res. Bull.*, 14, (1979) 1281–1294.

(115) Malov, Yu.I.; Fokin, V.N.; Troitskaya, S.L.; Fokina, E.E; Shilkin, S.P – *Russ. J. Inorg. Chem.*, 39, (1994) 1712–1714.

UNIVERSITY of the
WESTERN CAPE